TRIGONOMETRIC SERIES SOLUTION FOR ANALYSIS OF COMPOSITE LAMINATED PLATES

A THESIS SUBMITTED TO
THE GRADUATE SCHOOL OF NATURAL AND APPLIED SCIENCES
OF
MIDDLE EAST TECHNICAL UNIVERSITY

BY

SAMET KOÇ

IN PARTIAL FULFILLMENT OF THE REQUIREMENTS
FOR
THE DEGREE OF MASTER OF SCIENCE
IN
MECHANICAL ENGINEERING

JANUARY 2023

Approval of the thesis:

TRIGONOMETRIC SERIES SOLUTION FOR ANALYSIS OF COMPOSITE LAMINATED PLATES

submitted by **SAMET KOÇ** in partial fulfillment of the requirements for the degree of **Master of Science in Mechanical Engineering, Middle East Technical University** by,

Prof. Dr. Halil Kalıpçılar
Dean, Graduate School of **Natural and Applied Sciences** _____

Prof. Dr. M.A. Sahir Arıkan
Head of the Department, **Mechanical Engineering** _____

Prof. Dr. Serkan Dağ
Supervisor, **Mechanical Engineering, METU** _____

Examining Committee Members:

Prof. Dr. Suat Kadıoğlu
Mechanical Eng, METU _____

Prof. Dr. Serkan Dağ
Mechanical Eng, METU _____

Assoc. Prof. Dr. Merve Erdal
Mechanical Eng, METU _____

Assist. Prof. Dr. Orkun Özşahin
Mechanical Eng, METU _____

Prof. Dr. Mete Onur Kaman
Mechanical Eng., Fırat Uni. _____

Date: 27.01.2023

I hereby declare that all information in this document has been obtained and presented in accordance with academic rules and ethical conduct. I also declare that, as required by these rules and conduct, I have fully cited and referenced all material and results that are not original to this work.

Name Last name: Samet Koç

Signature:

ABSTRACT

TRIGONOMETRIC SERIES SOLUTION FOR ANALYSIS OF COMPOSITE LAMINATED PLATES

Koç, Samet
Master of Science, Mechanical Engineering
Supervisor: Prof. Dr. Serkan Dağ

January 2023, 142 pages

In this study, static bending and free vibrations of symmetric rectangular laminated composite plates are examined by using a new trigonometric series expansion technique and finite element analysis. Kirchhoff (Classical Laminated Plate) plate theory is applied in the analytical formulation of both bending and free vibration problems. Mid-plane displacement is expanded into a series of trigonometric shape functions, which allow exact satisfaction of the boundary conditions. In the case of static bending, application of the Rayleigh-Ritz method leads to a linear system for the coefficients of the trigonometric series. For free vibrations, minimization of the energy functional in conjunction with the Rayleigh-Ritz approach results in an eigenvalue problem. Finite element models for both bending and free vibrations are constructed by means of plate elements that incorporate first-order shear deformation theory. Numerical results are generated for simply-supported and fully-clamped composite plates as well as for a composite plate with a single free and three clamped edges. The trigonometric series technique developed is verified by comparisons to the outcomes of the finite element analyses. Presented numerical results illustrate the effects of geometrical parameters, boundary conditions, and composite plate

stacking sequence on deflection, transverse stresses, natural frequencies, and mode shapes. The proposed method leads to rapid convergence, possesses computational efficiency, and could be useful in design and optimization studies involving laminated composite structures.

Keywords: Rayleigh-Ritz Method, Symmetrically Laminated Composite, Bending, Free Vibration

ÖZ

KOMPOZİT LAMİNE LEVHALARIN ANALİZİ İÇİN TRİGONOMETRİK SERİSİ ÇÖZÜMÜ

Koç, Samet
Yüksek Lisans, Makina Mühendisliği
Tez Yöneticisi: Prof. Dr. Serkan Dağ

Ocak 2023, 142 sayfa

Bu çalışmada, simetrik dikdörtgen lamine kompozit plakaların statik eğilme ve serbest titreşimleri yeni bir trigonometrik seri genişletme tekniği ve sonlu elemanlar analizi kullanılarak incelenmiştir. Kirchhoff (Klasik Lamine Plaka) plaka teorisi, hem eğilme hem de serbest titreşim problemlerinin analitik formülasyonunda uygulanmaktadır. Orta düzlem yer değiştirmesi, sınır koşullarının tam olarak karşılanmasına izin veren bir dizi trigonometrik şekil fonksiyonuna genişletilir. Statik bükme durumunda, Rayleigh-Ritz yönteminin uygulanması, trigonometrik serilerin katsayıları için doğrusal bir sisteme yol açar. Serbest titreşimler için, Rayleigh-Ritz yaklaşımıyla bağlantılı olarak enerji fonksiyonelinin minimizasyonu, bir özdeğer problemiyle sonuçlanır. Hem eğilme hem de serbest titreşimler için sonlu eleman modelleri, birinci dereceden kesme deformasyon teorisini içeren plaka elemanlar vasıtasıyla oluşturulur. Basit destekli ve tam kenetlenmiş kompozit plakaların yanı sıra tek serbest ve üç kenetlenmiş kenarlı bir kompozit plaka için sayısal sonuçlar üretilir. Geliştirilen trigonometrik seri tekniği, sonlu eleman analizlerinin sonuçlarıyla karşılaştırmalar yapılarak doğrulanır. Sunulan sayısal sonuçlar, geometrik parametrelerin, sınır koşullarının ve kompozit plaka istifleme sırasının sapma, düzlem içi gerilmeler, doğal frekanslar ve mod şekilleri üzerindeki etkilerini göstermektedir. Önerilen yöntem, hızlı yakınsama sağlar, hesaplama

verimliliğine sahiptir ve katmanlı kompozit yapıları içeren tasarım ve optimizasyon çalışmalarında faydalı olabilir.

Anahtar Kelimeler: Rayleigh Ritz Metodu, Simetrik Lamine Kompozit, Eğilme, Serbest Titreşim

To my wife and parents.

ACKNOWLEDGMENTS

My supervisor, Professor Dr. Serkan Dağ, has provided me with consistent supervision, advice, support, and perspective throughout my project. I want to convey my greatest thanks to him for all these things.

In addition, I would like to express my gratitude to the jury members for their insightful remarks and recommendations.

I would like to express my gratitude to my family for their unwavering love, encouragement, and support during this time.

TABLE OF CONTENTS

LIST OF TABLES

TABLES

LIST OF FIGURES

FIGURES

CHAPTER 1

INTRODUCTION

In recent years, strength and cost requirements have pushed engineers and researchers to design lighter and more durable structures. Such design requirements led to investigations involving stronger and lighter components. Composites are alternative advanced materials that possess low weight and high strength. Composites have been used with increasing interest in material science, manufacturing technology, and theoretical analysis since they were considered structural materials. The term "composite" is used for structures formed by combining different materials, but in modern materials engineering, this term usually refers to a matrix material reinforced with fibers. These materials are called fiber-reinforced composites. Structures made of fiber-reinforced composites are used in many engineering projects, like aircrafts, machines, ships, and buildings due to their higher strength-weight ratios and more lightweight properties. Fiber-reinforced composite structures provide designers with the convenience of adjusting the fiber orientation and stacking sequence so that designers can make structures with the desired strength. A composite structure consists of many layers bonded to one another to form a high-strength fiber-reinforced laminated plate. Each lamina has a fiber-reinforced along a single direction. Adjacent layers usually have different fiber orientations. In order to accurately predict the static and dynamic behavior of fiber-reinforced plates, mathematical models should be established, and these models should be solved by analytical and computational techniques to evaluate the main variables. It is essential to choose the appropriate theories for the analysis and design studies. Different types of plate theories have been developed to predict these structures' static and dynamic behavior accurately.

Free or forced vibrations of composite plates are important under certain circumstances. A fiber-reinfoced plate's geometrical dimensions, material, and boundary conditions affect its natural frequency. The plate will vibrate with large deflections if the excitation frequency is equal to one of its natural frequencies. Knowledge of the natural frequencies of a fiber-reinforced plate under different boundary conditions might help engineers avoid such problems while designing structures. In addition, the fiber-reinforced plate must be able to withstand the intended structural load without cracking, so computation of deflection and stresses is also important. Mathematical techniques are needed to be developed to accurately describe their static and dynamic characteristics. These concepts are based on plate theories. Since most of the time, plates have a small thickness compared to other dimensions; they can be modeled as 2D (thin) objects instead of 3D objects. There are a number of plate theories proposed, each of which has its own computational efficiency.

In this study, a trigonometric series based approach is proposed to analyze the static and dynamic characteristics of laminated composite plates. The methods put forward are computationally efficient and shown to lead to results of high accuracy. Finite element analysis techniques are also used in modeling. The proposed approach in compared with different approximation method given in the literature. The methods presented in this thesis could be useful in design and analysis studies involving fiber-reinforced composite plates.

1.1 Review of Composite Materials

A material that is formed by combining at least two materials with different properties is called a composite material. The different materials that are brought together to form a composite structure may not possess the desired properties on their own. However, a structure that meets the desired performance criteria can be fabricated when they are brought together. The ability to be designed according to engineering requirements has made composites useful in different engineering fields.

Secondary structures in the aviation sector have long been made using composite materials. However, as techniques for producing and maintaining composites have advanced, composites have been employed as primary structures in the aviation sector. They are also used in the automotive industry because they can be recycled, could be more effective in crashes, and are low-weight. Composites are employed in structural parts of marine vehicles due to their corrosion resistance, in electrical panels due to their dielectric property, and in construction areas due to their lightweight and durability.

Composite materials can be classified and characterized by distinguishing between fibrous and particulate composite materials. Materials that are made of fibers and a matrix are called fibrous composites. The matrix holds the fibers together and prevents them from getting damaged. It also transfers the load from one fiber to another. Particulate composite materials are made of small particles of material that are placed together by a tough matrix, such as powders or small pieces of material in a ceramic matrix. Different fiber-reinforced laminas are bonded together to create a fiber-reinforced laminated composite plate. Composite plies have orthotropic material properties due to the existence of fibers. Composite materials have improved mechanical properties compared to isotropic materials due to reinforcement.

In this study, fiber-reinforced composite materials will be examined since they are the main part of a rectangular laminated plate structure. These structures consist of layers or plies made from fiber-reinforced material. Most of the time, the layers will be oriented in different directions to give the laminate specific strengths and stiffnesses. So, the strength and stiffness of the laminated fiber-reinforced composite plate can be changed to meet the structural element's design requirements. When designing a composite material, it is necessary to determine static and dynamic responses under different loadings. These responses depend on the fiber orientation, thickness, dimensions, and boundary conditions. It could be possible to experimentally evaluate the response of laminated composite plates under external loadings. Still, they may not always be practical due to the high cost of conducting

experiments. As described in this paper, numerical methods based on plate theories could be useful in this respect.

1.2 Literature Survey

Due to the increasing strength properties of fiber-reinforced composite plates, they have been frequently used in engineering fields in recent years. The orthotropic properties of fiber-reinforced composite plates have allowed them to be used in more specific areas than isotropic materials. It has become challenging to understand the static and dynamic responses of laminated fiber-reinforced composite plates due to the different material properties of each layer. Applying advanced mathematical models to understand these responses has become imperative. For this reason, many researchers develop other mathematical models and apply these models to different problems to analyze fiber-reinforced plates.

To understand the static and dynamic behavior of laminated fiber-reinforced plates, two different approaches are evaluated based on the three-dimensional or two-dimensional properties of the plates. These approaches can be called Equivalent Single Layer (ESL) and Layerwise theory (LW). ESL is displacement-based, and LW is a mixed formulation-based theory. Carrera [1], Reddy [2], Liew et al. [3], and Kreja [4] has explained these theories. In three-dimensional approaches, displacement and stresses at each layer are treated as unknowns. There are different studies on three-dimensional methods, Srinivas and Rao [5] have explained the bending, vibration, and buckling behavior of simply supported rectangular plates. Exact solutions of laminated bi-directional composite plates and shells have been investigated by Pagano [6]. Ye and Soldatos [7] have studied on the free vibration of the symmetrical and unsymmetrical laminated cylindrical plates and cylinders in a three-dimensional approach. Static and dynamic response of the thick laminated plates analyzed by Fan and Ye [8]. Vel and Batra [9,10,11] have researched thick laminated piezoelectric composite plates with different boundary conditions. But these three-dimensional analytical solutions can only work for simple geometries

and boundary conditions. They are also more complicated to calculate than 2D theories.

Researchers improved two-dimensional theories since 3D theories are computationally expensive. In ESL theories, all variables are the same, so the number of variables does not depend on how many layers there are. In two-dimensional theories, there are different plate theories which are classical laminated plate theory (CLPT), first-order shear deformation theory (FSDT), and higher-order shear deformation theory (HSDT). There is plenty of research on laminated composite plates with CLPT. Equivalent single layer (ESL) theory can be used with CLPT for thin laminated composite plates and shells [12, 13]. For a non-linear geometric analysis of laminated composite plates, Sun and Chin [14] introduced the von Kármán-type CLPT model. Bending analysis of symmetrically laminated two orthotropic plies with CLPT has been researched by Reissner and Stavsky [15]. Because it does not consider transverse-shear deformation, the CLPT formulation is not very good at predicting how composites will behave elastically. An improved lamination theory that accounts for transverse shear deformation is required to eliminate this constraint. Whitney & Pagano [16] offered an extension of the First-Order Shear Deformation (FSDT) model for anisotropic composite plates, while Dong & Tso [17] introduced the FSDT model for composite shells. Also, static analysis of cylindrical shells was conducted by Chandrashekhara and Pavan Ku [18] with both CLPT and FSDT. In the higher-order shear deformation theory (HSDT), classic displacement equations of FSDT are put into the higher-order terms of the equation. This can significantly improve the results of thick laminated composite plates. A typical method is expanding the displacement and strains with power series concerning thickness coordinates. This formula can get a shear deformation model of any order. Assuming a cubic description of the displacements for the thickness coordinate, Reddy [19] proposed a Third Order Transverse Shear Deformation (TOSD) theory for laminated plates in 1984. Also, Khdeir et al. [20] TOSD theory has been revised for laminated rectangular composite plates using a Lévy type solution and state-space approach. From all these theories, it can be understood that

due to the high processing cost of three-dimensional studies, plate theories based on simplified kinematic assumptions have been developed even though plate geometry is three-dimensional. Transverse shear deformations, normal deformations, and rotating inertia are neglected by the classical (Kirchhoff) laminated plate theory (CLPT). The CLPT yields appropriate solutions for plates with a thickness/side length (h/b) less than 0.01 and for plates with h/b between 0.01 and 0.05.

The finite element method (FEM) and Ritz method can solve initial boundary value problems. Ritz method uses shape (approximating) functions that satisfy the essential boundary conditions to solve the problem. The Ritz method's degree of freedom is fewer than the FEM [21, 22]. Linear combination of shape functions is put into the displacement equation in the Ritz method. Choosing shape functions is the most critical part of the Ritz method because the precision and speed of convergence of the problem vary according to these functions. Until now, many shape functions have been used in problems solved by the Ritz method. The most widely used of these are polynomial shape functions because these functions are simple to use and have fast convergence properties. However, due to numerical instability and poor conditioning problems in high-order polynomials [23, 24], researchers have also turned to other shape functions. These problems are avoided by using orthogonal polynomials. Bhat [25] developed a new technique by using the orthogonal polynomial shape functions that meet the boundary conditions with Gram-Schmidt orthogonalization technique. In this approach, the initial term of the orthogonal polynomial shape function fulfills the boundary conditions. After finding these orthogonal polynomial shape functions, Bhat [26, 27, 28] solved different plate problems. Free vibration problems in laminated composite plates with the Ritz method have been solved by many researchers using different shape functions. Leissa [29] solved the free vibration problem of rectangular composite plates with two opposite sides is simply supported by using hyperbolic functions. Later, Narita and Leissa [30] used a double sine trigonometric shape function to solve symmetrically laminated composite plates in 1989. Liew and Lam [31] also used the Graham-Schmidt operation to calculate isotropic and anisotropic laminated composite trapezium plates with orthogonal

approximation functions. Chow et al. [32] showed free vibration and mode shapes with orthogonal approximating functions for rectangular laminated plates. Composite plates with different forms of free vibration results have been investigated by Geannakakes [33]. Different boundary conditions of symmetric and unsymmetric plates have been studied by Chai [34] with sine shape functions. Wang [35] analyzed the free vibration of an obliquely laminated composite plate with small thickness, including coupling terms into the governing equations. This study shows that it is essential to strengthen composite plates. Also, Cheung and Zhou [36, 37] researched the reinforcement of composite plates with using point support and line support. Free vibration results have been examined with beam shape functions for different edge conditions. Another study of strengthening the laminated composite plates with plies layered obliquely (skew) is reviewed by Anlas and Göker [38]. Clamped and simply supported conditions were analyzed with orthogonal polynomials in this research. Some composite plates have elastic edge conditions. Amirahmadi and Ansari [39] have shown buckling and vibration responses of symmetrically laminated plates with two distinct types of shape functions: polynomial and beam. Functionally graded composite plates can be analyzed by using the Rayleigh-Ritz method. Chakraverty and Pradhan [40] studied this type of composite plate for examining free vibration results under different boundary conditions. Free vibration of plates with too small in-plane dimensions, which are nanoplates, has also been solved using the Ritz method. Chakraverty and Behera [41] studied this problem using polynomial approximating functions. Deghboudj et al. [42] reviewed a cross-ply thin laminated composite plate utilizing the polynomial and trigonometric sine functions as shape functions and compared them with FEM results. Nguyen et al. [43] developed approximating functions as a trigonometric series to solve buckling and free vibration characteristic of laminated beams with utilizing Ritz method. Static bending comparison with FEM results of symmetrically laminated composite plate has been studied by Carrol and Gutierrez-Miravete [44]. This study has been done when all boundary conditions of plate simply supported and under uniformly distributed loading. Larita and Leissa [45] researched on buckling of symmetric

laminate composite plate with edges are all simply supported. Five different loading has been applied on a composite plate and approximating double sine series has been used in Ritz method.

1.3 Motivation and Scope

This study aims to accurately obtain static bending and free vibration responses of symmetrically laminated fiber-reinforced composite plates by a trigonometric series approach. Kirchhoff plate theory is used in the formulation of the problems. Mid-plane transverse deformation of laminated composite plate is developed using trigonometric shape functions that satisfy the essential boundary conditions. The Rayleigh-Ritz method was applied to solve the static bending and the free vibration problems. The deformation of the mid-plane is expressed in terms of the new trigonometric shape functions. Solution of a linear system is required to find the unknown coefficients [2]. The Rayleigh-Ritz method was applied to the energy function in the solution of the free vibration problem [30], [32], [42]. An eigenvalue problem is obtained, and natural frequencies and mode shapes are calculated by solving the eigenvalue problem. A finite element model is used in the verification of the developed techniques. Numerical results are obtained for simply-supported and clamped composite plates as well as those with one free edge and three clamped edges. Parametric analyses are carried out to observe how the results are affected by different parameters like thickness-to-length ratio, lamination scheme, and aspect ratio.

This study presents a new method for bending and free vibrations of fiber-reinforced symmetrically laminated composite plates. The method is computationally efficient and provided insight into the behavior of composite structures.

CHAPTER 2

GOVERNING EQUATIONS

2.1 The Classical Laminated Plate Theory

The classical laminated plate theory is a type of classical plate theory that uses laminated composites. So, this theory applies to the fiber-reinforced laminated plates seen in Figure 2-1. It is assumed that the Kirchhoff hypothesis holds in classical laminated plate theory [2]:

- Straight lines perpendicular to the mid surface remained straight after the deformation.
- There is no elongation experienced by the transverse normals.
- After deformation, the transverse normals rotate to stay perpendicular to the mid surface.

The transverse displacement is independent of the transverse coordinate, and the normal transverse strain ε_z is assumed to be zero by the first two assumptions. There are no transverse shear strains $\varepsilon_{xz}, \varepsilon_{yz}$ as a result of the third assumption.

- Classical plate theory utilizes the plane stress assumption; that is, the out of plane stress σ_z is zero since the plate is thin.
- This is a reasonable assumption for thin plates as these stresses do not develop significantly over small thicknesses.

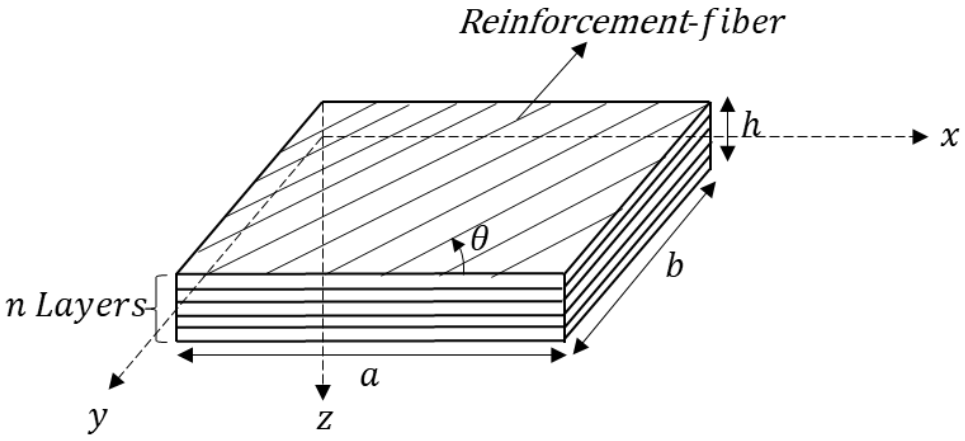

Figure 2-1. Configuration of fiber-reinforced laminated plate

2.2 Displacements and Strains

Assume that a plate with *n* orthotropic layers and a total thickness of *h* has the principal material coordinates of the *kth* lamina aligned at an angle θ to the laminate coordinate, *x* as seen in Figure 2-1. It is advantageous, but not necessary, to locate the undeformed mid-plane of the laminate in the problem's *xy* plane. The *z*-axis is taken positively downward from the mid-plane. The *kth* layer lies between the positions and in the thickness direction (see Figure 2-2).

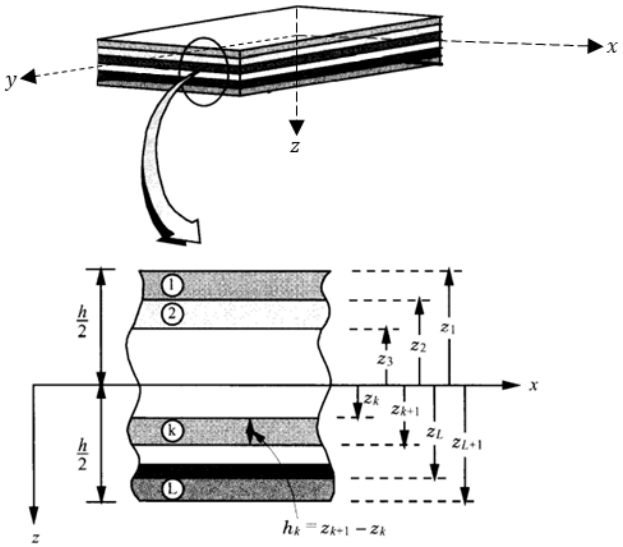

Figure 2-2.Stacking sequence numbering of a fiber-reinforced laminated plate [2]

It is possible to develop specific assumptions or set limitations when developing the theory [2], as given here:

- There is a perfect bond between the layers (assumption).
- The material of each layer is linearly elastic and symmetric in three planes. (limitation)
- There is uniform thickness for each layer (limitation)
- There are small displacement and strains (limitation)
- There is no shear stresses on the top and bottom surfaces of the laminate (limitation)

A material point at coordinates (x, y, z) in the undeformed laminate shifts to coordinates $(x + u, y + v, z + w)$ in the deformed laminate, where (u, v, w) are components of the total displacement vector *r* along the (x, y, z) axes, as predicted by the Kirchhoff hypotheses.

$$r = u\hat{e}_x + v\hat{e}_y + w\hat{e}_z \qquad (2\text{-}1)$$

Where $(\hat{e}_x, \hat{e}_y, \hat{e}_z)$ are unit vectors along the (x, y, z) directions. No differentiation is made between the material coordinates and the spatial coordinates, between the finite Green strain tensor and infinitesimal strain tensor, and between the second Piola-Kirchhoff stress tensor and Cauchy stress tensor due to the small strain and small displacement assumptions.

The displacements (u, v, w), according to the Kirchhoff hypothesis, must be such that:

$$u(x, y, z) = u_0(x, y) - z\,\frac{\partial w_0}{\partial x} \qquad (2\text{-}2)$$

$$v(x, y, z) = v_0(x, y) - z\,\frac{\partial w_0}{\partial y} \qquad (2\text{-}3)$$

$$w(x,y,z) = w_0(x,y) \tag{2-4}$$

Under some assumptions of Kirchhoff's hypothesis, the linear strain-displacement relations are used to calculate the strains associated with displacement. The linear strain-displacement relation can be written as:

$$\varepsilon_x = \frac{\partial u}{\partial x}, \varepsilon_y = \frac{\partial v}{\partial y}, \varepsilon_z = \frac{\partial w}{\partial z}, \gamma_{xy} \equiv 2\varepsilon_{xy} = \frac{\partial u}{\partial y} + \frac{\partial v}{\partial x}$$
$$\gamma_{xz} \equiv 2\varepsilon_{xz} = \frac{\partial u}{\partial z} + \frac{\partial w}{\partial x}, \gamma_{yz} \equiv 2\varepsilon_{yz} = \frac{\partial v}{\partial z} + \frac{\partial w}{\partial y} \tag{2-5}$$

Kirchhoff's hypothesis assumptions for strain-displacement relations imply that the transverse shear strains $\varepsilon_{xz}, \varepsilon_{yz}$ and transverse normal strain ε_z are zero in the equation (2-5). Substitute equation (2-2) -(2-4) into the equation (2-5), it can be obtained strain-displacement relations of classical laminated plate theory:

$$\begin{Bmatrix} \varepsilon_x \\ \varepsilon_y \\ \gamma_{xy} \end{Bmatrix} = \begin{Bmatrix} {\varepsilon_x}^{(0)} \\ {\varepsilon_y}^{(0)} \\ {\gamma_{xy}}^{(0)} \end{Bmatrix} + z \begin{Bmatrix} {\varepsilon_x}^{(1)} \\ {\varepsilon_y}^{(1)} \\ {\gamma_{xy}}^{(1)} \end{Bmatrix} \tag{2-6}$$

$$\begin{Bmatrix} \varepsilon_x \\ \varepsilon_y \\ \gamma_{xy} \end{Bmatrix} = \begin{Bmatrix} \frac{\partial u}{\partial x} \\ \frac{\partial v}{\partial y} \\ \frac{\partial u}{\partial y} + \frac{\partial v}{\partial x} \end{Bmatrix} = \begin{Bmatrix} \frac{\partial u_0}{\partial x} \\ \frac{\partial v_0}{\partial y} \\ \frac{\partial u_0}{\partial y} + \frac{\partial v_0}{\partial x} \end{Bmatrix} + z \begin{Bmatrix} -\frac{\partial^2 w_0}{\partial x^2} \\ -\frac{\partial^2 w_0}{\partial y^2} \\ -2\frac{\partial^2 w_0}{\partial x \partial y} \end{Bmatrix} \tag{2-7}$$

${\varepsilon_x}^{(0)}$, ${\varepsilon_y}^{(0)}$, ${\varepsilon_z}^{(0)}$ are the membrane strains and ${\varepsilon_x}^{(1)}$, ${\varepsilon_y}^{(1)}$, ${\varepsilon_z}^{(1)}$ are flexural strains [2].

2.3 Lamina Constitutive Law

The transverse strain components $\varepsilon_z, \varepsilon_{xz}, \varepsilon_{yz}$ are zero with classical laminated plate theory assumptions. A thin plate with plane stress assumption is used in formulations since the thickness is small per in-plane dimensions.

Strain-stress relationship for plane stress (reduced) is given by:

$$\begin{Bmatrix} \varepsilon_1 \\ \varepsilon_2 \\ \gamma_{12} \end{Bmatrix} = \begin{bmatrix} \frac{1}{E_{11}} & \frac{-v_{21}}{E_{22}} & 0 \\ \frac{-v_{12}}{E_{11}} & \frac{1}{E_{22}} & 0 \\ 0 & 0 & \frac{1}{G_{12}} \end{bmatrix} \begin{Bmatrix} \sigma_1 \\ \sigma_2 \\ \tau_{12} \end{Bmatrix} \quad (2\text{-}8)$$

$$[S] = \begin{bmatrix} \frac{1}{E_{11}} & \frac{-v_{21}}{E_{22}} & 0 \\ \frac{-v_{12}}{E_{11}} & \frac{1}{E_{22}} & 0 \\ 0 & 0 & \frac{1}{G_{12}} \end{bmatrix} \quad (2\text{-}9)$$

Stress-strain relationship can be determined from inversion of equation (2-8):

$$\begin{Bmatrix} \sigma_1 \\ \sigma_2 \\ \tau_{12} \end{Bmatrix} = \begin{bmatrix} Q_{11} & Q_{12} & 0 \\ Q_{21} & Q_{22} & 0 \\ 0 & 0 & 2Q_{66} \end{bmatrix} \begin{Bmatrix} \varepsilon_1 \\ \varepsilon_2 \\ \gamma_{12}/2 \end{Bmatrix} \quad (2\text{-}10)$$

$$[Q] = [S]^{-1} \quad (2\text{-}11)$$

$$Q_{11} = \frac{S_{22}}{S_{11}S_{22} - {S_{12}}^2} = \frac{E_{11}}{1 - v_{12}v_{21}} \quad (2\text{-}12)$$

$$Q_{22} = \frac{S_{11}}{S_{11}S_{22} - {S_{12}}^2} = \frac{E_{22}}{1 - v_{12}v_{21}} \quad (2\text{-}13)$$

$$Q_{12} = \frac{S_{12}}{S_{11}S_{22} - {S_{12}}^2} = \frac{v_{12}E_{22}}{1 - v_{12}v_{21}} \quad (2\text{-}14)$$

$$Q_{66} = \frac{1}{S_{66}} = G_{12} \quad (2\text{-}15)$$

E_{11} and E_{22} are the Young modulus in x_1 and x_2 directions. G_{12} is the shear modulus and v_{12} and v_{21} are the Poisson ratios. Q_{ij} are the reduced stiffnesses of *kth* lamina with plane stress assumptions and σ_i, ε_i are stresses and strains components, respectively. These stresses and strains are in material coordinates (x_1, x_2, x_3). Figure 2-3 shows the material and global coordinates of the fiber-reinforced plate.

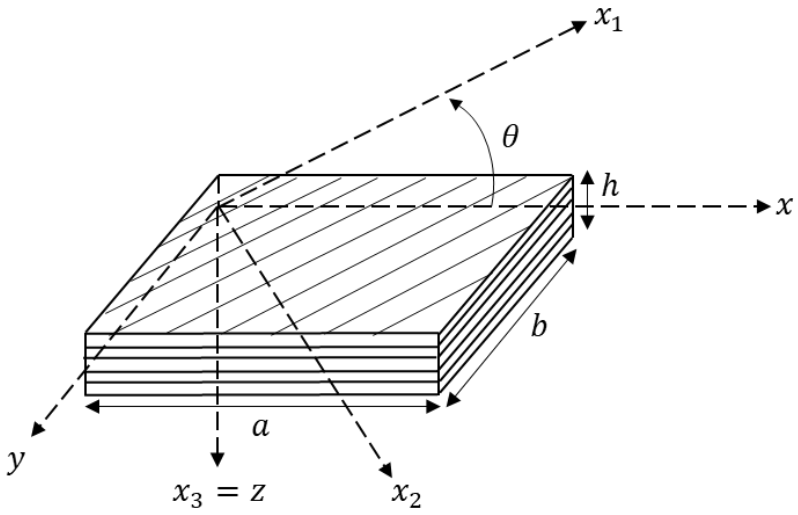

Figure 2-3. Representation of material and global coordinate system of fiber-reinforced laminated plate

The constitutive equations must be translated to the global coordinates since orthotropic layers are used in laminates with the material axis orientated with those coordinates. To find transformed constitutive equation, equation (2-10) is multiplied by transformation matrix [T]. In transformation matrix $m = cos\theta$ and $n = sin\theta$. Fibers are aligned at an angle of θ to the global coordinate as shown in Figure 2-3.

Transformation of constitutive equations to the global coordinate system can be expressed as follows:

$$\begin{Bmatrix}\sigma_1\\ \sigma_2\\ \tau_{12}\end{Bmatrix}=\begin{bmatrix} m^2 & n^2 & 2mn\\ n^2 & m^2 & -2mn\\ -mn & mn & m^2-n^2\end{bmatrix}\begin{Bmatrix}\sigma_x\\ \sigma_y\\ \tau_{xy}\end{Bmatrix}=[T]\begin{Bmatrix}\sigma_x\\ \sigma_y\\ \tau_{xy}\end{Bmatrix} \quad (2\text{-}16)$$

$$\begin{Bmatrix}\varepsilon_1\\ \varepsilon_2\\ \gamma_{12}\end{Bmatrix}=[T]\begin{Bmatrix}\varepsilon_x\\ \varepsilon_y\\ \gamma_{xy}\end{Bmatrix} \quad (2\text{-}17)$$

$$[T]\begin{Bmatrix}\sigma_x\\ \sigma_y\\ \tau_{xy}\end{Bmatrix}=\begin{bmatrix}Q_{11} & Q_{12} & 0\\ Q_{21} & Q_{22} & 0\\ 0 & 0 & 2Q_{66}\end{bmatrix}[T]\begin{Bmatrix}\varepsilon_x\\ \varepsilon_y\\ \gamma_{xy}\end{Bmatrix} \quad (2\text{-}18)$$

$$\begin{Bmatrix}\sigma_x\\ \sigma_y\\ \tau_{xy}\end{Bmatrix}=[T]^{-1}[Q][T]\begin{Bmatrix}\varepsilon_x\\ \varepsilon_y\\ \varepsilon_{xy}\end{Bmatrix} \quad (2\text{-}19)$$

$$\begin{Bmatrix}\sigma_x\\ \sigma_y\\ \tau_{xy}\end{Bmatrix}=\begin{bmatrix} m^2 & n^2 & 2mn\\ n^2 & m^2 & -2mn\\ -mn & mn & m^2-n^2\end{bmatrix}^{-1}\begin{bmatrix}Q_{11} & Q_{12} & 0\\ Q_{21} & Q_{22} & 0\\ 0 & 0 & 2Q_{66}\end{bmatrix}\begin{bmatrix} m^2 & n^2 & 2mn\\ n^2 & m^2 & -2mn\\ -mn & mn & m^2-n^2\end{bmatrix}\begin{Bmatrix}\varepsilon_x\\ \varepsilon_y\\ \varepsilon_{xy}\end{Bmatrix} \quad (2\text{-}20)$$

Finally, transformed constitutive equations can be written as:

$$\begin{Bmatrix}\sigma_x\\ \sigma_y\\ \tau_{xy}\end{Bmatrix}=\begin{bmatrix}\bar{Q}_{11} & \bar{Q}_{12} & \bar{Q}_{16}\\ \bar{Q}_{12} & \bar{Q}_{22} & \bar{Q}_{26}\\ \bar{Q}_{16} & \bar{Q}_{26} & \bar{Q}_{66}\end{bmatrix}\begin{Bmatrix}\varepsilon_x\\ \varepsilon_y\\ \varepsilon_{xy}\end{Bmatrix} \quad (2\text{-}21)$$

In equation (2-21), reduced stiffnesses are given by:

$$\bar{Q}_{11}=Q_{11}cos^4\theta+2(Q_{12}+2Q_{66})sin^2\theta cos^2\theta+Q_{22}sin^4\theta \quad (2\text{-}22)$$

$$\bar{Q}_{12} = (Q_{11} + Q_{22} - 4Q_{66})sin^2\theta cos^2\theta + Q_{12}(sin^4\theta + cos^4\theta) \quad (2\text{-}23)$$

$$\bar{Q}_{22} = Q_{11}sin^4\theta + 2(Q_{12} + 2Q_{66})sin^2\theta cos^2\theta + Q_{22}cos^4\theta \quad (2\text{-}24)$$

$$\bar{Q}_{16} = (Q_{11} - Q_{12} - 2Q_{66})sin\theta cos^3\theta + (Q_{12} - Q_{22} + 2Q_{66})sin^3\theta cos\theta \quad (2\text{-}25)$$

$$\bar{Q}_{26} = (Q_{11} - Q_{12} - 2Q_{66})sin^3\theta cos\theta + (Q_{12} - Q_{22} + 2Q_{66})sin\theta cos^3\theta \quad (2\text{-}26)$$

$$\bar{Q}_{26} = (Q_{11} - Q_{12} - 2Q_{66})sin^3\theta cos\theta + (Q_{12} - Q_{22} + 2Q_{66})sin\theta cos^3\theta \quad (2\text{-}27)$$

$\bar{Q}_{ij}$ are the plane-stress transformed reduced stiffnesses.

2.4 Force and Moment Resultants

The equilibrium of the differential element can be considered shown in the Figure 2-4. Since the stresses are functions of spatial coordinates, a first order Taylor series expansion is used to consider variations in term.

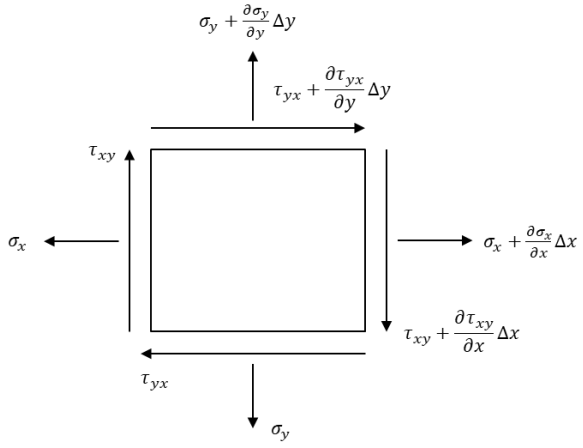

Figure 2-4. Small element of linear elastic body

Equilibrium requires that

$$\sum F_x = 0 \tag{2-28}$$

$$-\sigma_x(\Delta y \Delta z) + \left(\sigma_x + \frac{\partial \sigma_x}{\partial x}\Delta x\right)\Delta y \Delta z - \sigma_{xy}(\Delta x \Delta z) + \left(\sigma_{xy} + \frac{\partial \sigma_{xy}}{\partial y}\Delta y\right)\Delta x \Delta z = 0 \tag{2-29}$$

Equation (2-29) reduces to the following equation:

$$\frac{\partial \sigma_x}{\partial x} + \frac{\partial \sigma_{xy}}{\partial y} = 0 \tag{2-30}$$

Equilibrium equations in 3D are written as:

$$\frac{\partial \sigma_x}{\partial x} + \frac{\partial \sigma_{xy}}{\partial y} + \frac{\partial \sigma_{xz}}{\partial z} = 0 \tag{2-31}$$

$$\frac{\partial \sigma_{xy}}{\partial x} + \frac{\partial \sigma_y}{\partial y} + \frac{\partial \sigma_{yz}}{\partial z} = 0 \tag{2-32}$$

$$\frac{\partial \sigma_{xz}}{\partial x} + \frac{\partial \sigma_{yz}}{\partial y} + \frac{\partial \sigma_z}{\partial z} = 0 \tag{2-33}$$

Integrating the equilibrium equations (2-31), (2-32), and (2-33) through the thickness, the force (*N*) resultants can be found as follows:

$$\int_{-h/2}^{h/2} \begin{Bmatrix} \frac{\partial \sigma_x}{\partial x} + \frac{\partial \sigma_{xy}}{\partial y} + \frac{\partial \sigma_{xz}}{\partial z} + b_x \\ \frac{\partial \sigma_{xy}}{\partial x} + \frac{\partial \sigma_y}{\partial y} + \frac{\partial \sigma_{yz}}{\partial z} + b_y \\ \frac{\partial \sigma_{xz}}{\partial x} + \frac{\partial \sigma_{yz}}{\partial y} + \frac{\partial \sigma_z}{\partial z} + b_z \end{Bmatrix} dz = 0 \tag{2-34}$$

$$\frac{\partial}{\partial x}\int_{-h/2}^{h/2} \sigma_x dz + \frac{\partial}{\partial y}\int_{-h/2}^{h/2} \sigma_{xy} dz + [\sigma_{xz}]_{-h/2}^{h/2} = 0 \tag{2-35}$$

$$\frac{\partial}{\partial x}\int_{-h/2}^{h/2}\sigma_{xy}dz + \frac{\partial}{\partial y}\int_{-h/2}^{h/2}\sigma_{y}dz + \left[\sigma_{yz}\right]_{-h/2}^{h/2} = 0 \quad (2\text{-}36)$$

$$\frac{\partial}{\partial x}\int_{-h/2}^{h/2}\sigma_{xz}dz + \frac{\partial}{\partial y}\int_{-h/2}^{h/2}\sigma_{yz}dz + \left[\sigma_{zz}\right]_{-h/2}^{h/2} = 0 \quad (2\text{-}37)$$

Force resultants can be written from equations (2-35) and (2-36):

$$\begin{bmatrix} N_x \\ N_y \\ N_{xy} \end{bmatrix} = \int_{-h/2}^{h/2}\begin{bmatrix} \sigma_x \\ \sigma_y \\ \sigma_{xy} \end{bmatrix}dz \quad (2\text{-}38)$$

Since the plate is multi-layered with n-plies, the integral can be re-written as follows:

$$\begin{bmatrix} N_x \\ N_y \\ N_{xy} \end{bmatrix} = \sum_{k=1}^{n}\int_{z_{k-1}}^{z_k}\begin{bmatrix} \sigma_x \\ \sigma_y \\ \sigma_{xy} \end{bmatrix}dz \quad (2\text{-}39)$$

Considering the moments about the x and y axis respectively, it can be written as:

$$\frac{\partial}{\partial x}\int_{-h/2}^{h/2}z\sigma_{x}dz + \frac{\partial}{\partial y}\int_{-h/2}^{h/2}z\sigma_{xy}dz + \frac{\partial}{\partial z}\int_{-h/2}^{h/2}z\sigma_{zx}dz = 0 \quad (2\text{-}40)$$

$$\frac{\partial}{\partial x}\int_{-h/2}^{h/2}z\sigma_{xy}dz + \frac{\partial}{\partial y}\int_{-h/2}^{h/2}z\sigma_{y}dz + \frac{\partial}{\partial z}\int_{-h/2}^{h/2}z\sigma_{zy}dz = 0 \quad (2\text{-}41)$$

Moment resultants can be written from these integral equations (2-40) and (2-41).

$$\begin{bmatrix} M_x \\ M_y \\ M_{xy} \end{bmatrix} = \int_{-h/2}^{h/2}\begin{bmatrix} \sigma_x \\ \sigma_y \\ \sigma_{xy} \end{bmatrix}zdz \quad (2\text{-}42)$$

Since the plate is multi-layered with n-plies, the integral can be re-written as follows:

$$\begin{bmatrix} M_x \\ M_y \\ M_{xy} \end{bmatrix} = \sum_{k=1}^{n}\int_{z_{k-1}}^{z_k}\begin{bmatrix} \sigma_x \\ \sigma_y \\ \sigma_{xy} \end{bmatrix}zdz \quad (2\text{-}43)$$

Equations (2-39) and (2-43) shows the force and moment resultants of fiber-reinforced plate as seen in the Figure 2-5.

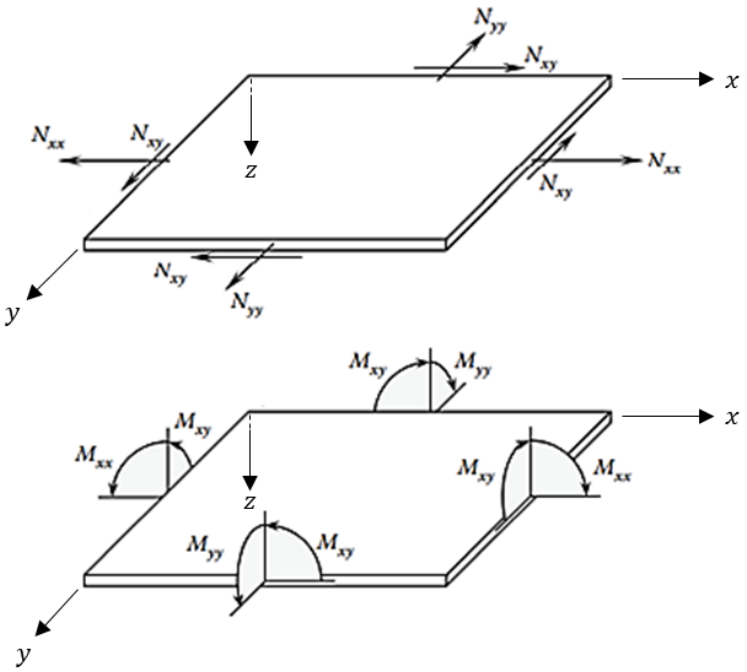

Figure 2-5. Force and moment resultants of fiber-reinforced laminated plate [13]

2.5 Equations of Motion

There are many possible configurations in a mechanical system. These configurations satisfy the geometric constraints of the system. Only one of these possible configurations matches the actual configuration, and from this configuration, the equilibrium equations or motion of the system can be found. These configurations are derived from infinitesimal variations of the actual configuration. Virtual displacement occurs when a mechanical system changes its configuration. While using the virtual displacement and forces, δ operator is used. It is called a variational operator [2]. δ operator shows a change in the given displacement. This operator is beneficial in obtaining governing equations from the virtual work principle. Equation (2-44) shows the first variation of F with using δ operator [2].

$$\delta F = \frac{\partial F}{\partial u}\delta u + \frac{\partial F}{\partial u'}\delta u' \qquad (2\text{-}44)$$

Functionals are integral expressions of dependent variables. Thus, a functional transforms dependent variable *u* to real number *I(u)*.

For example, consider functional *I(u)* expressed in interval *(a, b)* and obtaining the maximum or minimum of this functional [2]:

$$I(u) = \int_a^b F(x, u(x), u(x)')dx \qquad u(a) = u_a, \quad u(b) = u_b \tag{2-45}$$

In order to have minimum or maximum of the functional, the first variation of functional, equation (2-45) should be zero:

$$\delta I = 0 \tag{2-46}$$

To calculate governing equations of equilibrium configuration, mechanical system is subjected to virtual displacements $\delta u, \delta v, and\ \delta w$ from its actual configuration. These virtual displacements are continuous functions and satisfy the geometric boundary conditions of the mechanical system.

In this study, the principle of virtual displacements are used to obtain equations of motion of the fiber-reinforced plate with using equations (2-44) – (2-46). If the mechanical system is in equilibrium, work of external and internal forces done over virtual displacements is zero. The principle of virtual displacements can be expressed as follows [2]:

$$\delta U + \delta V \equiv \delta T \tag{2-47}$$

In equation (2-47), δU and δT represents variation strain energy and variation kinetic energy of fiber-reinforced plate. Externally applied forces on the fiber-reinforced plate cause virtual work δV.

Virtual strain energy of the system, virtual work done by the applied forces, and virtual work done by the inertia force ma can be expressed as [2]:

$$\delta U = \int\int\int \sigma_{ij}\delta\varepsilon_{ij}dv \tag{2-48}$$

$$\delta V = -\int\int p\delta w ds \tag{2-49}$$

$$\delta T = \int\int\int \rho_0 \frac{\partial^2 w}{\partial t^2}\delta w dv = \int\int\int \rho_0 \frac{\partial w}{\partial t}\frac{\partial \delta w}{\partial t} dv \tag{2-50}$$

Where dv is volume, ds is surface, and ρ_0 is the mass density of the fiber-reinforced plate. p is the applied force on the fiber-reinforced plate.

Equation (2-47) is known as principle of virtual displacement. Equations of motion of laminated fiber-reinforced plate can be found using the virtual work principle or known as Hamilton's principle [2].

Integrate the equation (2-47) with respect to time leads to the Hamilton's principle [2]:

$$0 = \int_0^T (\delta U + \delta V - \delta T) dt \tag{2-51}$$

Virtual strain energy δU can be written for fiber-reinforced laminated plate as [2]:

$$\delta U = \int_0^a \int_0^b \int_{-h/2}^{h/2} (\sigma_x \delta\varepsilon_x + \sigma_y \delta\varepsilon_y + 2\sigma_{xy}\delta\varepsilon_{xy}) dz dy dx \tag{2-52}$$

Virtual work done by externally applied force δV for fiber-reinforced laminated plate can be written as [2]:

$$\delta V = \int_0^a \int_0^b (p(x,y)\ \delta w_0(x,y)) dy dx \tag{2-53}$$

Virtual kinetic energy δT for fiber-reinforced laminated plate can be written as [2]:

$$\delta T = \int_0^a \int_0^b \int_{-h/2}^{h/2} \rho_0 [(\dot{u}_0 \delta\dot{u}_0 + \dot{v}_0 \delta\dot{v}_0 + \dot{w}_0 \delta\dot{w}_0)] dz dy dx \tag{2-54}$$

$p(x,y)$ is the pressure distribution on top of the fiber-reinforced plate.

Substituting equations (2-52) -(2-54) into the equation (2-51) and integrating through thickness, it can be obtained [2]:

$$0 = \int_0^T \left\{ \int_0^a \int_0^b [N_x \delta {\varepsilon_x}^{(0)} + M_x \delta {\varepsilon_x}^{(1)} + N_y \delta {\varepsilon_y}^{(0)} + M_y \delta {\varepsilon_y}^{(1)} + N_{xy} \delta {\gamma_{xy}}^{(0)} + M_{xy} \delta {\gamma_{xy}}^{(1)} - p \delta w_0 - I_0 (\dot{u}_0 \delta \dot{u}_0 + \dot{v}_0 \delta \dot{v}_0 + \dot{w}_0 \delta \dot{w}_0)] \, dx dy \right\} dt \quad (2\text{-}55)$$

I_0 is the mass per unit area of the fiber-reinforced laminated plate [2].

$$I_0 = \int_{-h/2}^{h/2} \rho_0 dz \quad (2\text{-}56)$$

Virtual strains can be represented in terms of virtual displacement as equation (2-7) real strain in terms of real displacement [2].

$$\delta {\varepsilon_x}^{(0)} = \frac{\partial \delta u_0}{\partial x} + \frac{\partial w_0}{\partial x} \frac{\partial \delta w_0}{\partial x} \quad (2\text{-}57)$$

$$\delta {\varepsilon_y}^{(0)} = \frac{\partial \delta v_0}{\partial y} + \frac{\partial w_0}{\partial y} \frac{\partial \delta w_0}{\partial y} \quad (2\text{-}58)$$

$$\delta {\gamma_{xy}}^{(0)} = \frac{\partial \delta u_0}{\partial y} + \frac{\partial \delta v_0}{\partial x} + \frac{\partial \delta w_0}{\partial x} \frac{\partial w_0}{\partial y} + \frac{\partial w_0}{\partial x} \frac{\partial \delta w_0}{\partial y} \quad (2\text{-}59)$$

$$\delta {\varepsilon_x}^{(1)} = -\frac{\partial^2 \delta w_0}{\partial x^2} \quad (2\text{-}60)$$

$$\delta {\varepsilon_y}^{(1)} = -\frac{\partial^2 \delta w_0}{\partial y^2} \quad (2\text{-}61)$$

$$\delta {\gamma_{xy}}^{(1)} = -2 \frac{\partial^2 \delta w_0}{\partial x \partial y} \quad (2\text{-}62)$$

$\delta {\varepsilon_x}^{(0)}$, $\delta {\varepsilon_y}^{(0)}$, $\delta {\varepsilon_z}^{(0)}$ are the virtual membrane strains and $\delta {\varepsilon_x}^{(1)}$, $\delta {\varepsilon_y}^{(1)}$, $\delta {\varepsilon_z}^{(1)}$ are the virtual flexural strains.

Substituting equation (2-57) -(2-62) into the equation (2-55), it is found [2]:

$$0 = \int_0^T \left\{ \int_0^a \int_0^b \left[-(N_{x,x} + N_{xy,y} - I_0 \ddot{u}_0)\delta u_0 - (N_{xy,x} + N_{y,y} - I_0 \ddot{v}_0)\delta v_0 - (M_{x,xx} + 2M_{xy,xy} + M_{y,yy} + p - I_0 \ddot{w}_0)\delta w_0 \right] dy dx \right\} dt \quad (2\text{-}63)$$

Setting the $\delta u_0, \delta v_0$, and δw_0 coefficients of equation (2-63) zero separately, gives the equation of motion of fiber-reinforced laminated plate [2].

$$\partial u_0 : \frac{\partial N_x}{\partial x} + \frac{\partial N_{xy}}{\partial y} = I_0 \frac{\partial^2 \delta u_0}{\partial t^2} \quad (2\text{-}64)$$

$$\partial v_0 : \frac{\partial N_{xy}}{\partial x} + \frac{\partial N_y}{\partial y} = I_0 \frac{\partial^2 \delta v_0}{\partial t^2} \quad (2\text{-}65)$$

$$\partial w_0 : \frac{\partial^2 M_x}{\partial x^2} + \frac{2\partial^2 M_{xy}}{\partial x \partial y} + \frac{\partial^2 M_y}{\partial y^2} + p(x,y) = I_0 \frac{\partial^2 w_0}{\partial t^2} \quad (2\text{-}66)$$

2.6 Laminate Stress Resultant-Strain Relationship

Substitute force resultant equation (2-39) into the constitutive law equation (2-21), force resultant relation with strains are obtained.

$$\begin{bmatrix} N_x \\ N_y \\ N_{xy} \end{bmatrix} = \sum_{k=1}^{N} \int_{z_{k-1}}^{z_k} \begin{bmatrix} \bar{Q}_{11} & \bar{Q}_{12} & \bar{Q}_{16} \\ \bar{Q}_{12} & \bar{Q}_{22} & \bar{Q}_{26} \\ \bar{Q}_{16} & \bar{Q}_{26} & \bar{Q}_{66} \end{bmatrix} \left[\begin{Bmatrix} {\varepsilon_x}^{(0)} \\ {\varepsilon_y}^{(0)} \\ {\gamma_{xy}}^{(0)} \end{Bmatrix} + z \begin{Bmatrix} {\varepsilon_x}^{(1)} \\ {\varepsilon_y}^{(1)} \\ {\gamma_{xy}}^{(1)} \end{Bmatrix} \right] dz \quad (2\text{-}67)$$

$$\begin{bmatrix} N_x \\ N_y \\ N_{xy} \end{bmatrix} = \begin{bmatrix} A_{11} & A_{12} & A_{16} \\ A_{12} & A_{22} & A_{26} \\ A_{16} & A_{26} & A_{66} \end{bmatrix} \begin{Bmatrix} {\varepsilon_x}^{(0)} \\ {\varepsilon_y}^{(0)} \\ {\gamma_{xy}}^{(0)} \end{Bmatrix} + \begin{bmatrix} B_{11} & B_{12} & B_{16} \\ B_{12} & B_{22} & B_{26} \\ B_{16} & B_{26} & B_{66} \end{bmatrix} \begin{Bmatrix} {\varepsilon_x}^{(1)} \\ {\varepsilon_y}^{(1)} \\ {\gamma_{xy}}^{(1)} \end{Bmatrix} \quad (2\text{-}68)$$

$$A_{ij} = \sum_{k=1}^{N} {\bar{Q}_{ij}}^{(k)} (z_k - z_{k-1}) \quad (2\text{-}69)$$

$$B_{ij} = \frac{1}{2} \sum_{k=1}^{N} {\bar{Q}_{ij}}^{(k)} ({z_k}^2 - {z_{k-1}}^2) \quad (2\text{-}70)$$

A_{ij} are extensional stiffnesses and B_{ij} are bending extensional coupling stiffnesses. These stiffnesses are in terms of the plane-stress transformed reduced stiffnesses $\bar{Q}_{ij}$.

Substitute moment resultant equation (2-43) into the constitutive law equation (2-21), it is obtained moment resultant relation with strains.

$$\begin{bmatrix} M_x \\ M_y \\ M_{xy} \end{bmatrix} = \sum_{k=1}^{N} \int_{z_{k-1}}^{z_k} \begin{bmatrix} \bar{Q}_{11} & \bar{Q}_{12} & \bar{Q}_{16} \\ \bar{Q}_{12} & \bar{Q}_{22} & \bar{Q}_{26} \\ \bar{Q}_{16} & \bar{Q}_{26} & \bar{Q}_{66} \end{bmatrix} \left[z \begin{Bmatrix} {\varepsilon_x}^{(0)} \\ {\varepsilon_y}^{(0)} \\ {\gamma_{xy}}^{(0)} \end{Bmatrix} + z^2 \begin{Bmatrix} {\varepsilon_x}^{(1)} \\ {\varepsilon_y}^{(1)} \\ {\gamma_{xy}}^{(1)} \end{Bmatrix} \right] dz \quad (2\text{-}71)$$

$$\begin{bmatrix} M_x \\ M_y \\ M_{xy} \end{bmatrix} = \sum_{k=1}^{N} \begin{bmatrix} \bar{Q}_{11} & \bar{Q}_{12} & \bar{Q}_{16} \\ \bar{Q}_{12} & \bar{Q}_{22} & \bar{Q}_{26} \\ \bar{Q}_{16} & \bar{Q}_{26} & \bar{Q}_{66} \end{bmatrix}^k \left[\frac{1}{2} ({z_k}^2 - {z_{k-1}}^2) \begin{Bmatrix} {\varepsilon_x}^{(0)} \\ {\varepsilon_y}^{(0)} \\ {\gamma_{xy}}^{(0)} \end{Bmatrix} + \frac{1}{3} ({z_k}^3 - {z_{k-1}}^3) \begin{Bmatrix} {\varepsilon_x}^{(1)} \\ {\varepsilon_y}^{(1)} \\ {\gamma_{xy}}^{(1)} \end{Bmatrix} \right] \quad (2\text{-}72)$$

Finally, moment resultants are written as:

$$\begin{bmatrix} M_x \\ M_y \\ M_{xy} \end{bmatrix} = \begin{bmatrix} B_{11} & B_{12} & B_{16} \\ B_{12} & B_{22} & B_{26} \\ B_{16} & B_{26} & B_{66} \end{bmatrix} \begin{Bmatrix} {\varepsilon_x}^{(0)} \\ {\varepsilon_y}^{(0)} \\ {\gamma_{xy}}^{(0)} \end{Bmatrix} + \begin{bmatrix} D_{11} & D_{12} & D_{16} \\ D_{12} & D_{22} & D_{26} \\ D_{16} & D_{26} & D_{66} \end{bmatrix} \begin{Bmatrix} {\varepsilon_x}^{(1)} \\ {\varepsilon_y}^{(1)} \\ {\gamma_{xy}}^{(1)} \end{Bmatrix} \quad (2\text{-}73)$$

$$D_{ij} = \frac{1}{3} \sum_{k=1}^{N} {\bar{Q}_{ij}}^{(k)} ({z_k}^3 - {z_{k-1}}^3) \quad (2\text{-}74)$$

D_{ij} are bending stiffnesses. These stiffnesses are in terms of the plane-stress transformed reduced stiffnesses $\bar{Q}_{ij}$.

2.7 Governing Equations for a Fiber-Reinforced Symmetrically Laminated Plate

Substitution of strain equation (2-7) into the force resultant equation (2-68) and moment resultant equation (2-73) leads to force and moment resultants in terms of displacements.

$$\begin{bmatrix} N_x \\ N_y \\ N_{xy} \end{bmatrix} = \begin{bmatrix} A_{11} & A_{12} & A_{16} \\ A_{12} & A_{22} & A_{26} \\ A_{16} & A_{26} & A_{66} \end{bmatrix} \begin{Bmatrix} \dfrac{\partial u_0}{\partial x} \\ \dfrac{\partial v_0}{\partial y} \\ \dfrac{\partial u_0}{\partial y} + \dfrac{\partial v_0}{\partial x} \end{Bmatrix} + \begin{bmatrix} B_{11} & B_{12} & B_{16} \\ B_{12} & B_{22} & B_{26} \\ B_{16} & B_{26} & B_{66} \end{bmatrix} \begin{Bmatrix} -\dfrac{\partial^2 w_0}{\partial x^2} \\ -\dfrac{\partial^2 w_0}{\partial y^2} \\ -2\dfrac{\partial^2 w_0}{\partial x \partial y} \end{Bmatrix} \quad (2\text{-}75)$$

$$\begin{bmatrix} M_x \\ M_y \\ M_{xy} \end{bmatrix} = \begin{bmatrix} B_{11} & B_{12} & B_{16} \\ B_{12} & B_{22} & B_{26} \\ B_{16} & B_{26} & B_{66} \end{bmatrix} \begin{Bmatrix} \dfrac{\partial u_0}{\partial x} \\ \dfrac{\partial v_0}{\partial y} \\ \dfrac{\partial u_0}{\partial y} + \dfrac{\partial v_0}{\partial x} \end{Bmatrix} + \begin{bmatrix} D_{11} & D_{12} & D_{16} \\ D_{12} & D_{22} & D_{26} \\ D_{16} & D_{26} & D_{66} \end{bmatrix} \begin{Bmatrix} -\dfrac{\partial^2 w_0}{\partial x^2} \\ -\dfrac{\partial^2 w_0}{\partial y^2} \\ -2\dfrac{\partial^2 w_0}{\partial x \partial y} \end{Bmatrix} \quad (2\text{-}76)$$

Substituting equation (2-75) and (2-76) into the equation of motion of fiber-reinforced laminated plate (2-64) -(2-66), leads to the governing equations.

$$A_{11}\frac{\partial^2 u^0}{\partial x^2} + 2A_{16}\frac{\partial^2 u^0}{\partial x \partial y} + A_{66}\frac{\partial^2 u^0}{\partial y^2} + A_{16}\frac{\partial^2 v^0}{\partial x^2} + (A_{12} + A_{66})\frac{\partial^2 v^0}{\partial x \partial y} + A_{26}\frac{\partial^2 v^0}{\partial y^2} - B_{11}\frac{\partial^3 w^0}{\partial x^3} - 3B_{16}\frac{\partial^3 w^0}{\partial x^2 \partial y} - (B_{12} + 2B_{66})\frac{\partial^3 w^0}{\partial x \partial y^2} - B_{26}\frac{\partial^3 w^0}{\partial y^3} = I_0\frac{\partial^2 \delta u_0}{\partial t^2} \quad (2\text{-}77)$$

$$A_{16}\frac{\partial^2 u^0}{\partial x^2} + 2A_{26}\frac{\partial^2 v^0}{\partial x \partial y} + A_{26}\frac{\partial^2 u^0}{\partial y^2} + A_{66}\frac{\partial^2 v^0}{\partial x^2} + (A_{12} + A_{66})\frac{\partial^2 u^0}{\partial x \partial y} + A_{22}\frac{\partial^2 v^0}{\partial y^2} - B_{16}\frac{\partial^3 w^0}{\partial x^3} - 3B_{26}\frac{\partial^3 w^0}{\partial x \partial y^2} - (B_{12} + 2B_{66})\frac{\partial^3 w^0}{\partial x^2 \partial y} - B_{22}\frac{\partial^3 w^0}{\partial y^3} = I_0\frac{\partial^2 \delta v_0}{\partial t^2} \quad (2\text{-}78)$$

$$D_{11}\frac{\partial^4 w^0}{\partial x^4} + D_{22}\frac{\partial^4 w^0}{\partial y^4} + 2(D_{12} + D_{66})\frac{\partial^4 w^0}{\partial x^2 \partial y^2} + 4D_{16}\frac{\partial^4 w^0}{\partial x^3 \partial y} + 4D_{26}\frac{\partial^4 w^0}{\partial x \partial y^3}$$

$$-B_{11}\frac{\partial^3 u^0}{\partial x^3} - 3B_{16}\frac{\partial^3 u^0}{\partial x^2 \partial y} - (B_{12} + 2B_{66})\frac{\partial^3 u^0}{\partial x \partial y^2} - B_{26}\frac{\partial^3 u^0}{\partial y^3} - B_{16}\frac{\partial^3 v^0}{\partial x^3} - (B_{12} + 2B_{66})\frac{\partial^3 v^0}{\partial x^2 \partial y} - 3B_{26}\frac{\partial^3 v^0}{\partial x \partial y^2} - B_{22}\frac{\partial^3 v^0}{\partial y^3} = p(x,y) - I_0\frac{\partial^2 w_0}{\partial t^2} \quad (2\text{-}79)$$

Simplifications for governing equations of a symmetric fiber-reinforced laminate:

- For symmetrically laminated plates, the coupling stiffnesses B_{ij} are equal to zero. The governing equation is simplified by removing the bending extension coupling.
- The governing equations for in-plane deformation (2-77), (2-78) and governing equation for bending of symmetric laminates can be decoupled when the strain-displacement equations are linear.
- If there are no in-plane forces or displacements, the in-plane strain is zero, and the only equation to solve is the bending one (2-79).

Under these simplifications the governing equations are simplified as follows [2]:

$$-D_{11}\frac{\partial^4 w_0}{\partial x^4} - 2(D_{12} + 2D_{66})\frac{\partial^4 w_0}{\partial x^2 \partial y^2} - D_{22}\frac{\partial^4 w_0}{\partial y^4} - 4D_{16}\frac{\partial^4 w_0}{\partial x^3 \partial y} - 4D_{26}\frac{\partial^4 w_0}{\partial x \partial y^3} + p(x,y) = I_0\frac{\partial^2 w_0}{\partial t^2} \quad (2\text{-}80)$$

Presence of the bending-twisting coupling stiffnesses (D_{16}, D_{26}) prevent to obtain exact Navier solutions, so the solution of the governing equation is required to apply the Ritz or finite element approach. In the following sections, Ritz method will be applied to bending and free vibration problems.

CHAPTER 3

TRIGONOMETRIC SERIES SOLUTION OF FIBER-REINFORCED LAMINATED PLATES

3.1.1 Rayleigh Ritz Approach

The virtual displacements concept provides the equilibrium equations as Euler-Lagrange equations. These governing equations are differential equations, which can sometimes be challenging to solve analytically. These differential equations can be resolved using approximation techniques. Ritz [47] proposed a method for approximating the results. The Ritz method uses weak form of governing equation and minimum total potential energy principle, as well as variable expressions that are identical to the fundamental differential equations, as natural boundary conditions.

The basic ideas of the Ritz approach are described here using virtual displacements or minimum total potential energy principles. In the Ritz approach, the dependent unknown of a given problem is estimated using a finite linear combination of the u [2].

$$u \approx U_N = \sum_{j=1}^{N} c_j \varphi_j \qquad (3\text{-}1)$$

c_j will be determined that the principal of virtual displacement provide for the approximate solution which minimize the minimum total potential energy with respect to c_j.

In the above equation c_j is the undetermined parameters, and φ_j is approximating (shape) function which was selected to satisfy the geometric boundary conditions.

3.2 Static Bending and Stress of Fiber-Reinforced Laminated Plates with Rayleigh-Ritz Method

In static equilibrium, the total forces acting on the fiber-reinforced laminated plate is zero according to Newton's second law. Thus, total virtual work i.e. sum of internal and external works is zero for conservative system. In other words, the total virtual work done due to virtual displacement for a fiber-reinforced plate in equilibrium is zero. The idea behind this argument is called the theory of virtual displacement.

The concept of minimum total potential energy is a specific case of the principle of virtual displacements that applies to both linear and nonlinear elastic bodies [2]. The first variation of strain energy δU and variational work is done by externally applied force δV of fiber reinforced laminated plate expressed in equations (2-52) and (2-53).

The principle of minimum total potential energy of the fiber-reinforced plate can be expressed as [2]:

$$\delta\Pi = \delta U + \delta V = 0 \tag{3-2}$$

Substitute equations (2-52) and (2-53) into equation (3-2), it is found [2]:

$$0 = \int_0^a \int_0^b [N_x \delta {\varepsilon_x}^{(0)} + M_x \delta {\varepsilon_x}^{(1)} + N_y \delta {\varepsilon_y}^{(0)} + M_y \delta {\varepsilon_y}^{(1)} + N_{xy} \delta {\gamma_{xy}}^{(0)} + M_{xy} \delta {\gamma_{xy}}^{(1)} - p(x,y)\delta w_0]\, dxdy \tag{3-3}$$

Substitute equation (2-57) -(2-62) into the equation (3-3), it is obtained minimum potential energy principle with virtual displacements expressions [2]:

$$0 = \int_0^a \int_0^b [-(N_{x,x}+N_{xy,y})\delta u_0 - (N_{xy,x}+N_{y,y})\delta v_0 - (M_{x,xx} + 2M_{xy,xy} + M_{y,yy} + p(x,y))\delta w_0] dydx \tag{3-4}$$

Under assumptions of governing equation of the symmetrically laminated fiber-reinforced plate, equation (3-4) can be simplified as:

$$0 = \int_0^a \int_0^b -[(M_{x,xx} + 2M_{xy,xy} + M_{y,yy} + p(x,y))\delta w_0]dydx \quad (3\text{-}5)$$

Substitute equation (2-77) into the equation (3-5), it can be obtained [2]:

$$\int_0^a \int_0^b -[(-D_{11}\frac{\partial^4 w_0}{\partial x^4} - 2(D_{12} + 2D_{66})\frac{\partial^4 w_0}{\partial x^2 \partial y^2} - D_{22}\frac{\partial^4 w_0}{\partial y^4} - 4D_{16}\frac{\partial^4 w_0}{\partial x^3 \partial y} - 4D_{26}\frac{\partial^4 w_0}{\partial x \partial y^3} + p(x,y))\delta w_0]dxdy \quad (3\text{-}6)$$

Recall that weak form or virtual displacement form of partial differential equation can be expressed as:

$$\int \frac{\partial^2 u}{\partial x^2}\delta u dx = \int \frac{\partial u}{\partial x}\frac{\partial \delta u}{\partial x}dx \quad (3\text{-}7)$$

The weak or principle of virtual displacement forms of the equation (3-6) of the symmetrically laminated fiber-reinforced plate can be written with using principle of equation (3-7) as follows [2]:

$$\begin{aligned} 0 = \int_0^b \int_0^a \Bigg\{ & D_{11}\frac{\partial^2 w_0}{\partial x^2}\frac{\partial^2 \delta w_0}{\partial x^2} + D_{12}\left(\frac{\partial^2 w_0}{\partial y^2}\frac{\partial^2 \delta w_0}{\partial x^2} + \frac{\partial^2 w_0}{\partial x^2}\frac{\partial^2 \delta w_0}{\partial y^2}\right) \\ & + D_{22}\frac{\partial^2 w_0}{\partial y^2}\frac{\partial^2 \delta w_0}{\partial y^2} + 4D_{66}\frac{\partial^2 w_0}{\partial x \partial y}\frac{\partial^2 \delta w_0}{\partial x \partial y} \\ & + 2D_{16}\left(\frac{\partial^2 w_0}{\partial x \partial y}\frac{\partial^2 \delta w_0}{\partial x^2} + \frac{\partial^2 w_0}{\partial x^2}\frac{\partial^2 \delta w_0}{\partial x \partial y}\right) \\ & + 2D_{26}\left(\frac{\partial^2 w_0}{\partial x \partial y}\frac{\partial^2 \delta w_0}{\partial y^2} + \frac{\partial^2 w_0}{\partial y^2}\frac{\partial^2 \delta w_0}{\partial x \partial y}\right) \\ & - p(x,y)\delta w_0 \Bigg\} dxdy \end{aligned} \quad (3\text{-}8)$$

Static bending problems for different boundary conditions can be solved by using the Ritz method. The Ritz approach is based on variational statements, often called

the weak form, that is equivalent to the governing differential equations and the natural boundary conditions, such as those provided by the principle of virtual displacements or the minimum total potential energy.

Linear combination of displacement variable of symmetrically laminated fiber-reinforced plate can be expressed as:

$$w_0(x,y) \approx W_{MN}(x,y) = \sum_{i=1}^{M}\sum_{j=1}^{N} c_{ij}\varphi_{ij}(x,y) \tag{3-9}$$

$\varphi_{ij}(x,y)$ denotes the approximating or shape function of the fiber-reinforced plate and can be represented as:

$$\varphi_{ij}(x,y) = X_i(x)Y_j(y) \tag{3-10}$$

$X_i(x)$ and $Y_j(y)$ are the approximating (shape) functions which satisfy the geometric boundary conditions in *x* and *y* direction. Substituting equation (3-9) and (3-10) into the weak form of the static bending governing equation (3-8), it can be found [2]:

$$\begin{aligned}
0 = \sum_{i=1}^{M}\sum_{j=1}^{N}\Bigg\{ \int_0^b \int_0^a \Bigg[& D_{11}\frac{d^2X_i}{dx^2}Y_j\frac{d^2X_p}{dx^2}Y_q \\
& + D_{12}\left(X_i\frac{d^2Y_j}{dy^2}\frac{d^2X_p}{dx^2}Y_q + \frac{d^2X_i}{dx^2}Y_jX_p\frac{d^2Y_q}{dy^2}\right) \\
& + D_{22}X_i\frac{d^2Y_j}{dy^2}X_p\frac{d^2Y_q}{dy^2} + 4D_{66}\frac{dX_i}{dx}\frac{dY_j}{dy}\frac{dX_p}{dx}\frac{dY_q}{dy} \\
& + 2D_{16}\left(\frac{dX_i}{dx}\frac{dY_j}{dy}\frac{d^2X_p}{dx^2}Y_q + \frac{d^2X_i}{dx^2}Y_j\frac{dX_p}{dx}\frac{dY_q}{dy}\right) \\
& + 2D_{26}\left(\frac{dX_i}{dx}\frac{dY_j}{dy}X_p\frac{d^2Y_q}{dy^2}\right. \\
& \left. + X_i\frac{d^2Y_j}{dy^2}\frac{dX_p}{dx}\frac{dY_q}{dy}\right)\Bigg] dxdy\Bigg\} c_{ij} \\
& - \int_0^b \int_0^a p(x,y)X_pY_q dxdy
\end{aligned} \tag{3-11}$$

for $p = 1, 2, \dots, M$ and $q = 1, 2, \dots, N$. M and N are the order of Ritz series expansion of the admissible functions in x and y directions

Equation (3-11) can be used to solve bending problems when using appropriate shape functions which simulate the essential (geometric) boundary conditions. Equation (3-11) can be expressed as matrix form:

$$[H]_{ijpq}[c]_{ij} = [P]_{pq} \quad (3\text{-}12)$$

In order to solve the undetermined parameters c_{ij}, inverse of $[H]_{ijpq}$ matrix is multiplied with $[P]_{pq}$matrix as:

$$[c]_{ij} = [H]_{ijpq}{}^{-1}[P]_{pq} \quad (3\text{-}13)$$

In this study, three different boundary conditions have been used to obtain static bending and stress results of the fiber-reinforced laminated plate. These boundary conditions are simply-supported, clamped, and one free and three clamped edges. While obtaining these results, shape functions are used with the Ritz method. In order to use shape functions for boundary conditions, it is necessary to know the behavior of boundary conditions. Table 3-1 shows the behavior of different types of boundary conditions of the fiber-reinforced plate. In this table, M_x, M_y, and M_{xy} denotes the bending moment in x and y direction and twisting moment, respectively. Q_x and Q_y represents the shear forces. In-plane dimensions of fiber-reinforced plate are a and b in x and y direction.

Table 3-1. Conditions of edges of the laminated fiber-reinforced plate [31] [37]

BCs	Edges	Boundary Equations	
Simply-Supported	$x = 0$	$w_0(0,y) = 0,$	$M_x(0,y) = 0$
	$x = a$	$w_0(a,y) = 0,$	$M_x(a,y) = 0$
	$y = 0$	$w_0(x,0) = 0,$	$M_y(x,0) = 0$
	$y = b$	$w_0(x,b) = 0,$	$M_y(x,b) = 0$
Clamped	$x = 0$	$w_0(0,y) = 0,$	$\frac{dw_0(0,y)}{dx} = 0$
	$x = a$	$w_0(a,y) = 0,$	$\frac{dw_0(a,y)}{dx} = 0$
	$y = 0$	$w_0(x,0) = 0,$	$\frac{dw_0(x,0)}{dy} = 0$
	$y = b$	$w_0(x,b) = 0,$	$\frac{dw_0(x,b)}{dy} = 0$
Free	$x = 0$	$M_x(0,y) = 0,$	$\frac{dM_{xy}(0,y)}{dx} + Q_x = 0$
	$x = a$	$M_x(a,y) = 0,$	$\frac{dM_{xy}(a,y)}{dx} + Q_x = 0$
	$y = 0$	$M_y(x,0) = 0,$	$\frac{dM_{xy}(x,0)}{dx} + Q_y = 0$
	$y = b$	$M_y(x,b) = 0,$	$\frac{dM_{xy}(x,b)}{dx} + Q_y = 0$

New trigonometric shape functions have been developed in accordance with the behavior of the boundary conditions given in Table 3-1. These functions are used in trigonometric series expansion Ritz solution for different boundary conditions to solve the bending problems. The shape functions to be used are provided in Table 3-2. In this table, S-S-S-S, C-C-C-C, and C-F-C-C represents simply-supported, clamped, and single free- three clamped plate.

Table 3-2. New Trigonometric shape functions used in bending problems

Shape Function	Boundary Conditions		
	S-S-S-S	C-C-C-C	C-F-C-C
$\varphi_{ij}(x,y)$	$\sin\frac{i\pi x}{a}\sin\frac{j\pi y}{b}$	$\sin\frac{\pi x}{a}\sin\frac{i\pi x}{a}\sin\frac{\pi y}{b}\sin\frac{j\pi y}{b}$	$(1-\cos\left(\frac{(2i-1)\pi}{2a}x\right)\sin\frac{\pi y}{b}\sin\frac{j\pi y}{b}$

These trigonometric shape functions are substituted into the Ritz series expansion equation (3-9). Then, this series expansion equation is used in conjunction with weak form of the bending governing equation to solve c_{ij}. After finding these parameters, transverse deflection $w_0(x,y)$ can be calculated. This procedure is integrated into the math package MATLAB.

Equation (2-21) is used when calculating the transverse stresses of the *kth* layer of fiber-reinforced plates. Substitute strain-displacement relation equation (2-7) into the equation (2-21) and neglect the in-plane deformations because of symmetrically laminated fiber-reinforced assumptions, it is obtained:

$$\begin{Bmatrix}\sigma_{xx}\\ \sigma_{yy}\\ \sigma_{xy}\end{Bmatrix}^k = -z\begin{bmatrix}\bar{Q}_{11} & \bar{Q}_{12} & \bar{Q}_{16}\\ \bar{Q}_{12} & \bar{Q}_{22} & \bar{Q}_{26}\\ \bar{Q}_{16} & \bar{Q}_{26} & \bar{Q}_{66}\end{bmatrix}^k \begin{Bmatrix}\frac{\partial^2 w_0}{\partial x^2}\\ \frac{\partial^2 w_0}{\partial y^2}\\ 2\frac{\partial^2 w_0}{\partial x\partial y}\end{Bmatrix} \quad (3\text{-}14)$$

In order to calculate transverse stresses of fiber-reinforced plate with Ritz method, substitute equation (3-9) into the equation (3-14), transverse stresses with shape functions are given by:

$$\begin{Bmatrix}\sigma_{xx}\\ \sigma_{yy}\\ \sigma_{xy}\end{Bmatrix}^k = \sum_{i=1}^{N} -z\begin{bmatrix}\bar{Q}_{11} & \bar{Q}_{12} & \bar{Q}_{16}\\ \bar{Q}_{12} & \bar{Q}_{22} & \bar{Q}_{26}\\ \bar{Q}_{16} & \bar{Q}_{26} & \bar{Q}_{66}\end{bmatrix}^k \begin{Bmatrix}\frac{\partial^2 \varphi_{ij}}{\partial x^2}\\ \frac{\partial^2 \varphi_{ij}}{\partial y^2}\\ 2\frac{\partial^2 \varphi_{ij}}{\partial x\partial y}\end{Bmatrix} c_{ij} \quad (3\text{-}15)$$

Finally, normal and shear stresses of plies can be calculated since c_{ij} are determined for different boundary conditions at previous part. ${\sigma_{xx}}^k$, ${\sigma_{yy}}^k$, and ${\sigma_{xy}}^k$ of kth layer can be expressed as:

$$ {\sigma_{xx}}^k = \sum_{i=1}^{N} -z \left[\bar{Q}_{11} \times \frac{\partial^2 \varphi_{ij}}{\partial x^2} + \bar{Q}_{12} \times \frac{\partial^2 \varphi_{ij}}{\partial y^2} + \bar{Q}_{16} \times 2 \frac{\partial^2 \varphi_{ij}}{\partial x \partial y} \right] c_{ij} \qquad (3\text{-}16) $$

$$ {\sigma_{yy}}^k = \sum_{i=1}^{N} -z \left[\bar{Q}_{12} \times \frac{\partial^2 \varphi_{ij}}{\partial x^2} + \bar{Q}_{22} \times \frac{\partial^2 \varphi_{ij}}{\partial y^2} + \bar{Q}_{26} \times 2 \frac{\partial^2 \varphi_{ij}}{\partial x \partial y} \right] c_{ij} \qquad (3\text{-}17) $$

$$ {\sigma_{xy}}^k = \sum_{i=1}^{N} -z \left[\bar{Q}_{16} \times \frac{\partial^2 \varphi_{ij}}{\partial x^2} + \bar{Q}_{26} \times \frac{\partial^2 \varphi_{ij}}{\partial y^2} + \bar{Q}_{66} \times 2 \frac{\partial^2 \varphi_{ij}}{\partial x \partial y} \right] c_{ij} \qquad (3\text{-}18) $$

Substituting the undetermined parameters c_{ij} and shape functions φ_{ij} which is taken from Table 3-2, transverse stresses are calculated. This procedure is integrated into the math package MATLAB.

3.3 Free Vibration of Fiber-Reinforced Plates with Rayleigh-Ritz Eigenvalue Formulation

A thin, symmetrically laminated rectangular fiber-reinforced plate made of fiber composite that is in the *x-y* plane and is limited $0 < x < a$ and $0 < x < b$ is shown in Fig.3-1. Plies are orthotropic that are bonded to one another by a matrix material to give it thickness *h* in the *z* direction. The number of plies is *n*, according to Fig. 3-1, the baseline plane $z = 0$ is the mid-plane. The angle θ denotes the fiber direction within a layer. E_{11} and E_{22} are the Young modulus for layers that are parallel and perpendicular to the fibers.

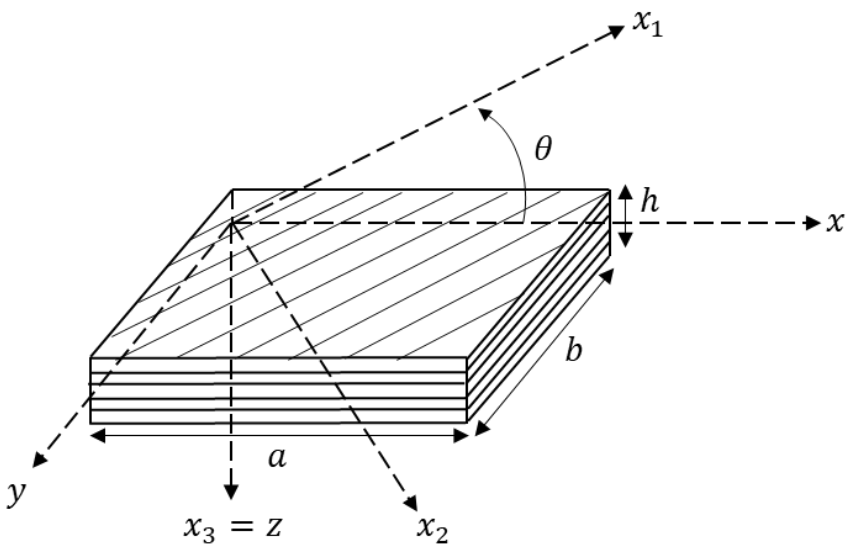

Figure 3-1. Representation of laminated fiber-reinforced plate

In this problem, the layers are set up in a way that creates a mid-plane symmetry. This technique eliminates transverse bending and in-plane stretching, as mentioned before. The natural frequencies and mode shapes of these problems can be solved by using the Rayleigh-Ritz method and approximate trigonometric series shape functions. Minimization of energy function ($\mathcal{R}$) which is defined as total vibration energy is used to calculate natural frequencies and mode shapes of fiber-reinforced plate [30] [32] [42].

Energy function of fiber-reinforced plate can be expressed as follows [42]:

$$\mathcal{R} = U_{max} - T_{max} \qquad (3\text{-}19)$$

Where U_{max} is the maximum strain energy of fiber-reinforced plate due to the bending and T_{max} is the maximum kinetic energy as a result of the mass of fiber-reinforced plate.

Strain energy of the fiber-reinforced plate can be written by simplifying the virtual potential energy equation (3-6) by removing the external work and virtual displacement term [36] [37]:

$$U_{max} = \frac{1}{2}\int_0^a \int_0^b \left\{ D_{11}\left[\frac{\partial^2 w_0}{\partial x^2}\right]^2 + D_{12}\left[\frac{\partial^2 w_0}{\partial x^2}\frac{\partial^2 w_0}{\partial y^2}\right] + D_{22}\left[\frac{\partial^2 w_0}{\partial y^2}\right]^2 + 4D_{16}\left[\frac{\partial^2 w_0}{\partial x^2}\frac{\partial^2 w_0}{\partial x \partial y}\right] + 4D_{26}\left[\frac{\partial^2 w_0}{\partial y^2}\frac{\partial^2 w_0}{\partial x \partial y}\right] + 4D_{66}\left[\frac{\partial^2 w_0}{\partial x \partial y}\right]^2 \right\} dxdy \quad (3\text{-}20)$$

Kinetic energy of the fiber-reinforced plate can be written by simplifying the virtual kinetic energy equation (2-50) by removing virtual displacement term as follows [2]:

$$T_{max} = \frac{1}{2}\int\int\int \rho_0 \frac{\partial^2 w}{\partial t^2} dv = \frac{1}{2}\int\int\int \rho_0 \frac{\partial w}{\partial t}\frac{\partial \delta w}{\partial t} dv \quad (3\text{-}21)$$

Here, ρ_0 is the mass per unit volume of the fiber-reinforced plate and *w* denotes the displacement term in the free vibration problems. Displacement function can be expressed as:

$$w(x, y, z) = w_0(x, y)e^{i\omega t} \quad (3\text{-}22)$$

Substitute the equation (3-22) into the equation (3-21) and integrate through the thickness of the fiber-reinforced plate, we obtain [36]:

$$T_{max} = \frac{1}{2}\rho_0 h\omega^2 \iint {w_0}^2(x, y)dxdy \quad (3\text{-}23)$$

Where ω denotes the natural frequency of fiber-reinforced plate.

In order to solve the free vibration problem of the fiber-reinforced plate, an eigenvalue equation will be developed using equation (3-19). To write the eigenvalue equation, in-plane dimensions of the plate can be normalized. For normalization of in plane dimensions, letting $\xi = x/a$ and $\eta = y/b$. So, the linear combination of displacement variable of symmetrically laminated fiber-reinforced plate can be expressed with using equation (3-9) as [36]:

$$w_0(\xi, \eta) = \sum_{i=1}^{M} \sum_{j=1}^{N} c_{ij}\varphi_{ij}(\xi, \eta) \quad (3\text{-}24)$$

Where c_{ij} is the undetermined coefficient, M and N are the order of Ritz series expansion of the admissible functions in x and y directions. $\varphi_{ij}(x,y)$ denotes the approximating or shape function that represent boundary condition of the fiber-reinforced plate and can be represented as:

$$\varphi_{ij}(\xi,\eta) = X_i(\xi)Y_j(\eta) \qquad (3\text{-}25)$$

In trigonometric series solution, Ritz series deformation expansion equation (3-22) is substituted into the maximum strain energy equation (3-20) and maximum kinetic energy equation (3-23), we find U_{max} and T_{max} as follows:

$$\begin{aligned}
&U_{max}\\
&= \frac{1}{2}\int_0^a\int_0^b \left\{ \frac{D_{11}}{a^4}\left[\frac{\partial^2 \sum_{i=1}^{M}\sum_{j=1}^{N} c_{ij}\phi_{ij}(\xi,\eta)}{\partial\xi^2}\right]^2 \right.\\
&+ \frac{D_{12}}{a^2b^2}\left[\frac{\partial^2 \sum_{i=1}^{M}\sum_{j=1}^{N} c_{ij}\phi_{ij}(\xi,\eta)}{\partial\xi^2} x \frac{\partial^2 \sum_{i=1}^{M}\sum_{j=1}^{N} c_{ij}\phi_{ij}(\xi,\eta)}{\partial\eta^2}\right]\\
&+ \frac{D_{22}}{b^4}\left[\frac{\partial^2 \sum_{i=1}^{M}\sum_{j=1}^{N} c_{ij}\phi_{ij}(\xi,\eta)}{\partial\eta^2}\right]^2\\
&+ \frac{4D_{16}}{a^3b}\left[\frac{\partial^2 \sum_{i=1}^{M}\sum_{j=1}^{N} c_{ij}\phi_{ij}(\xi,\eta)}{\partial\xi^2} x \frac{\partial^2 \sum_{i=1}^{M}\sum_{j=1}^{N} c_{ij}\phi_{ij}(\xi,\eta)}{\partial\xi\partial\eta}\right]\\
&+ 4\frac{D_{26}}{ab^3}\left[\frac{\partial^2 \sum_{i=1}^{M}\sum_{j=1}^{N} c_{ij}\phi_{ij}(\xi,\eta)}{\partial\eta^2} x \frac{\partial^2 \sum_{i=1}^{M}\sum_{j=1}^{N} c_{ij}\phi_{ij}(\xi,\eta)}{\partial\xi\partial\eta}\right]\\
&\left.+ 4\frac{D_{66}}{a^2b^2}\left[\frac{\partial^2 \sum_{i=1}^{M}\sum_{j=1}^{N} c_{ij}\phi_{ij}(\xi,\eta)}{\partial\xi\partial\eta}\right]^2 \right\} d\xi d\eta
\end{aligned} \qquad (3\text{-}26)$$

$$T_{max} = \frac{1}{2}\rho h\omega^2 \int_0^a\int_0^b \left(\sum_{i=1}^{M}\sum_{j=1}^{N} c_{ij}\varphi_{ij}(\xi,\eta)\right)^2 d\xi d\eta \qquad (3\text{-}27)$$

To minimize the energy function ($\mathcal{R} = U_{max} - T_{max}$) equation (3-19) with respect to undetermined coefficient c_{ij}, we write [36]:

$$\frac{\partial}{\partial c_{ij}}(U_{max} - T_{max}) = 0 \qquad (3\text{-}28)$$

which leads to the eigenvalue equation:

$$\left([K_{ijmn}] - \lambda^2[M_{ijmn}]\right)\{c_{ij}\} = \{0\} \qquad (3\text{-}29)$$

The matrix $[K_{ijmn}]$ denotes the symmetric stiffness matrix, while the matrix $[M_{ijmn}]$ indicates the diagonal mass matrix. The unknown coefficients c_{ij} are used to define a set of $i \times j$ homogeneous linear equations that can be solved simultaneously. These equations are called eigenvalue equations. The determinant of the coefficient matrix of equation (3-29) is set to zero in order to solve the eigenvalue problem. There are $i \times j$ values of λ that satisfy the eigenvalue equation.

$[K_{ijmn}]$ stiffness and $[M_{ijmn}]$ mass matrices in equation (3-29) can be written as follows [36]:

$$\begin{aligned}[K_{ijmn}] = \Bigg[& \frac{D_{11}P^{22}{}_{im}Q^{00}{}_{jn}}{\alpha^2} + 4D_{66}P^{11}{}_{im}Q^{11}{}_{jn} \\ & + D_{22}\alpha^2 P^{00}{}_{im}Q^{22}{}_{jn} \\ & + D_{12}\left(P^{02}{}_{im}Q^{20}{}_{jn} + P^{20}{}_{im}Q^{02}{}_{jn}\right) \\ & + \frac{2D_{16}\left(P^{12}{}_{im}Q^{10}{}_{jn} + P^{21}{}_{im}Q^{01}{}_{jn}\right)}{\alpha} \\ & + 2D_{26}\alpha(P^{10}{}_{im}Q^{12}{}_{jn} + P^{01}{}_{im}Q^{21}{}_{jn})\Bigg]/D_0 \end{aligned} \qquad (3\text{-}30)$$

$$[M_{ijmn}] = P^{00}{}_{im}Q^{00}{}_{jn} \qquad (3\text{-}31)$$

$i, m = 1, 2, 3, \dots, M$

$j, n = 1, 2, 3, \dots, N$

λ is the nondimensional eigenfrequency parameter and it can be written as:

$$\lambda = \omega ab\sqrt{\rho_0 h/D_0} \quad (3\text{-}32)$$

D_0 and α are parameters used to develop the eigenvalue equation. D_0 is called bending stiffness parameter and represents with Young's modulus E_{11} and Poisson's ratios v_{12} and v_{21}. α is a ratio of in-plane dimensions of fiber-reinforced plate. D_0 and α are expressed as follows:

$$D_0 = \frac{E_{11}h^3}{12(1 - v_{12}v_{21})} \quad (3\text{-}33)$$

$$\alpha = a/b \quad (3\text{-}34)$$

The form of unknown coefficients used in the eigenvalue solution of the equation (3-29) is written as:

$$\{c_{ij}\} = [c_{11}, c_{12}, \dots, c_{1N}, c_{21}, c_{22}, \dots, c_{2N}, c_{M1}, c_{M2}, \dots, c_{MN}]^T \quad (3\text{-}35)$$

When the eigenvalues λ are substituted back into the equation (3-29), the eigenvector components c_{ij} corresponding to eigenvalues are calculated. Then, substituting these eigenvectors into the equation (3-24) gives mode shapes of the fiber-reinforced laminated plate.

$[K_{ijmn}]$ and $[M_{ijmn}]$ in equations (3-30) and (3-31) have integral expressions with shape functions [36]. These integrals can be expressed as follows [36]:

$$P^{rs}{}_{im} = \int_0^1 \frac{d^r X_i}{d\xi^r}\frac{d^s X_m}{d\xi^s}\,d\xi \quad (3\text{-}36)$$

$$Q^{rs}{}_{jn} = \int_0^1 \frac{d^r Y_j}{d\eta^r}\frac{d^s Y_n}{d\eta^s}\,d\eta \quad (3\text{-}37)$$

$r, s = 0, 1, 2$

X_i and Y_j are the components of $\varphi_{ij}(\xi, \eta)$ in *x* and *y* direction. $\varphi_{ij}(\xi, \eta)$ is the shape function that satisfies the boundary conditions. These functions are used in Ritz solution for different boundary conditions. In this study, new trigonometric shape

functions are developed for solving the free vibration problems of the fiber-reinforced plate. These trigonometric shape functions are provided in Table 3-3.

Table 3-3. New Trigonometric shape functions used in free vibration problems

Shape Function	Boundary Conditions		
	S-S-S-S	C-C-C-C	C-F-C-C
$\varphi_{ij}(\xi,\eta)$	$\sin i\pi\xi \sin j\pi\eta$	$\sin \pi\xi \sin i\pi\xi \sin \pi\eta \sin j\pi\eta$	$(1-\cos\left(\frac{(2i-1)\pi}{2}\xi\right))\sin \pi\eta \sin j\pi\eta$

Trigonometric shape functions are substituted into the Ritz series expansion equation. Then, this series expansion equation is used in conjunction with the minimization of the energy function, which leads to the eigenvalue equation. After finding the eigenvalues and eigenvectors of this equation, the natural frequencies and mode shapes of the fiber-reinforced plate can be calculated. This procedure is integrated into the math package MATLAB.

CHAPTER 4

NUMERICAL RESULTS

4.1 Finite Element Model with ANSYS

The finite element method is used to validate numerical results obtained from the analytical solution using the new trigonometric series shape functions. ANSYS is utilized to perform finite element analysis.

The ANSYS program's ACP (Pre) module is used to set up the analysis model, as seen in Figure 4-1. This module is a component system used for composites. In this module, the properties of the composite material used in the problem are first defined in the engineering data tab. Then, the problem's geometry is drawn to perform a two-dimensional analysis. The dimensions of the problem geometry are defined. The ACP setup is used to construct the lamination scheme and problem coordinates.

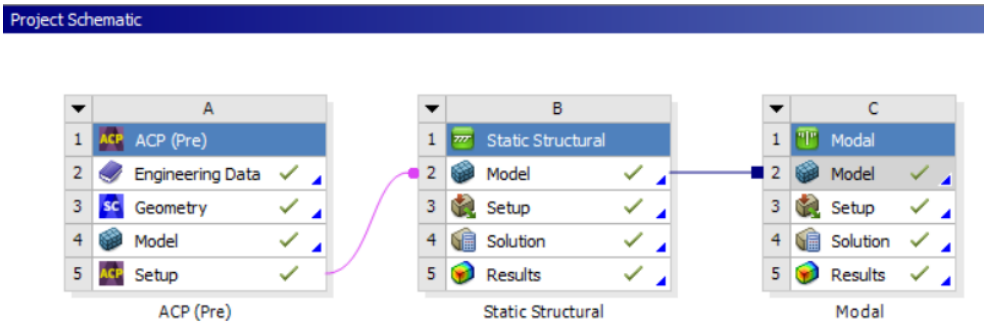

Figure 4-1. ANSYS project schema of static bending and free vibration problem of fiber-reinforced plate

The mesh structure required for a numerical solution is defined in ANSYS. While defining this mesh structure, the element order and size are chosen to be linear and 5 mm by 5 mm. The SHELL181 element is used for the mesh element type as seen in Figure 4-2. This element type is suitable for analyzing thin composite plates. An element has four nodes, and these nodes have six degrees of freedom: translation and

rotation around the *x*, *y*, and *z* axes. The SHELL181 element is suitable for linear and large rotation applications. Used in the analysis of composite shells or sandwich structures, the accuracy of this element is governed by the first-order shear deformation theory. Figure 4-3 shows the mesh model of the analysis model. There are 1600 elements and 1681 nodes in the FEM model.

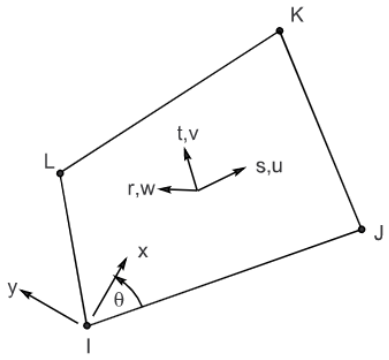

Figure 4-2. SHELL181 element geometry

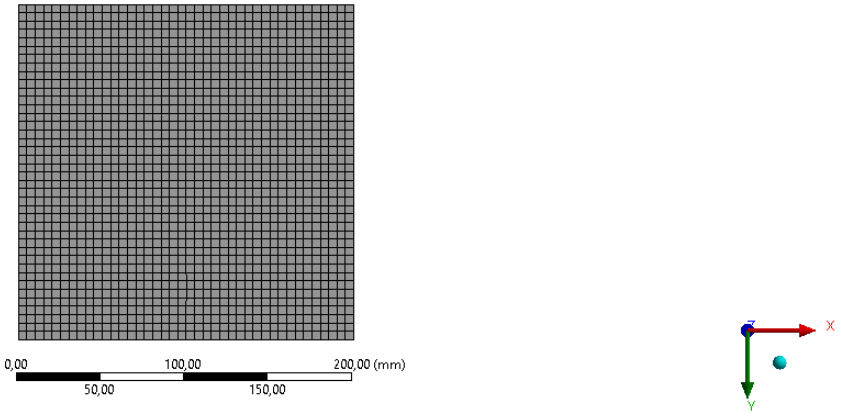

Figure 4-3. Mesh model of fiber-reinforced plate in ANSYS

Later, static structural and modal software is added to the ACP (Pre) to solve the static bending and free vibration problems. To solve these problems, the boundary conditions of the composite plate are defined. These boundary conditions seen in Figure 4-4 are defined as simply supported, clamped, and three edges clamped with one edge free, respectively, by the problem definition.

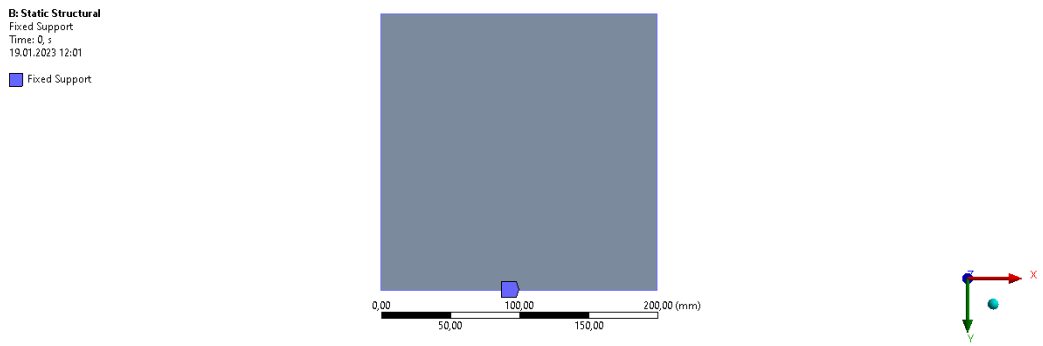

Figure 4-4. Example of clamped boundary conditions in ANSYS

The Figure 4-5 shows the distributed pressure given in the problem description is applied to the composite plate.

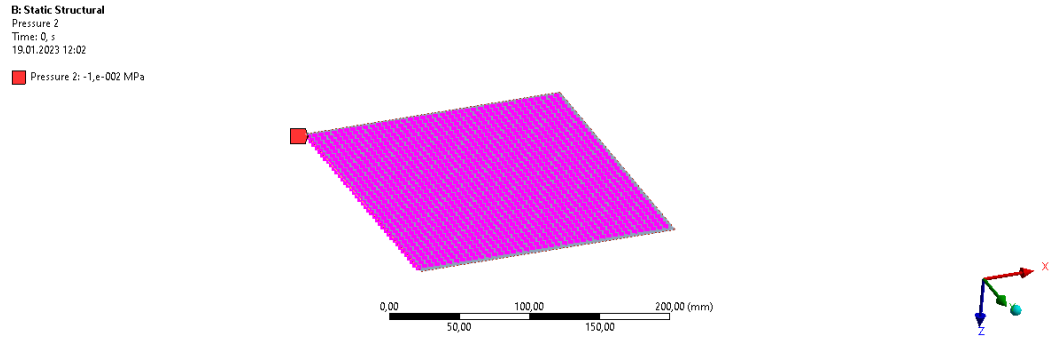

Figure 4-5. Distributed pressure of composite plate in ANSYS

After all the necessary definitions for the numerical solution were made, the static bending and free vibration solutions were solved using the ANSYS.

4.2 Static Bending Analysis

In this section, the static analysis of fiber-reinforced laminated plate has been determined using trigonometric series solution (TSS) for three different boundary conditions. For these boundary conditions, newly developed trigonometric shape functions are used. Firstly, the deformation values of fiber-reinforced laminated plates with three different boundary conditions are found under uniformly distributed load. Then, the transverse stress values of each layer of these plates are obtained

under this load. The results calculated by the trigonometric series solution method are verified by the finite element method described in the previous section.

Material and geometric properties of fiber-reinforced laminated plate are given in Table 4-1 and Table 4-2 while validating the static bending analytical solutions.

Table 4-1.Material properties of T300-934 carbon/epoxy for static bending analysis [49]

Name	Material Property	Value	Unit
Longitudinal Young Modulus	E_{11}	148×10^9	$\mathrm{N/m^2}$
Transverse Young Modulus	E_{22}	9.65×10^9	$\mathrm{N/m^2}$
In-plane Shear Modulus	G_{12}	4.55×10^9	$\mathrm{N/m^2}$
In-plane Poisson Ratio	ν_{12}	0.30	-
Thickness of Lamina	t	0.2×10^{-3}	m

Table 4-2. Geometric properties [49]

Name	Geometric Parameter	Value	Unit
X axis Dimension	a	0.2	m
Y axis Dimension	b	0.2	m
Uniform Load	q	10000	$\mathrm{N/m^2}$
Number of Plies	n	16	-

Using the material and geometric properties of the fiber-reinforced plate given in Table 4-1 and Table 4-2, a stacking sequence is built to compare it with the finite element method. This stacking sequence is $[0_2/-45_2/45_2/90_2]_s$. The number of plies are 16 in this lamination scheme, and plies are laminated symmetrically in the

mid-plane of the fiber-reinforced plate. The problem geometry used in validation is given in Figure 4-6.

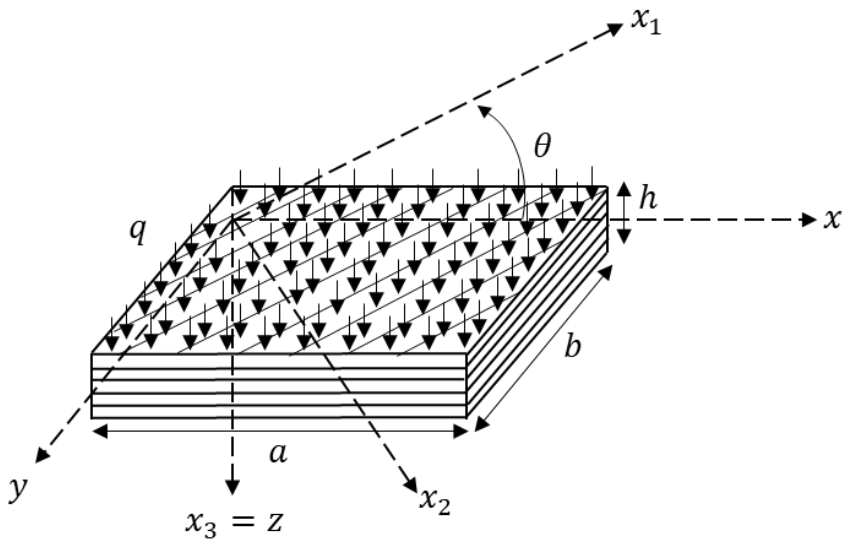

Figure 4-6. Bending problem geometry of fiber-reinforced $[0_2/-45_2/45_2/90_2]_s$ laminated plate

4.2.1 Analysis for a Simply-Supported Plate

Deformations of the fiber-reinforced laminated plate, whose material and geometric properties are taken from Table 4-1 and Table 4-2, under uniformly distributed lateral load, have been determined by trigonometric series shape functions. In the trigonometric series solution (TSS), a convergence study is performed for a simply-supported plate by increasing the *M* and *N* orders of the Ritz solution. The results of the convergence study using the trigonometric series solution are shown in Table 4-3, along with the maximum static bending of the simply supported plate. When all edges are simply supported, the trigonometric shape function, $\sin(\frac{i\pi}{a}x)\sin(\frac{j\pi}{b}y)$, is used in the Rayleigh-Ritz method solution. Validation has been done using the finite element analysis program ANSYS and the trigonometric series approach with M=12 and N=12 given in Table 4-4.

Table 4-3. Convergence study of maximum deflection for a simply-supported fiber-reinforced $[0_2/-45_2/45_2/90_2]_s$ laminated plate with $q = 0.01$ MPa, $a/b = 1$, $h/a = 0.016$ at $x = a/2$ and $y = b/2$ using trigonometric series solution

Number of Series $(M \times N)$	Maximum Deflection (mm) $w_0(a/2, b/2)$
2×2	0.41473
4×4	0.41596
6×6	0.41607
8×8	0.41609
10×10	0.41610
12×12	0.41611

Table 4-4.Maximum deflection of fiber-reinforced simply supported plate with $q = 0.01\ MPa,\ a/b = 1,\ h/a = 0.016$ at $x = a/2\ and\ y = b/2$ using trigonometric series solution with *M*=12 and *N*=12 and ANSYS

Solution Type	Maximum Deflection (mm) $w_0(a/2, b/2)$	Difference %
TSS	0.41611	0.24
ANSYS	0.41783	

Figure 4-7 shows the distribution of deformation results of the simply supported plate using trigonometric series solution. While obtaining the distribution of deformation, order of trigonometric series *M* and *N* are taken 12 in Figure 4-7.

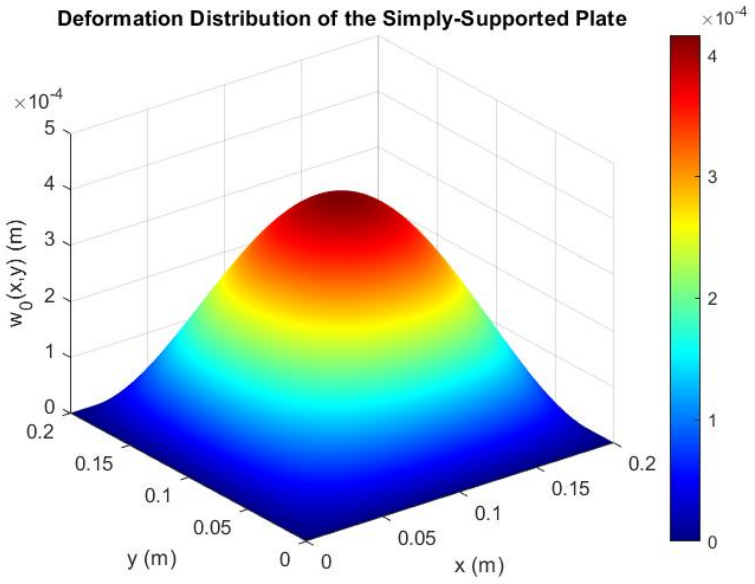

Figure 4-7. Distribution of deformation of the simply supported fiber-reinforced $[0_2/-45_2/45_2/90_2]_s$ laminated plate with $q = 0.01$ MPa, $a/b = 1$, $h/a = 0.016$ using the trigonometric series solution with M=12 and N=12

The deformation distribution of the simply supported plate modeled with the finite element program is given in Figure 4-8. In this figure, the ACP module of ANSYS is used. The edges of the fiber-reinforced plate are modeled as simply supported. The number of elements is 1600. The SHELL181 element is used in the model.

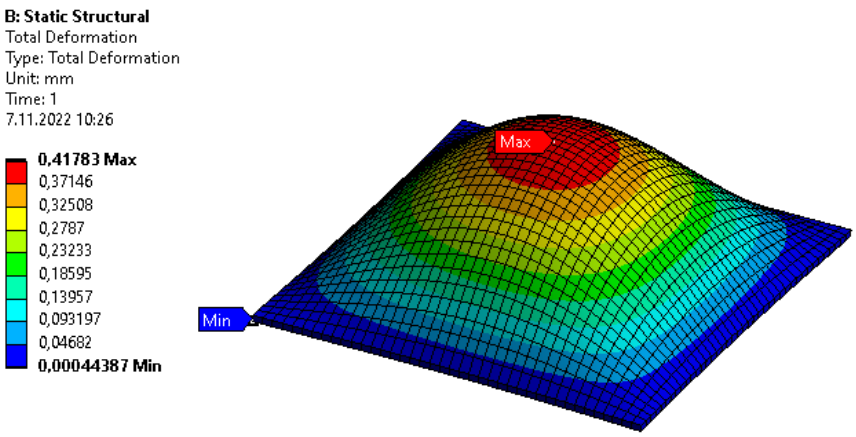

Figure 4-8. Distribution of deformation of the simply supported fiber-reinforced $[0_2/-45_2/45_2/90_2]_s$ laminated plate with $q = 0.01$ MPa, $a/b = 1$, $h/a = 0.016$ using ANSYS

Validation of a simply supported fiber-reinforced plate has also been done at $y = b/2$ and along the *x* axis with using the trigonometric series solution and ANSYS. Using the results seen in Figures 4-7 and 4-8, the deformation comparison plot along with the *x* axis is given in Figure 4-9. The results are very close to each other.

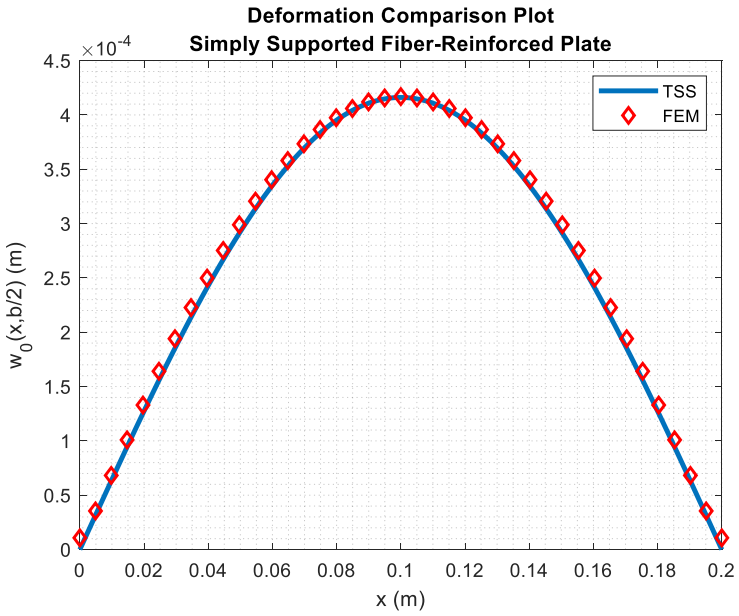

Figure 4-9. Deformation comparison plot of the fiber-reinforced $[0_2/-45_2/45_2/90_2]_s$ laminated simply-supported plate with $q = 0.01$ MPa, $a/b = 1, h/a = 0.016$ between results of trigonometric series solution and ANSYS at along with *x* axis and $y = b/2$

4.2.2 Analysis for a Clamped Plate

The same loading condition, material and geometric properties are used for a fiber-reinforced laminated plate given in the previous section. Still the analysis is done by changing the boundary conditions. Trigonometric series solution and finite element analysis are used to obtain deformation results. In the trigonometric series solution (TSS), a convergence study is performed for a clamped plate by increasing the *M* and *N* orders of the Ritz solution. The results of the convergence study using the trigonometric series solution are shown in Table 4-5, along with the maximum static bending of the clamped plate. When all edges are clamped, the trigonometric shape function, $\sin\left(\frac{i\pi}{a}x\right)\sin\left(\frac{\pi}{a}x\right)\sin\left(\frac{j\pi}{b}y\right)\sin\left(\frac{\pi}{b}y\right)$, is used in the Rayleigh-Ritz method solution. Validation has been done using the finite element analysis program ANSYS and the trigonometric series solution with *M*=12 and *N*=12 given in Table 4-6.

Table 4-5. Convergence study of maximum deflection for a fiber-reinforced $[0_2/-45_2/45_2/90_2]_s$ laminated clamped plate with $q = 0.01$ MPa, $a/b = 1$, $h/a = 0.016$ at $x = a/2$ and $y = b/2$ using trigonometric series solution

Number of Series $(M \times N)$	Maximum Deflection (mm) $w_0(a/2, b/2)$
2×2	0.12377
4×4	0.11535
6×6	0.11741
8×8	0.11884
10×10	0.11939
12×12	0.11942

Table 4-6. Maximum deflection of fiber-reinforced $[0_2/-45_2/45_2/90_2]_s$ laminated clamped plate with $q = 0.01$ MPa, $a/b = 1$, $h/a = 0.016$ at $x = a/2$ and $y = b/2$ using trigonometric series solution with *M*=12 and *N*=12 and ANSYS

Solution Type	Maximum Deflection (mm) $w_0(a/2, b/2)$	Difference %
TSS	0.11942	1.28
ANSYS	0.12097	

The distribution of deformation results of the clamped plate using trigonometric series solution is given in Figure 4-10. Order of trigonometric series *M* and *N* are taken 12 in obtaining the distribution of deformation.

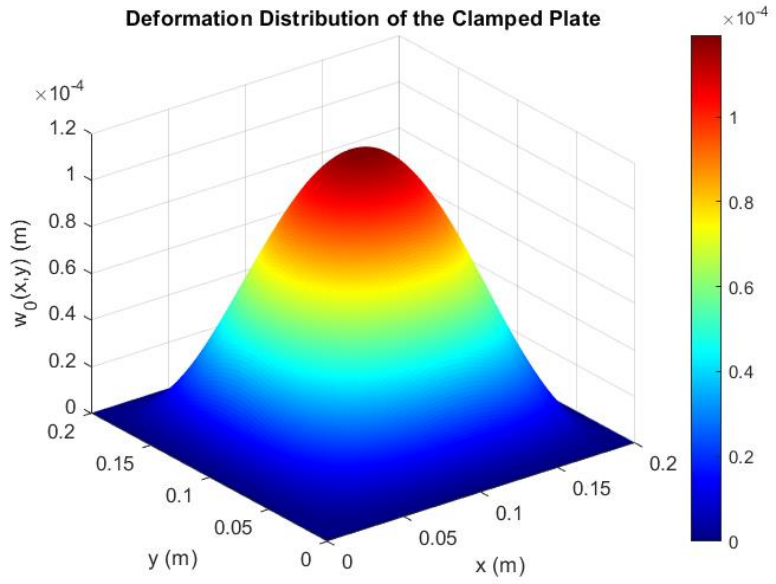

Figure 4-10. Distribution of deformation of the fiber-reinforced $[0_2/-45_2/45_2/90_2]_s$ laminated clamped plate with $q = 0.01$ MPa, $a/b = 1$, $h/a = 0.016$ using the trigonometric series solution with M=12 and N=12

The deformation distribution of the clamped plate modeled with the finite element program is given in Figure 4-11. In this figure, the ACP module of ANSYS is used. The edges of the fiber-reinforced plate are modeled as clamped.

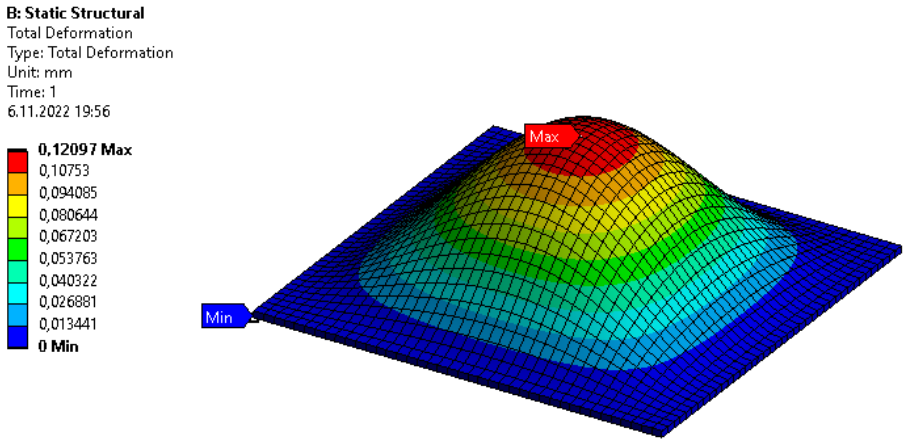

Figure 4-11. Distribution of deformation of the fiber-reinforced $[0_2/-45_2/45_2/90_2]_s$ laminated clamped plate with $q = 0.01$ MPa, $a/b = 1$, $h/a = 0.016$ using ANSYS

Deformations of the clamped fiber-reinforced plate at $y = b/2$ and along the *x* axis are compared with using the trigonometric series approach and ANSYS, as seen in Figure 4-12. The trigonometric series solution gave close results as FEM.

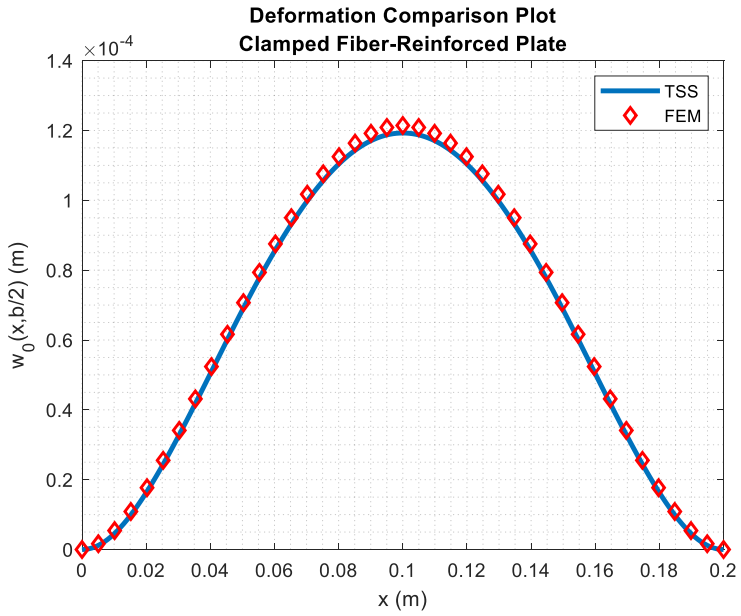

Figure 4-12. Deformation comparison plot of the fiber-reinforced $[0_2/-45_2/45_2/90_2]_s$ laminated clamped plate with $q = 0.01$ MPa, $a/b = 1$, $h/a = 0.016$ between results of trigonometric series solution and ANSYS at along with *x* axis and $y = b/2$

4.2.3 Analysis for a Single Free Edge and Three Clamped Edges

Deformations of the fiber-reinforced plate under the same load condition, material and geometric properties as in the previous two parts have been calculated for a single free and three clamped boundary conditions with the trigonometric series solution and finite element analysis. In the trigonometric series solution (TSS), a convergence study is performed for a single free and three-clamped plate by increasing the *M* and *N* orders of the Ritz solution. The results of the convergence study using the trigonometric series solution are shown in Table 4–7. When a fiber-reinforced plate has these boundary conditions, the trigonometric shape function, $(1-\cos\left(\frac{(2i-1)\pi}{2a}x\right))\sin\left(\frac{j\pi}{b}y\right)\sin\left(\frac{\pi}{b}y\right)$, is used in the Rayleigh-Ritz method solution. Validation has been done using the finite element analysis program ANSYS and the trigonometric series solution with M=12 and N=12 given in Table 4-8.

Table 4-7. Convergence study of maximum deflection for a fiber-reinforced $[0_2/-45_2/45_2/90_2]_s$ laminated single free and three clamped plate with $q = 0.01$ MPa, $a/b = 1$, $h/a = 0.016$ at $x = a$ and $y = b/2$ using trigonometric series solution

Number of Series $(M \times N)$	Maximum Deflection (mm) $w_0(a, b/2)$
2×2	0.58733
4×4	0.60105
6×6	0.61220
8×8	0.61334
10×10	0.61527
12×12	0.61579

Table 4-8. Maximum deflection of fiber-reinforced $[0_2/-45_2/45_2/90_2]_s$ laminated single free and three clamped plate with $q = 0.01$ MPa, $a/b = 1$, $h/a = 0.016$ at $x = a$ and $y = b/2$ using trigonometric series solution with *M*=12 and *N*=12 and ANSYS

Solution Type	Maximum Deflection (mm) $w_0(a, b/2)$	Difference %
Trigonometric Series Solution	0.61579	1.84
ANSYS	0.62736	

Figure 4-13 expresses the distribution of deformation results of the single free and three clamped plate using trigonometric series solution. While obtaining the distribution of deformation, order of trigonometric series *M* and *N* are taken 12 in Figure 4-13.

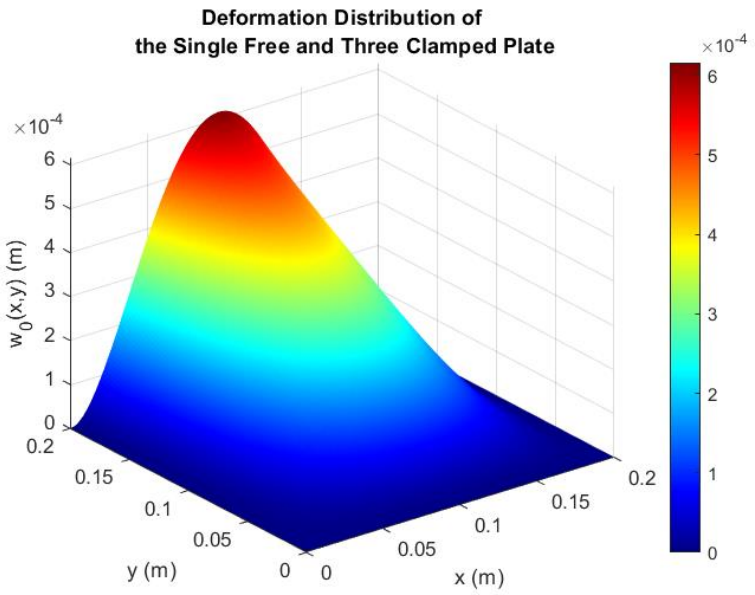

Figure 4-13. Distribution of deformation of the fiber-reinforced $[0_2/-45_2/45_2/90_2]_s$ laminated single free and three clamped plate with $q = 0.01$ MPa, $a/b = 1$, $h/a = 0.016$ using the trigonometric series solution with M=12 and N=12

The deformation distribution of the single free and three clamped plate determined with ANSYS is given in Figure 4-14. In this figure, the ACP module of ANSYS is used. The edges of the fiber-reinforced plate are modeled as single free and three clamped.

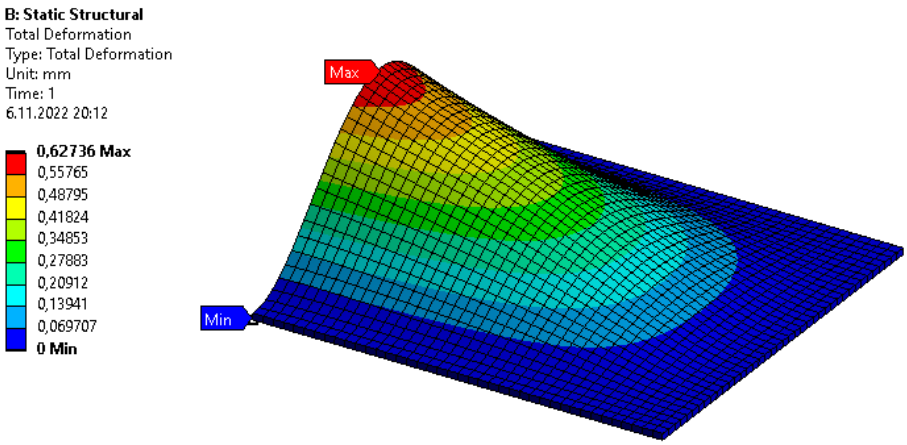

Figure 4-14. Distribution of deformation of the fiber-reinforced $[0_2/-45_2/45_2/90_2]_s$ laminated single free and three clamped plate with $q = 0.01$ MPa, $a/b = 1$, $h/a = 0.016$ using ANSYS

ANSYS and a trigonometric series solution are used to validate a single free and three clamped fiber-reinforced plate. This comparison is made at $y = b/2$ and along the *x* axis. Figure 4-15 shows the deformation comparison plot along with the *x*-axis based on the results shown in Figures 4-13 and 4-14.

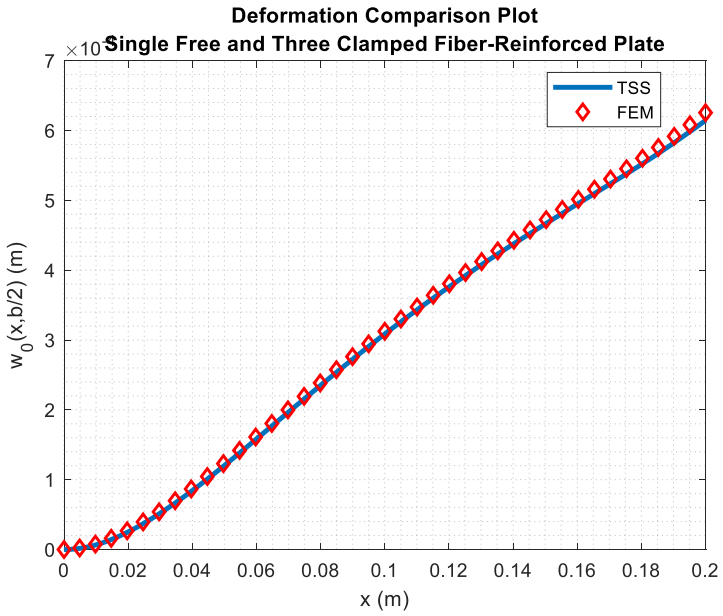

Figure 4-15. Deformation comparison plot of the fiber-reinforced $[0_2/-45_2/45_2/90_2]_s$ laminated single free and three clamped plate with $q = 0.01$ MPa, $a/b = 1$, $h/a = 0.016$ between results of trigonometric series solution and ANSYS at along with x axis and $y = b/2$

4.2.4 Transverse Stresses for a Simply Supported Plate

Transverse stresses of each ply of the fiber-reinforced laminated plate under uniformly distributed lateral load are calculated with the trigonometric series solution (TSS). Material and geometric properties of fiber-reinforced plate are taken in Table 4-1 and Table 4-2. The lamination scheme of the simply-supported plate is $[0_2/-45_2/45_2/90_2]_s$. To calculate σ_{xx}, σ_{yy}, and σ_{xy} of the *kth* layer a of the simply-supported plate, equations (3-16), (3-17), and (3-18) are used with $\sin(\frac{i\pi}{a}x)\sin(\frac{j\pi}{b}y)$ trigonometric shape function. Transverse stresses are validated with the finite element analysis program ANSYS. Normal stresses and shear stresses are validated at the mid-point of the fiber-reinforced simply-supported plate.

Figure 4-16 shows the validation of σ_{xx} of the *kth* layer of fiber-reinforced simply-supported plate. Mid-point stresses are determined using ANSYS, and trigonometric series solution (TSS) with *M* and *N* are taken 12. There are 16 plies in the laminated plate. The vertical axis represents the thickness coordinates of each layer while the horizontal axis indicates σ_{xx} values of these plies.

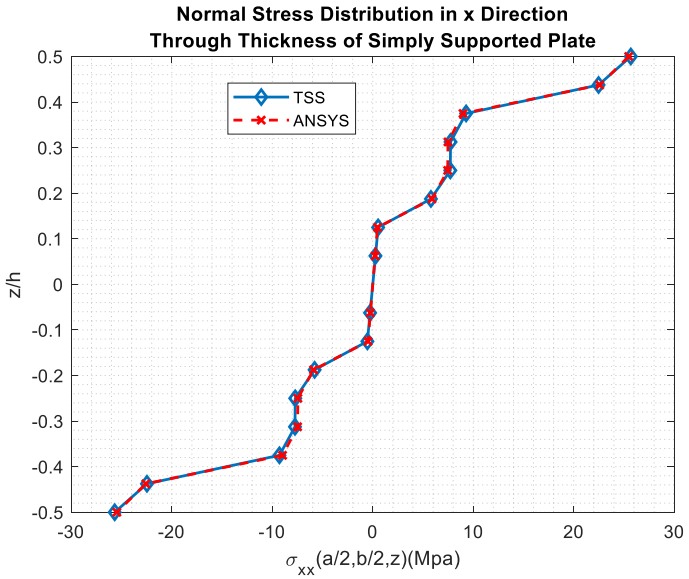

Figure 4-16. Comparison of σ_{xx} distribution with TSS and ANSYS through thickness of fiber-reinforced $[0_2/-45_2/45_2/90_2]_s$ laminated simply supported plate with $q = 0.01$ MPa, $a/b = 1$, $h/a = 0.016$

When Figure 4-16 is examined, it is understood that in the mid-point σ_{xx} distribution through the thickness, the $0°$ oriented fibers are exposed to the higher stress, and the $90°$ oriented fibers are exposed to the lower stress. It is understood that the $45°$ and $-45°$ oriented fibers have moderate stress values.

Figure 4-17 indicates the validation of σ_{yy} of the *kth* layer of fiber-reinforced simply-supported plate. Mid-point stress of each layer is determined using ANSYS, and trigonometric series solution (TSS) with *M* and *N* are taken 12.

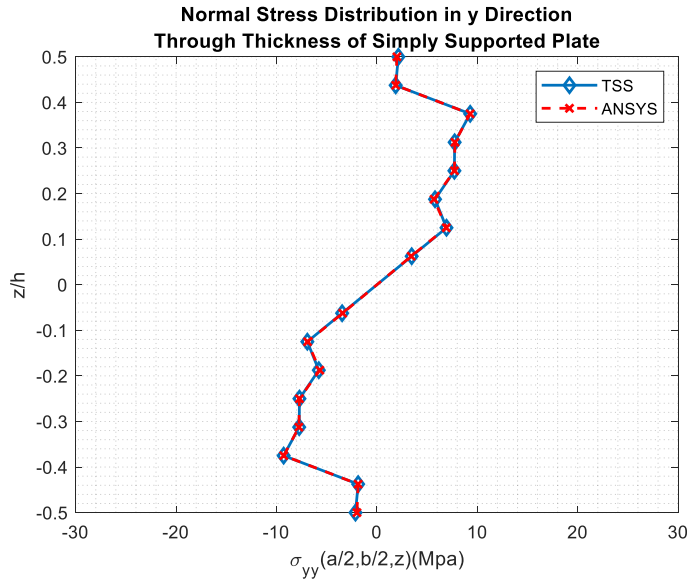

Figure 4-17. Comparison of σ_{yy} distribution with TSS and ANSYS through thickness of fiber-reinforced $[0_2/-45_2/45_2/90_2]_s$ laminated simply supported plate with $q = 0.01$ MPa, $a/b = 1$, $h/a = 0.016$

In Figure 4-17, σ_{yy} distributions through the thickness at the mid-point are shown. 90° oriented fibers are expected to undergo more significant stress since the *y*-direction is in the direction of the plies that are layered at 90°. Still, the 90° oriented fibers are subjected to less deformation as they are laminated in the mid-plane of the fiber-reinforced plate. This causes the 45° and −45° oriented fibers to be more stressed than the 90° oriented fibers. It is seen that the 0° oriented fibers are exposed to less stress in the *y* direction.

Figure 4-18 represents the validation of σ_{xy} of the *kth* layer of fiber-reinforced simply-supported plate. The mid-point stress of each layer is determined using ANSYS, and trigonometric series solution (TSS) with *M* and *N* are taken 12.

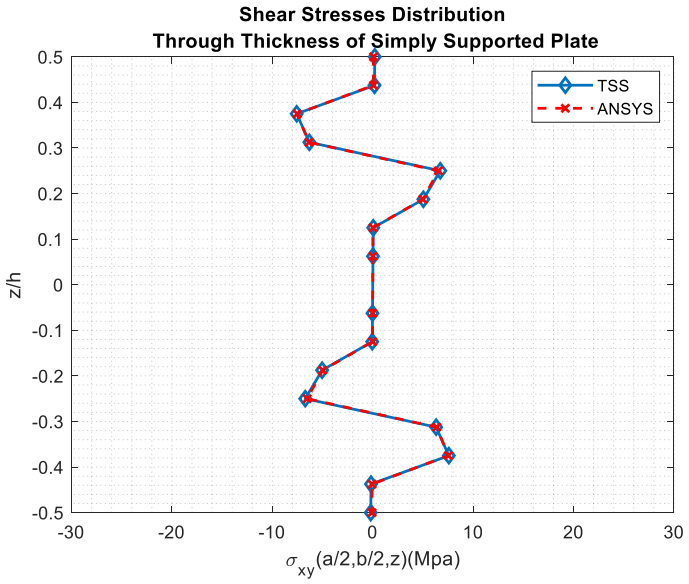

Figure 4-18. Comparison of σ_{xy} distribution with TSS and ANSYS through thickness of fiber-reinforced $[0_2/-45_2/45_2/90_2]_s$ laminated simply supported plate with $q = 0.01$ MPa, $a/b = 1$, $h/a = 0.016$

When the shear stress graph, Figure 4-18 is examined, it is seen that the $45°$ and $-45°$ layers are exposed to the highest stress, as expected. $0°$ and $90°$ oriented fibers are exposed to low shear stress.

Distribution of σ_{xx} in Layers:

There are four different fiber angles in the fiber-reinforced lamination scheme. The lamination scheme is $[0_2/-45_2/45_2/90_2]_s$ in the calculation of normal stress distribution of simply-supported plate. In the following parts, σ_{xx} distribution of different fiber angle plies will be examined.

Figure 4-19 shows the σ_{xx} distribution that is determined by a using trigonometric series solution (TSS) of $0°$ ply at $z = 1.6$ mm. Due to lateral load and edges are simply-supported, maximum stress occurred at the mid-point of the ply.

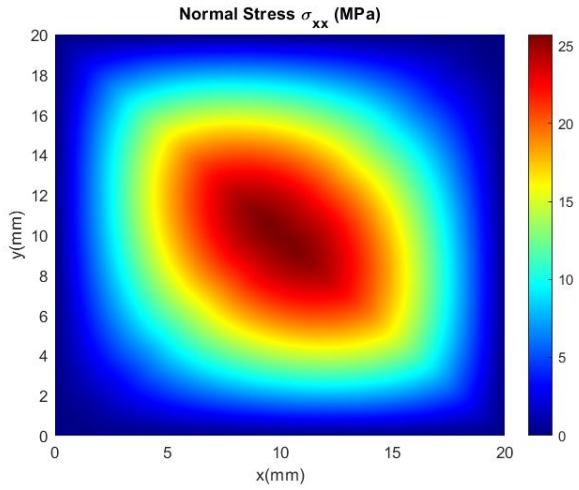

Figure 4-19. σ_{xx} distribution determined by trigonometric series solution with *M*, *N*=12 at $z = 1.6$ mm of 0°ply in fiber-reinforced laminated simply supported plate

σ_{xx} distribution that is determined by using trigonometric series solution (TSS) of -45° ply at $z = 1.2$ mm is indicated in Figure 4-20. Maximum stress occurred longitudinal direction of the ply.

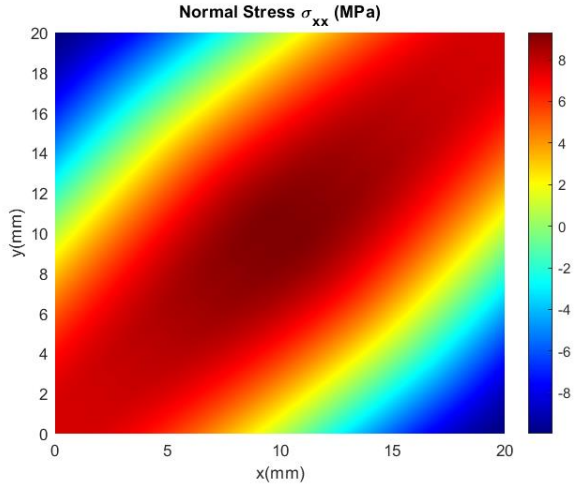

Figure 4-20. σ_{xx} distribution determined by trigonometric series solution with *M*, *N*=12 at $z = 1.2$ mm of -45°ply in fiber-reinforced laminated simply supported plate

Figure 4-21 indicates the σ_{xx} distribution which is obtained by using trigonometric series solution (TSS) of 45° ply at $z = 0.8$ mm.

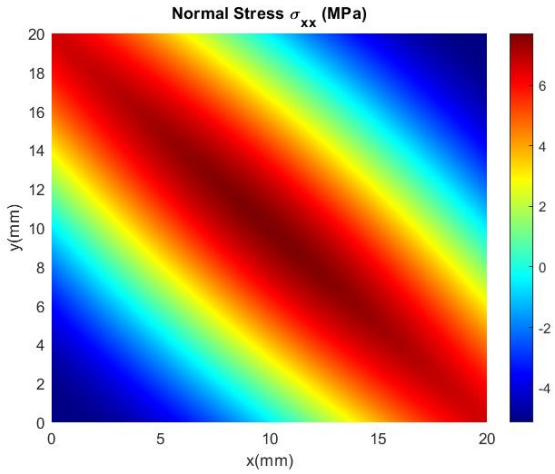

Figure 4-21. σ_{xx} distribution determined by trigonometric series solution with *M*, *N*=12 at $z = 0.8$ mm of 45° ply in fiber-reinforced laminated simply supported plate

σ_{xx} distribution that is determined by using trigonometric series solution (TSS) of 90° ply at $z = 0.4$ mm is given in Figure 4-22. 90° oriented fiber's strength is weak in the x direction, as expected.

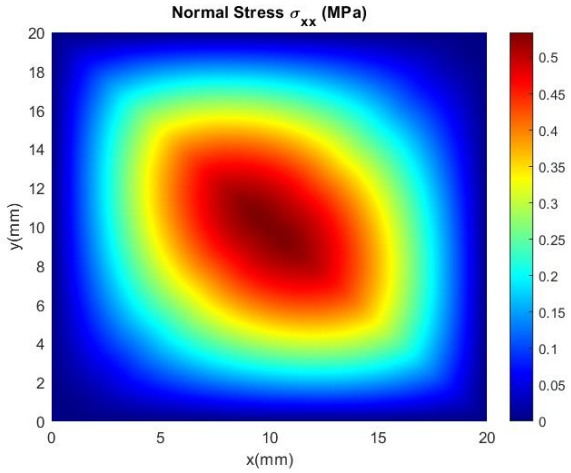

Figure 4-22. σ_{xx} distribution determined by trigonometric series solution with *M*, *N*=12 at $z = 0.4$ mm of 90° ply in fiber-reinforced laminated simply supported plate

Distribution of σ_{yy} in Layers:

While obtaining the σ_{yy} distribution of the *kth* layer of the fiber-reinforced simply-supported plate, $[0_2/-45_2/45_2/90_2]_s$ lamination scheme is used. In this lamination scheme, four different fiber orientations are used. To understand the normal stress distribution of layers in the y direction at different thickness coordinates, the trigonometric series solution (TSS) method is used. σ_{yy} distribution of these plies will be determined in the following parts.

Figure 4-23 shows the σ_{yy} distribution that is determined by using a trigonometric series solution (TSS) of $0°$ ply at $z = 1.6$ mm. When the fiber orientation is $0°$ in the ply, σ_{yy} is small compared to $90°$ fiber orientation.

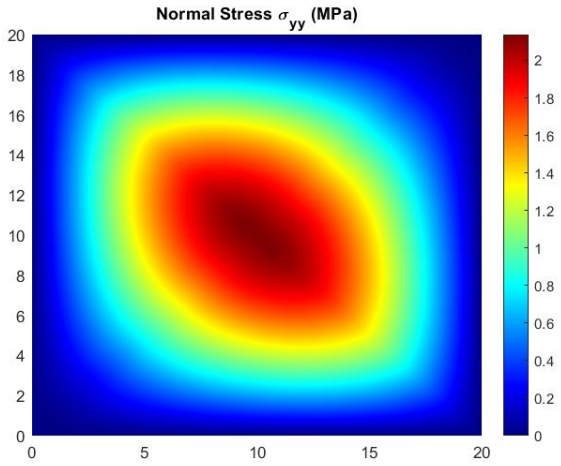

Figure 4-23. σ_{yy} distribution determined by trigonometric series solution with *M*, *N*=12 at $z = 1.6$ mm of 0° ply in fiber-reinforced laminated simply supported plate

σ_{yy} distribution that is obtained by using trigonometric series solution (TSS) of $-45°$ ply at $z = 1.2$ mm is indicated in Figure 4-24. Maximum stress occurred longitudinal direction of the ply.

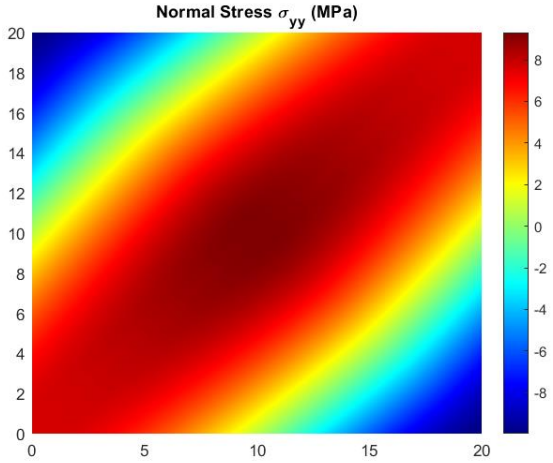

Figure 4-24. σ_{yy} distribution determined by trigonometric series solution with *M*, *N*=12 at $z = 1.2$ mm of -45°ply in fiber-reinforced laminated simply supported plate

Figure 4-25 expresses the σ_{yy} distribution which is obtained by using trigonometric series solution (TSS) of 45° ply at $z = 0.8$ mm.

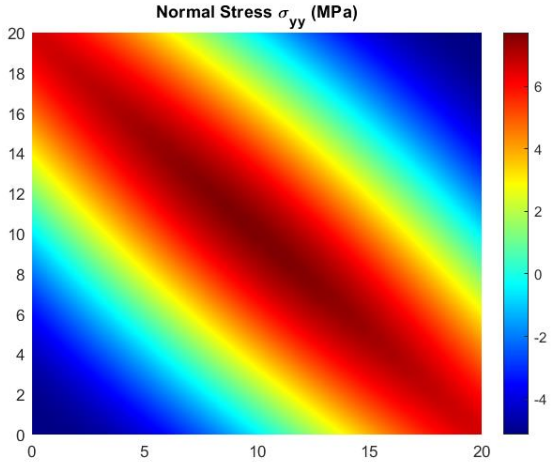

Figure 4-25. σ_{yy} distribution determined by trigonometric series solution with *M*, *N*=12 at $z = 0.8$ mm of 45°ply in fiber-reinforced laminated simply supported plate

σ_{yy} distribution which is calculated by using trigonometric series solution (TSS) of 90° ply at $z = 0.4$ mm is given in Figure 4-26. Strength of 90° oriented fiber is strong in the y direction compared to 0° oriented fiber, as expected.

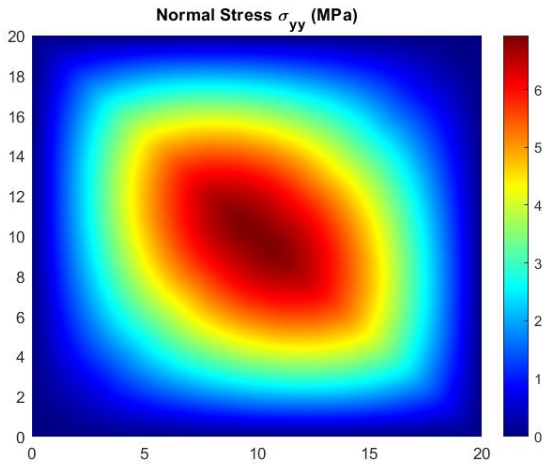

Figure 4-26. σ_{yy} distribution determined by trigonometric series solution with *M*, *N*=12 at $z = 0.4$ mm of 90°ply in fiber-reinforced laminated simply supported plate

Distribution of σ_{xy} in Layers:

While determining the shear stress distribution in the xy direction at different thickness coordinates, the trigonometric series solution method is used, as in the previous two sections. σ_{xy} distribution of these plies will be determined in the following parts.

Figure 4-27 shows the σ_{xy} distribution that is determined by a using trigonometric series solution (TSS) of 0° ply at $z = 1.6$ mm. Maximum stresses occur at the intersection of the boundaries of the ply.

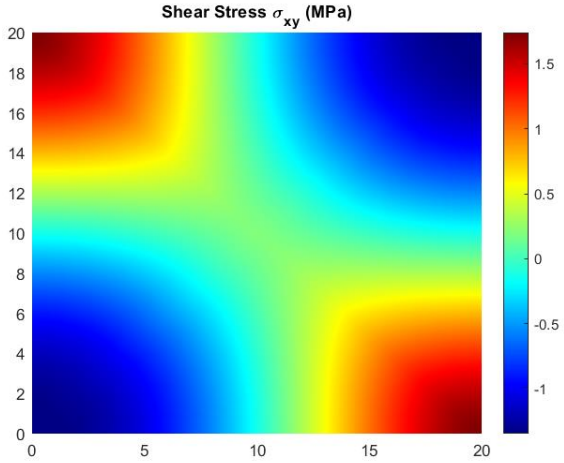

Figure 4-27. σ_{xy} distribution determined by trigonometric series solution with *M*, *N*=12 at $z = 1.6$ mm of 0°ply in fiber-reinforced laminated simply supported plate

σ_{xy} distribution that is determined by using trigonometric series solution (TSS) of -45° ply at $z = 1.2$ mm is expressed in Figure 4-28. Maximum shear stress occurred in 45° or $-45°$ fiber oriented plies.

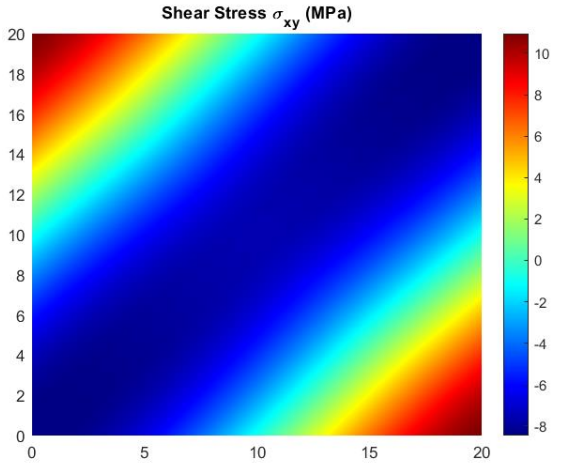

Figure 4-28. σ_{xy} distribution determined by trigonometric series solution with *M*, *N*=12 at $z = 1.2$ mm of -45°ply in fiber-reinforced laminated simply supported plate

Figure 4-29 gives the σ_{xy} distribution that is obtained by using trigonometric series solution (TSS) of 45° ply at $z = 0.8$ mm.

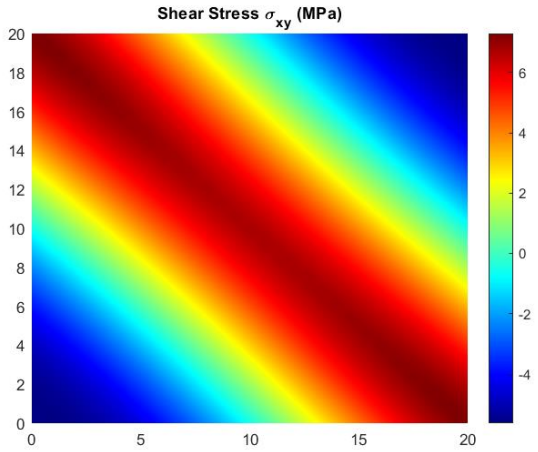

Figure 4-29. σ_{xy} distribution determined by trigonometric series solution with *M*, *N*=12 at $z = 0.8$ mm of 45°ply in fiber-reinforced laminated simply supported plate

σ_{xy} distribution which is calculated by using trigonometric series solution (TSS) of 90° ply at $z = 0.4$ mm is given in Figure 4-30.

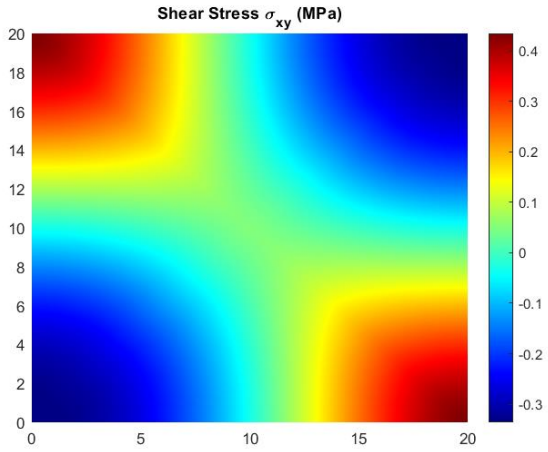

Figure 4-30. σ_{xy} distribution determined by trigonometric series solution with *M*, *N*=12 at $z = 0.4$ mm of 90°ply in fiber-reinforced laminated simply supported plate

4.2.5 Transverse Stresses for a Clamped Plate

As in the previous part, the transverse stresses of each ply of the fiber-reinforced laminated plate under the same load are calculated with the trigonometric series solution (TSS). Material and geometric properties of fiber-reinforced plate are also taken in Table 4-1 and Table 4-2. The lamination scheme of the clamped plate is $[0_2/-45_2/45_2/90_2]_s$ as mentioned before. σ_{xx}, σ_{yy}, and σ_{xy} of the *kth* layer a of the clamped plate are obtained with using equations (3-16), (3-17), and (3-18). Shape function is $\sin(\frac{i\pi}{a}x)\sin(\frac{\pi}{a}x)\sin(\frac{j\pi}{b}y)\sin(\frac{\pi}{b}y)$ for clamped plate in trigonometric series solution. Validations of transverse stresses are also done with the finite element analysis program ANSYS. Normal stresses and shear stresses are validated at the mid-point of the fiber-reinforced clamped plate.

Figure 4-31 shows the validation of σ_{xx} of the *kth* layer of fiber-reinforced clamped plate. Mid-point stress of each layer is determined using ANSYS, and trigonometric series solution (TSS) with *M* and *N* are taken 12.

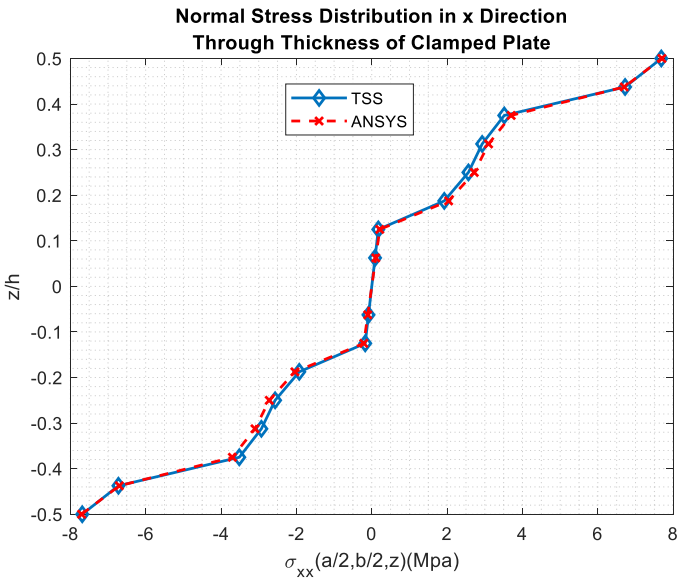

Figure 4-31. Comparison of σ_{xx} distribution with TSS and ANSYS through thickness of fiber-reinforced $[0_2/-45_2/45_2/90_2]_s$ laminated clamped plate with $q = 0.01$ MPa, $a/b = 1$, $h/a = 0.016$

Figure 4-31 shows that the 0° fiber oriented layers are subjected to the most stress in clamped fiber-reinforced plates. In contrast, the 90° fiber oriented layers are subjected to the least stress.

Figure 4-32 indicates the validation of σ_{yy} of the *kth* layer of fiber-reinforced clamped plate. Mid-point stress of each layer is determined using ANSYS, and trigonometric series solution (TSS) with *M* and *N* are taken 12.

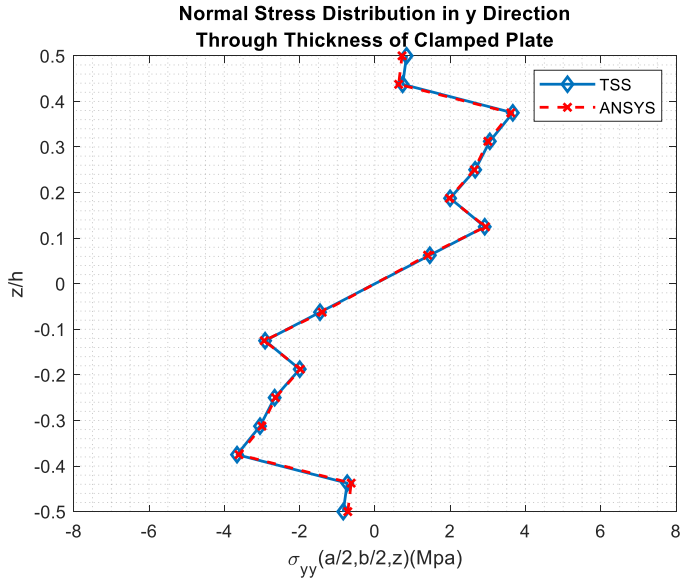

Figure 4-32. Comparison of σ_{yy} distribution with TSS and ANSYS through thickness of fiber-reinforced $[0_2/-45_2/45_2/90_2]_s$ laminated clamped plate with $q = 0.01$ MPa, $a/b = 1$, $h/a = 0.016$

At the mid-point of the σ_{yy} through the thickness, the 90° fiber oriented layers are less deformed as they are placed in the mid-plane of the composite plate. This causes the 45° and −45° fiber oriented layers to be more stressed than the 90° layers. It is seen that the 0° fiber oriented layers are exposed to less stress in the y direction.

Figure 4-33 represents the validation of σ_{xy} of the *kth* layer of fiber-reinforced clamped plate. The mid-point stress of each layer is determined using ANSYS, and trigonometric series solution (TSS) with *M* and *N* are taken 12.

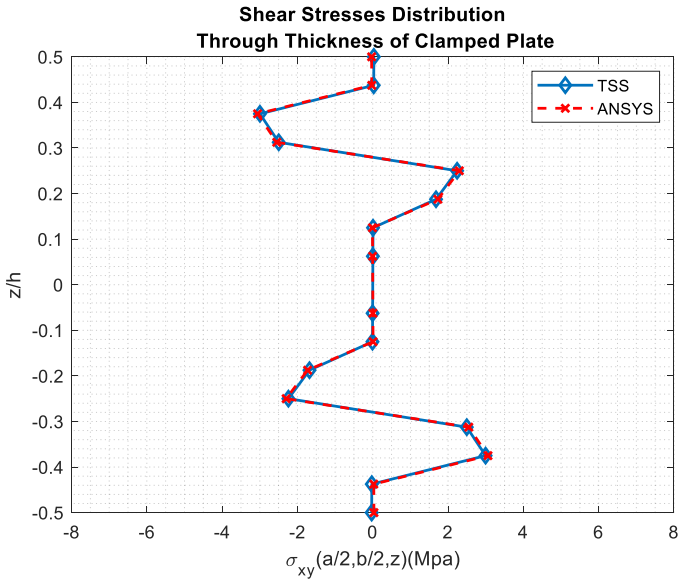

Figure 4-33. Comparison of σ_{xy} distribution with TSS and ANSYS through thickness of fiber-reinforced $[0_2/-45_2/45_2/90_2]_s$ laminated clamped plate with $q = 0.01$ MPa, $a/b = 1$, $h/a = 0.016$

When Figure 4-33 is examined, it is seen that the $45°$ and $-45°$ fiber oriented layers are exposed to the highest stress as expected.

The stress distributions in the middle of clamped composite plates are less than those of composite plates simply supported. This is because all degrees of freedom are limited at the boundary conditions of the clamped plates. Therefore, the boundary conditions are more stressed than the midpoints. This situation can be understood from the general stress distribution figures of the plates.

Distribution of σ_{xx} in Layers:

The lamination scheme is $[0_2/-45_2/45_2/90_2]_s$ in the calculation of normal stress distribution of clamped plate. As seen in the lamination scheme, four different fiber angles are present in this plate. In the following parts, σ_{xx} distribution of different fibre oriented plies will be examined.

Figure 4-34 shows the σ_{xx} distribution that is determined by using a trigonometric series solution (TSS) of $0°$ ply at $z = 1.6$ mm. Due to all degrees of freedom is

limited at the boundaries, maximum stress occurred at the edges. These edges are at the longitudinal direction of 0° fiber.

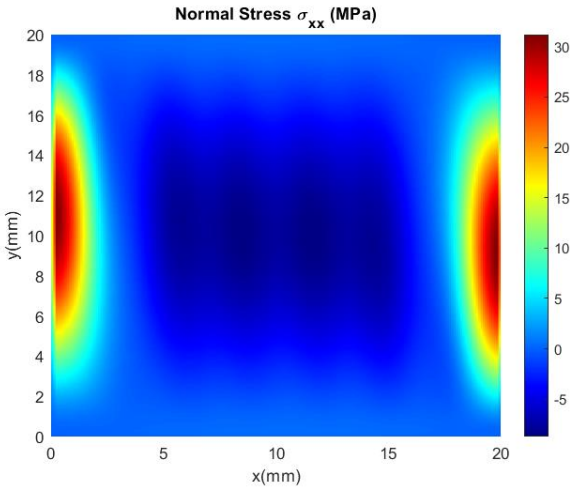

Figure 4-34. σ_{xx} distribution determined by trigonometric series solution with *M*, *N*=12 at $z = 1.6$ mm of 0° ply in fiber-reinforced laminated clamped plate

σ_{xx} distribution that is obtained by using trigonometric series solution (TSS) of -45° ply at $z = 1.2$ mm is indicated in Figure 4-35. Maximum stress occurred boundaries of the ply.

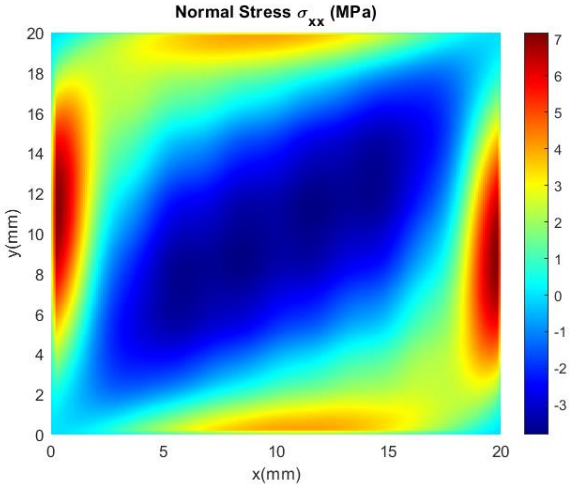

Figure 4-35. σ_{xx} distribution determined by trigonometric series solution with *M*, *N*=12 at $z = 1.2$ mm of -45° ply in fiber-reinforced laminated clamped plate

Figure 4-36 indicates the σ_{xx} distribution which is determined by using trigonometric series solution (TSS) of 45° ply at $z = 0.8$ mm.

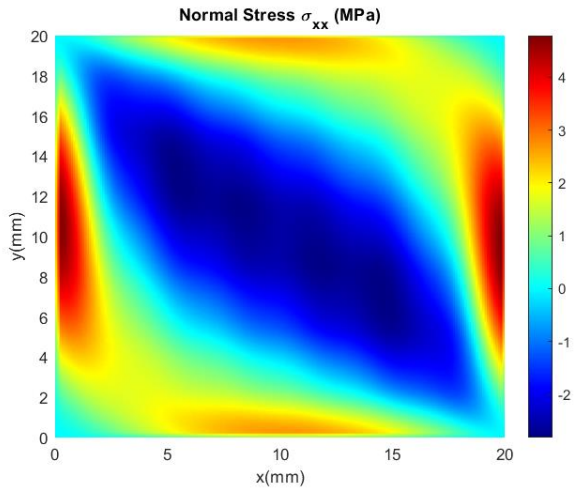

Figure 4-36. σ_{xx} distribution determined by trigonometric series solution with *M*, *N*=12 at $z = 0.8$ mm of 45°ply in fiber-reinforced laminated clamped plate

σ_{xx} distribution that is determined by using trigonometric series solution of 90° ply at $z = 0.4$ mm is given in Figure 4-37. Strength of fibers that is oriented 90° is weak in the x direction, as expected.

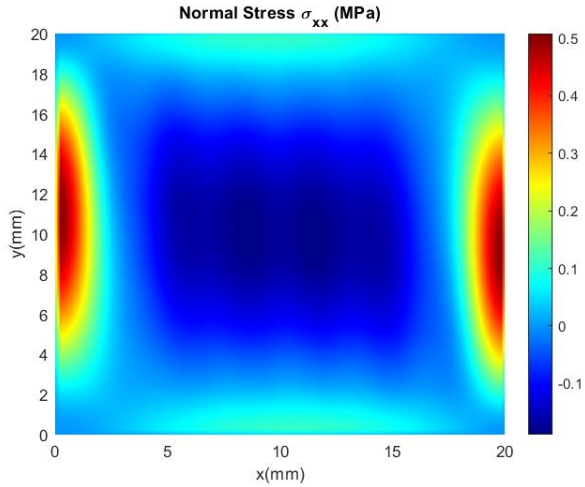

Figure 4-37. σ_{xx} distribution determined by trigonometric series solution with *M*, *N*=12 at $z = 0.4$ mm of 90°ply in fiber-reinforced laminated clamped plate

Distribution of σ_{yy} in Layers:

σ_{yy} distribution of *kth* layer of the fiber-reinforced clamped plate is obtained for $[0_2/-45_2/45_2/90_2]_s$ lamination scheme. In this lamination scheme, four different fiber orientations are used. To understand the normal stress distribution of layers in the y direction at different thickness coordinates, the trigonometric series solution (TSS) method is used. σ_{yy} distribution of these plies will be determined in the following parts.

Figure 4-38 shows the σ_{yy} distribution that is determined by using a trigonometric series solution (TSS) of $0°$ ply at $z = 1.6$ mm. When the fiber orientation is $0°$ in the ply, σ_{yy} is small compared to $90°$ fiber orientation.

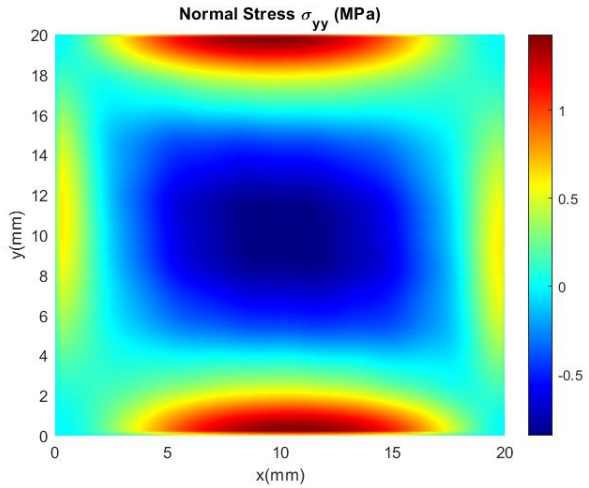

Figure 4-38. σ_{yy} distribution determined by trigonometric series solution with *M*, *N*=12 at $z = 1.6$ mm of 0° ply in fiber-reinforced laminated clamped plate

σ_{yy} distribution that is obtained by using trigonometric series solution (TSS) of $-45°$ ply at $z = 1.2$ mm is indicated in Figure 4-39. Maximum stress occurred edges of the ply.

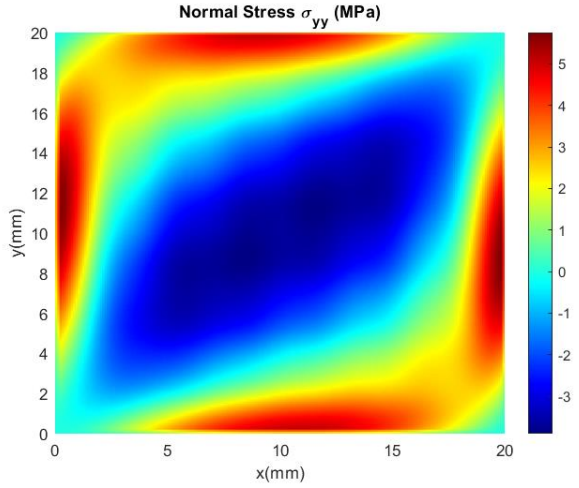

Figure 4-39. σ_{yy} distribution determined by trigonometric series solution with *M*, *N*=12 at $z = 1.2$ mm of -45° ply in fiber-reinforced laminated clamped plate

Figure 4-40 expresses the σ_{yy} distribution which is obtained by using trigonometric series solution (TSS) of $45°$ ply at $z = 0.8$ mm.

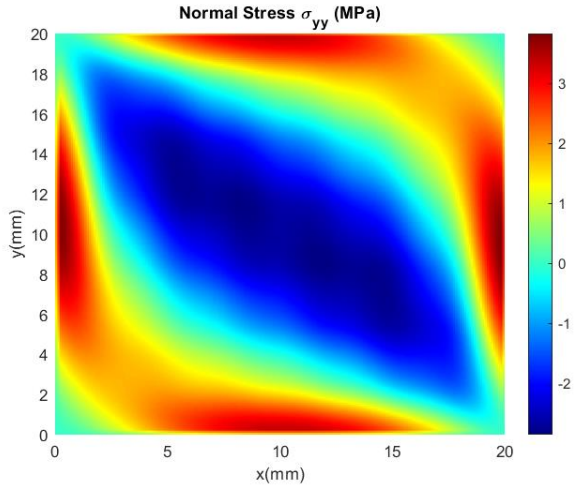

Figure 4-40. σ_{yy} distribution determined by trigonometric series solution with *M*, *N*=12 at $z = 0.8$ mm of 45° ply in fiber-reinforced laminated clamped plate

σ_{yy} distribution that is obtained by using trigonometric series solution (TSS) of $90°$ ply at $z = 0.4$ mm is given in Figure 4-41. Strength of $90°$ oriented fiber is strong in the y direction compared to $0°$ oriented fiber, as expected.

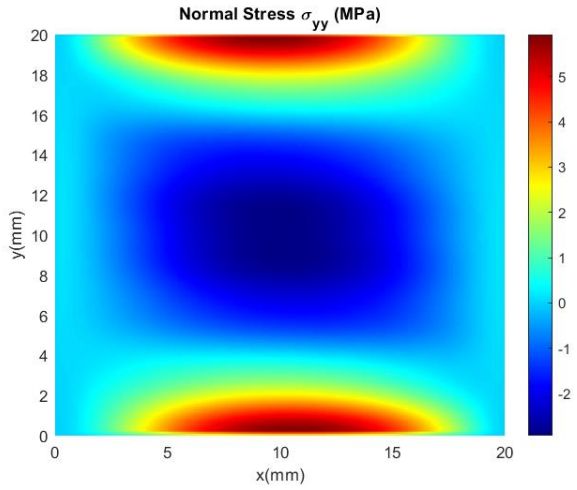

Figure 4-41. σ_{yy} distribution determined by trigonometric series solution with M, N=12 at $z = 0.4$ mm of 90° ply in fiber-reinforced laminated clamped plate

Distribution of σ_{xy} in Layers:

Shear stress distribution in the xy direction at different thickness coordinates is found by the trigonometric series solution (TSS) method, as in the previous sections. σ_{xy} distribution of these plies will be determined in the following parts.

Figure 4-42 shows the σ_{xy} distribution which is determined by using trigonometric series solution (TSS) of $0°$ ply at $z = 1.6$ mm. Maximum stresses take place at the corners of the ply.

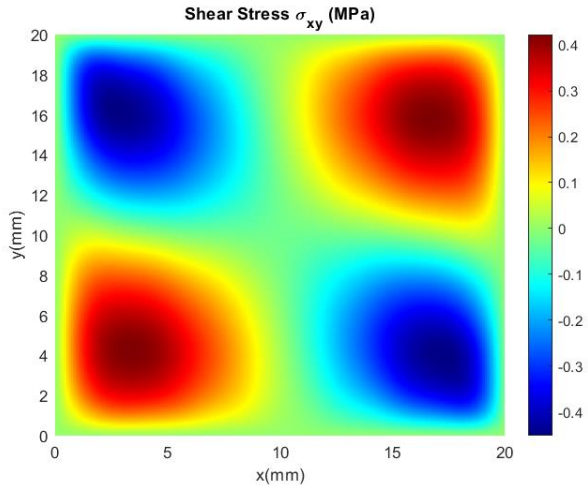

Figure 4-42. σ_{xy} distribution determined by trigonometric series solution with *M*, *N*=12 at $z = 1.6$ mm of 0°ply in fiber-reinforced laminated clamped plate

σ_{xy} distribution that is obtained by using trigonometric series solution (TSS) of -45° ply at $z = 1.2$ mm is shown in Figure 4-43. Maximum shear stress is at the longitudinal direction of fibers.

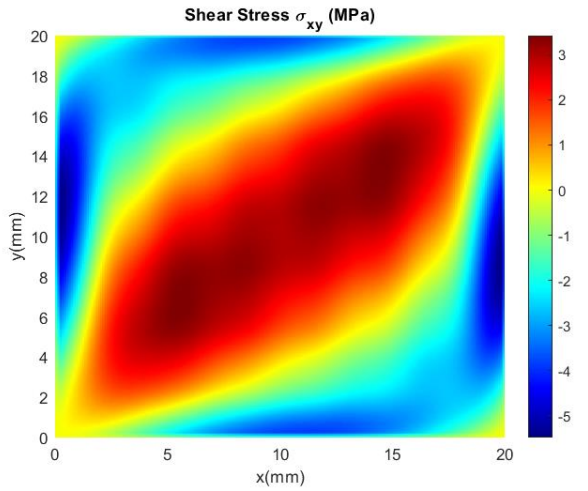

Figure 4-43. σ_{xy} distribution determined by trigonometric series solution with *M*, *N*=12 at $z = 1.2$ mm of -45°ply in fiber-reinforced laminated clamped plate

Figure 4-44 gives the σ_{xy} distribution that is determined by using trigonometric series solution (TSS) of 45° ply at $z = 0.8$ mm.

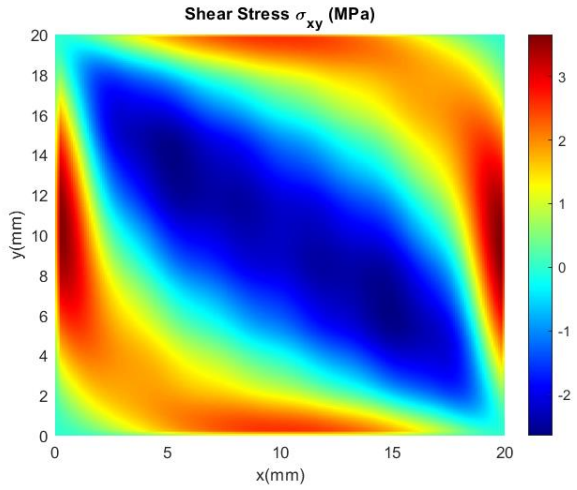

Figure 4-44. σ_{xy} distribution determined by trigonometric series solution with *M*, *N*=12 at $z = 0.8$ mm of 45°ply in fiber-reinforced laminated clamped plate

σ_{xy} distribution which is calculated by using trigonometric series solution (TSS) of 90° ply at $z = 0.4$ mm is given in Figure 4-45. Maximum stresses are also in the corner of the ply.

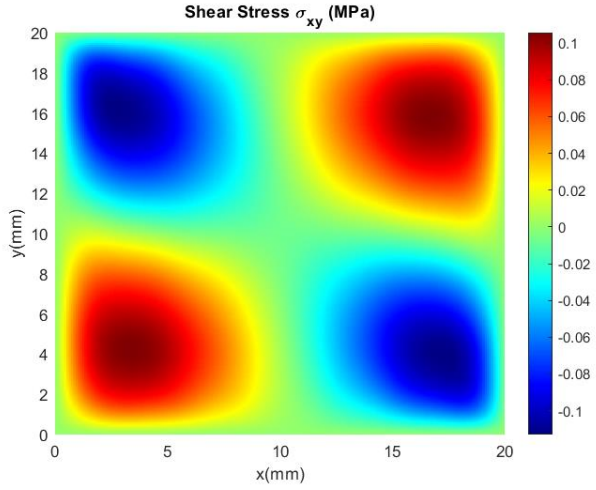

Figure 4-45. σ_{xy} distribution determined by trigonometric series solution with *M*, *N*=12 at $z = 0.4$ mm of 90°ply in fiber-reinforced laminated clamped plate

4.2.6 Transverse Stresses for a Single Free and Three Clamped Plate

Transverse stresses of each ply of the fiber-reinforced laminated plate under uniformly distributed lateral load are calculated with the trigonometric series solution (TSS). The material and geometric properties of fiber-reinforced plate are taken in the Table 4-1 and Table 4-2 as in previous two sections. Lamination scheme of single free and three clamped plate is $[0_2/-45_2/45_2/90_2]_s$. In order to calculate σ_{xx}, σ_{yy}, and σ_{xy} of the *kth* layer a of the fiber-reinforced plate, equations (3-16), (3-17), and (3-18) are used with $(1-\cos\left(\frac{(2i-1)\pi}{2a}x\right))\sin(\frac{j\pi}{b}y)\sin(\frac{\pi}{b}y)$, trigonometric shape function. Transverse stresses are validated with the finite element analysis program ANSYS for fiber-reinforced single free and three clamped plate. Normal stresses and shear stresses are validated at the mid-point of the fiber-reinforced plate.

Figure 4-46 shows the validation of σ_{xx} of the *kth* layer of fiber-reinforced single free and three clamped plate. Mid-point stress of each ply is determined using ANSYS, and trigonometric series solution (TSS) with *M* and *N* are taken 12.

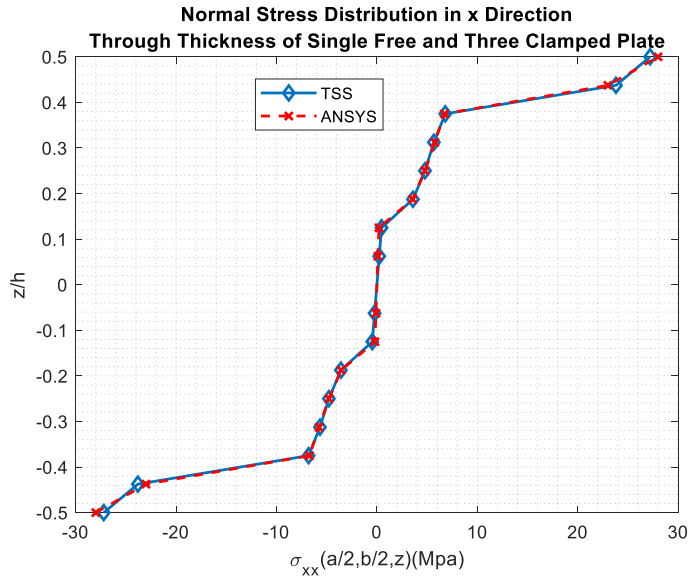

Figure 4-46. Comparison of σ_{xx} distribution with TSS and ANSYS through thickness of fiber-reinforced $[0_2/-45_2/45_2/90_2]_s$ laminated single free and three clamped plate with $q = 0.01$ MPa, $a/b = 1$, $h/a = 0.016$

It is known that in the midpoint normal stress distribution through the thickness in the *x*-direction, as in simply supported and clamped composite plates, the 0° fiber oriented layers are the most stressed. On the other hand, the layers at 90° fiber oriented are the least stressed, as shown in Figure 4-46.

Figure 4-47 indicates the validation of σ_{yy} of the *kth* layer of fiber-reinforced single free and three clamped plate. Mid-point stress of each layer is determined using ANSYS, and trigonometric series solution (TSS) with *M* and *N* are taken 12.

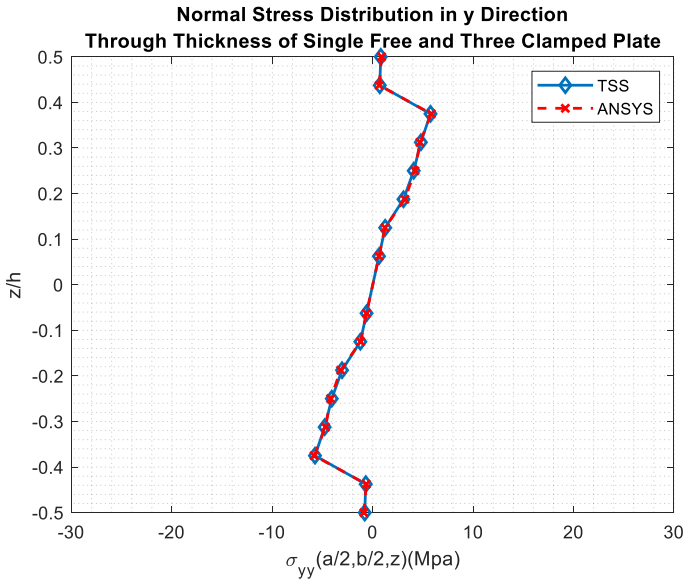

Figure 4-47. Comparison of σ_{yy} distribution with TSS and ANSYS through thickness of fiber-reinforced $[0_2/-45_2/45_2/90_2]_s$ laminated single free and three clamped plate with $q = 0.01$ MPa, $a/b = 1$, $h/a = 0.016$

When Figure 4-47 is examined, the $90°$ fiber oriented layers are in the middle of the composite plate, so they are less deformed compared to $45°$ and $-45°$ fiber oriented layers. This makes the layers at $45°$ and $-45°$ more stressed than the $90°$ fiber oriented layers in the y direction.

Figure 4-48 represents the validation of σ_{xy} of the *kth* layer of fiber-reinforced clamped plate. The mid-point stress of each layer is determined using ANSYS, and trigonometric series solution (TSS) with *M* and *N* are taken 12.

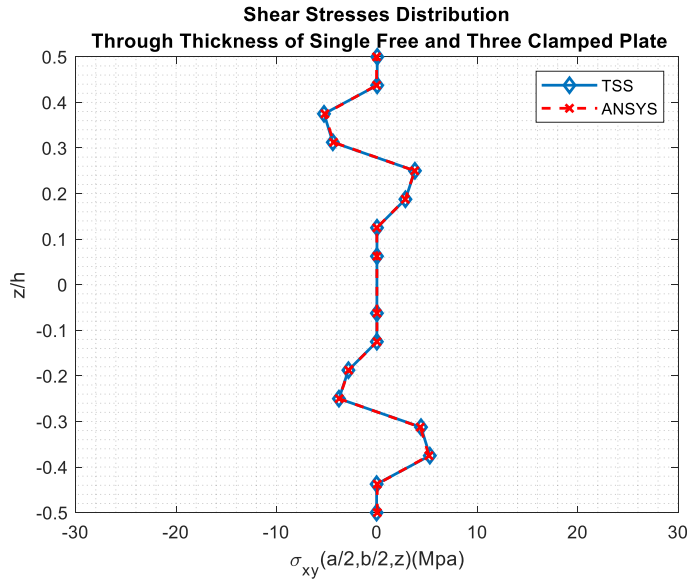

Figure 4-48. Comparison of σ_{xy} distribution with TSS and ANSYS through thickness of fiber-reinforced $[0_2/-45_2/45_2/90_2]_s$ laminated single free and three clamped plate with $q = 0.01$ MPa, $a/b = 1$, $h/a = 0.016$

When the Figure 4-48 of the maximum shear stress is looked at, it is clear that the $45°$ and $-45°$ fiber oriented layers have the most stress as expected.

The mid-point σ_{xx} distributions of single free and three clamped fiber-reinforced plate are greater than those of simply-supported and clamped fiber-reinforced plates because of free boundary condition that unlimited the degrees of freedom in all directions and rotations. Therefore, the mid-point of the fiber-reinforced single free and three clamped plate are more stressed. In other words, this stress spreads to different places on the plate since not much stress accumulates at the boundary condition. Since the free corner is in the x direction, the mid-point σ_{yy} on the simply-supported composite plate creates slightly more than a single free and three clamped fiber-reinforced plate.

Distribution of σ_{xx} in Layers:

σ_{xx} distributions of the fiber-reinforced single free and three clamped $[0_2/-45_2/45_2/90_2]_s$ plate are determined. As seen in the lamination scheme, four different fiber angles are present in this plate. In the following parts, σ_{xx} distribution of different fibre oriented plies will be examined.

Figure 4-49 shows the σ_{xx} distribution which is determined by using trigonometric series solution (TSS) of 0° ply at $z = 1.6$ mm. Due to clamped boundaries in *x* directions, maximum stress occurred at these edges. These edges are at the longitudinal direction of 0° fiber. The single free edge is at $y = 20$ mm, so this edge is under compressive σ_{xx} because of the lateral load.

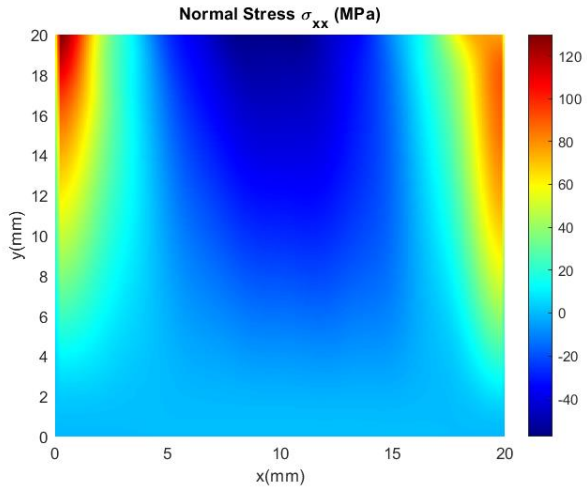

Figure 4-49. σ_{xx} distribution determined by trigonometric series solution with *M*, *N*=12 at $z = 1.6$ mm of 0° ply in fiber-reinforced laminated single free and three clamped plate

σ_{xx} distribution that is obtained by using trigonometric series solution (TSS) of -45° ply at $z = 1.2$ mm is indicated in Figure 4-50. Maximum stress occurred clamped boundaries of the ply.

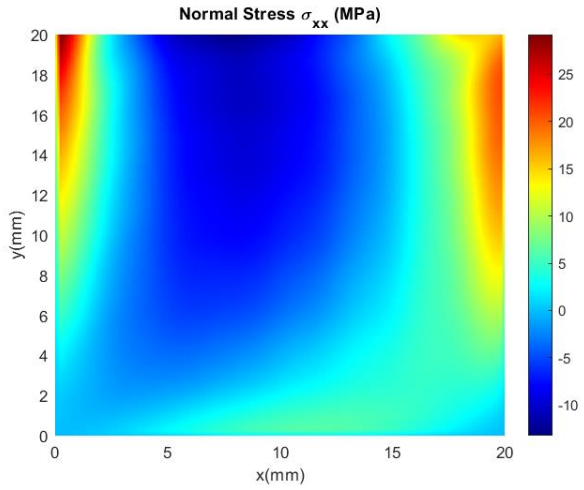

Figure 4-50. σ_{xx} distribution determined by trigonometric series solution with *M*, *N*=12 at $z = 1.2$ mm of -45°ply in fiber-reinforced laminated single free and three clamped plate

Figure 4-51 indicates the σ_{xx} distribution which is determined by using trigonometric series solution (TSS) of 45° ply at $z = 0.8$ mm.

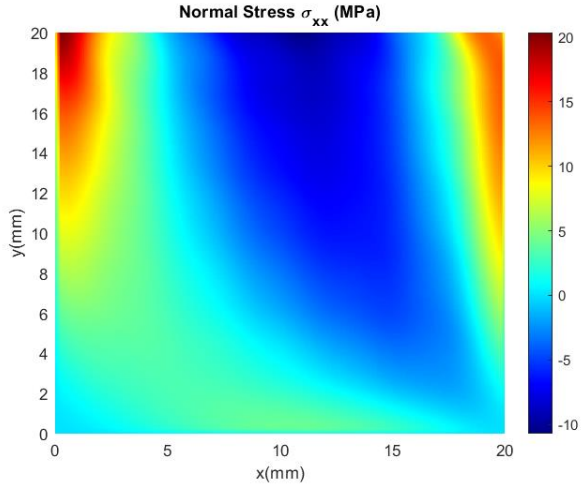

Figure 4-51. σ_{xx} distribution determined by trigonometric series solution with *M*, *N*=12 at $z = 0.8$ mm of 45°ply in fiber-reinforced laminated single free and three clamped plate

σ_{xx} distribution that is determined by using trigonometric series solution of 90° ply at $z = 0.4$ mm is given in Figure 4-52. Strength of fibers that is oriented 90° is weak in the x direction, as expected.

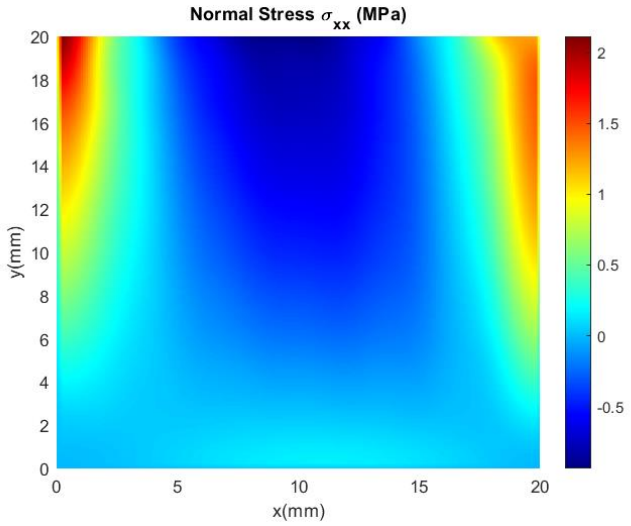

Figure 4-52. σ_{xx} distribution determined by trigonometric series solution with *M*, *N*=12 at $z = 0.4$ mm of 90° ply in fiber-reinforced laminated single free and three clamped plate

Distribution of σ_{yy} in Layers:

σ_{yy} distribution of *kth* layer of fiber-reinforced single free and three clamped plate is obtained for $[0_2/-45_2/45_2/90_2]_s$ lamination scheme. In this lamination scheme 4 different fiber orientations are used. To understand normal stress distribution of layers in y direction at different thickness coordinates, trigonometric series solution (TSS) method is used. σ_{yy} distribution of these plies will be determined in the following parts.

Figure 4-53 shows the σ_{yy} distribution that is determined by using trigonometric series solution (TSS) of 0° ply at $z = 1.6$ mm. When the fiber orientation is 0° in the ply, σ_{yy} is small compared to 90° fiber orientation. Maximum stresses occur at clamped boundaries.

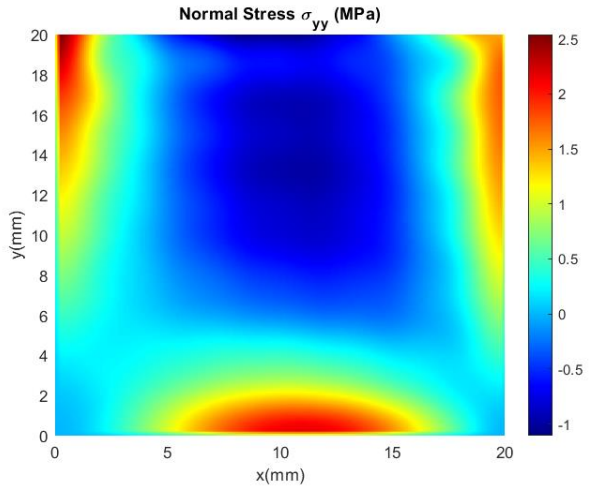

Figure 4-53. σ_{yy} distribution determined by trigonometric series solution with *M*, *N*=12 at $z = 1.6$ mm of 0°ply in fiber-reinforced laminated single free and three clamped plate

σ_{yy} distribution that is obtained by using trigonometric series solution (TSS) of $-45°$ ply at $z = 1.2$ mm is indicated in Figure 4-54. Maximum stress occurred on clamped edges except for free one of the ply.

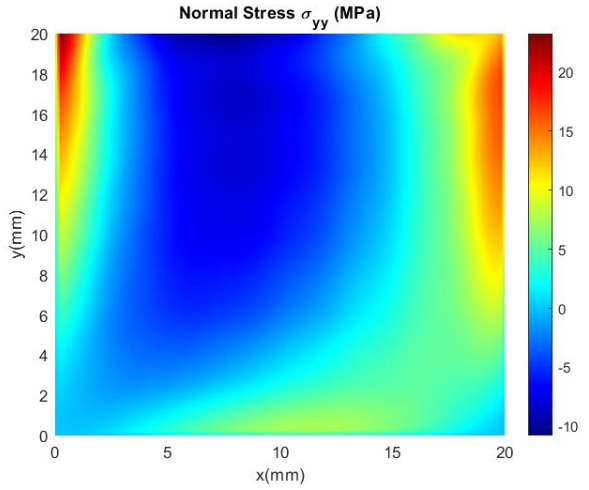

Figure 4-54. σ_{yy} distribution determined by trigonometric series solution with *M*, *N*=12 at $z = 1.2$ mm of -45°ply in fiber-reinforced laminated single free and three clamped plate

Figure 4-55 expresses the σ_{yy} distribution which is obtained by using trigonometric series solution (TSS) of 45° ply at $z = 0.8$ mm.

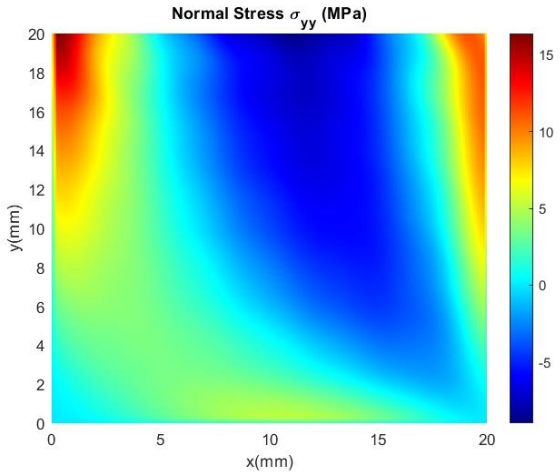

Figure 4-55. σ_{yy} distribution determined by trigonometric series solution with *M*, *N*=12 at $z = 0.8$ mm of 45°ply in fiber-reinforced laminated single free and three clamped plate

σ_{yy} distribution that is obtained by using trigonometric series solution (TSS) of 90° ply at $z = 0.4$ mm is given in Figure 4-56. Maximum stress is at one clamped edge in *y* direction of the fiber-reinforced plate since the other one is free.

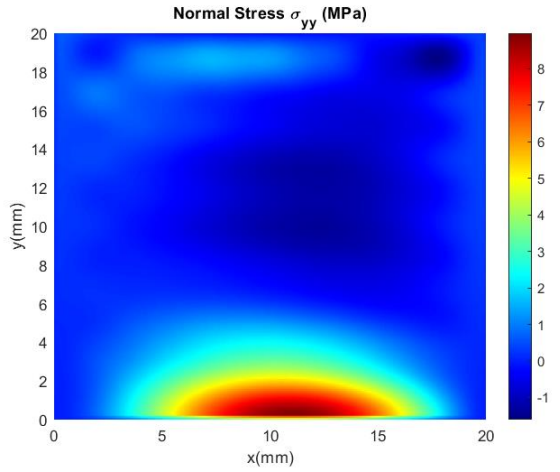

Figure 4-56. σ_{yy} distribution determined by trigonometric series solution with *M*, *N*=12 at $z = 0.4$ mm of 90°ply in fiber-reinforced laminated single free and three clamped plate

Distribution of σ_{xy} in Layers:

σ_{xy} distribution at different thickness coordinates is found by trigonometric series solution (TSS) method, as in the previous sections. σ_{xy} distribution of these plies will be determined in the following parts.

Figure 4-57 shows the σ_{xy} distribution that is determined by using trigonometric series solution (TSS) of 0° ply at $z = 1.6$ mm. Maximum tension and compression stress is symmetric about mid-point of the free edge.

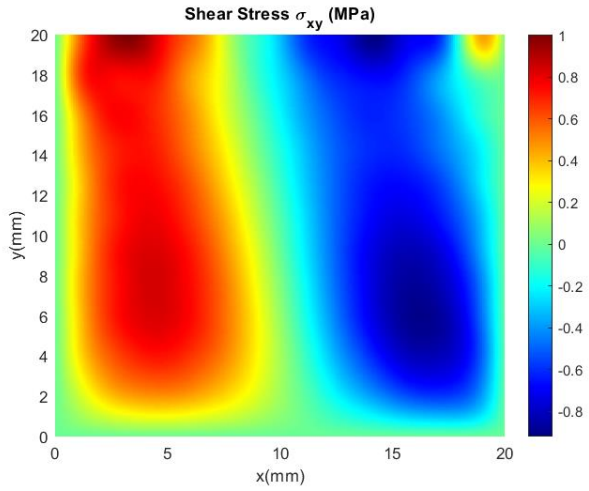

Figure 4-57. σ_{xy} distribution determined by trigonometric series solution with *M*, *N*=12 at $z = 1.6$ mm of 0° ply in fiber-reinforced laminated single free and three clamped plate

σ_{xy} distribution that is obtained by using trigonometric series solution (TSS) of -45° ply at $z = 1.2$ mm is shown in Figure 4-58. Maximum shear stress is at free boundary of the plate since the longitudinal direction of fibers cross this boundary.

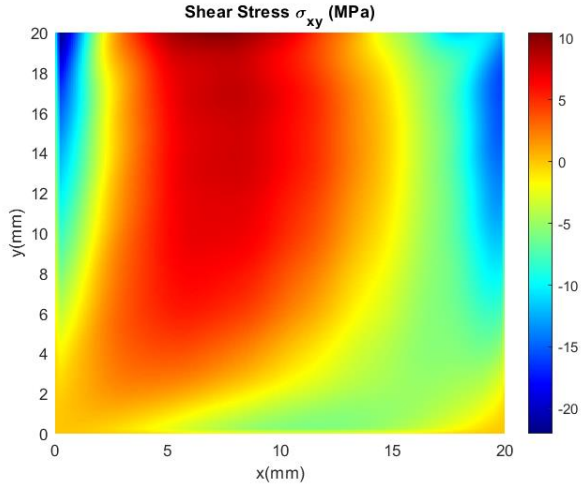

Figure 4-58. σ_{xy} distribution determined by trigonometric series solution with *M*, *N*=12 at $z = 1.2$ mm of -45°ply in fiber-reinforced laminated single free and three clamped plate

Figure 4-59 gives the σ_{xy} distribution that is determined by using trigonometric series solution (TSS) of 45° ply at $z = 0.8$ mm.

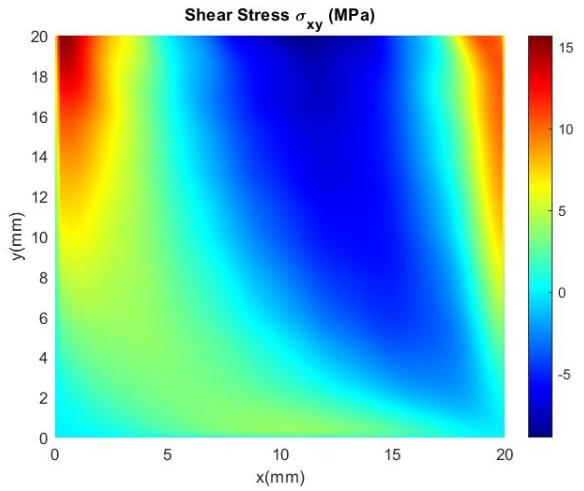

Figure 4-59. σ_{xy} distribution determined by trigonometric series solution with *M*, *N*=12 at $z = 0.8$ mm of 45°ply in fiber-reinforced laminated single free and three clamped plate

σ_{xy} distribution which is calculated by using trigonometric series solution (TSS) of 90° ply at $z = 0.4$ mm is given in Figure 4-60. Maximum stresses are also about free edge of the ply.

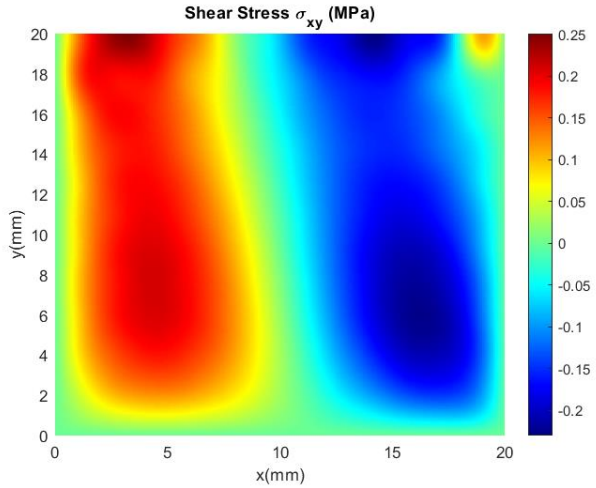

Figure 4-60. σ_{xy} distribution determined by trigonometric series solution with *M*, *N*=12 at $z = 0.4$ mm of 90° ply in fiber-reinforced laminated single free and three clamped plate

4.3 Free Vibration Analysis

Free vibration analysis of fiber-reinforced laminated plate has been obtained by using the trigonometric series solution (TSS) for three different boundary conditions. For these boundary conditions, new trigonometric shape functions are used. Firstly, the first four natural frequency values of fiber-reinforced laminated plates are found. Then, the four mode shapes of these plates are determined for their natural frequencies. The results calculated by the trigonometric series solution method are verified by the finite element method described in the first section.

Material and geometric properties of fiber-reinforced laminated plate are given in Table 4-9 and Table 4-10 while validating the free vibration solutions.

Table 4-9. Material properties of T300-934 carbon/epoxy for free vibration analysis [49]

Name	Material Property	Value	Unit
Longitudinal Young Modulus	E_{11}	148×10^9	$\mathrm{N/m^2}$
Transverse Young Modulus	E_{22}	9.65×10^9	$\mathrm{N/m^2}$
Longitudinal Shear Modulus	G_{12}	4.55×10^9	$\mathrm{N/m^2}$
Longitudinal Poisson Ratio	ν_{12}	0.30	-
Density	ρ_0	1.5×10^3	$\mathrm{kg/m^3}$
Thickness of Lamina	t	0.2×10^{-3}	m

Table 4-10. Geometric properties [49]

Name	Geometric Parameter	Value	Unit
X axis Dimension	a	0.2	m
Y axis Dimension	b	0.2	m
Number of Plies	n	16	-

A stacking sequence is constructed as $[0_2/-45_2/45_2/90_2]_s$ using material and geometric properties of the fiber-reinforced plate from Tables 4-9 and 4-10. The number of plies are 16 in this lamination sequence and plies are laminated symmetrically in the mid-plane of the fiber-reinforced plate. The problem geometry used in validation is given in Figure 4-61.

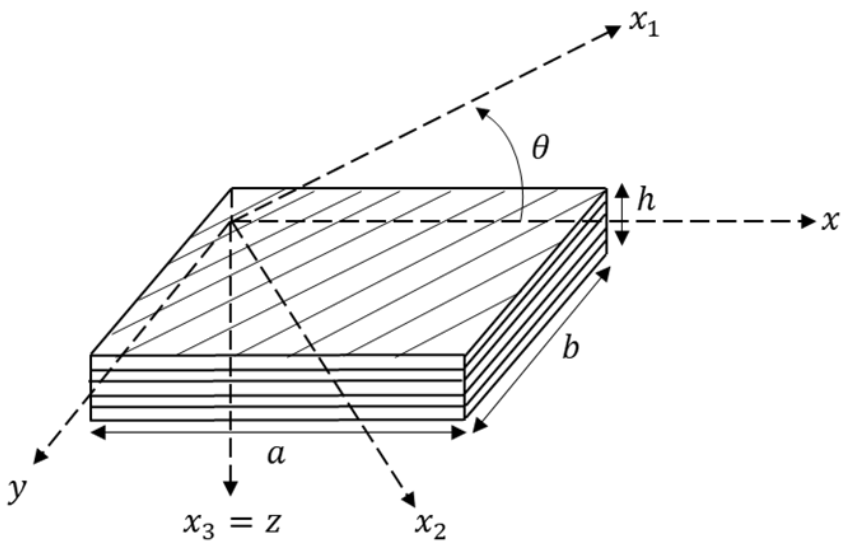

Figure 4-61. Free vibration problem geometry of fiber-reinforced $[0_2/-45_2/45_2/90_2]_s$ laminated plate

4.3.1 Analysis for a Simply-Supported Plate

The natural frequencies of the fiber-reinforced laminated plate, whose material and geometric properties are taken from Table 4-9 and Table 4-10, have been obtained with an analytical solution using trigonometric series shape functions. Lamination sequence of simply-supported plate is $[0_2/-45_2/45_2/90_2]_s$. In the trigonometric series solution (TSS), a convergence study is performed for a simply-supported plate by increasing the *M* and *N* orders of the Ritz solution. The results of the convergence study using the trigonometric series solution are shown in Table 4-11, with the frequency parameter λ of the simply supported plate. When all edges are simply supported, the trigonometric shape function, $\sin(i\pi\xi)\sin(j\pi\eta)$, is used in the Rayleigh-Ritz method solution. Validation has been done for the first four modes of natural frequency using the finite element analysis program ANSYS and the trigonometric series approach with M=12 and N=12 given in Table 4-12.

Table 4-11. Convergence study of frequency parameter $\lambda = \omega ab\sqrt{\rho h/D_0}$ for first four mode of the fiber-reinforced $[0_2/-45_2/45_2/90_2]_s$ laminated simply-supported plate with $a/b = 1, h/a = 0.016$

Number of Series (M× N)	Mode1 λ_1	Mode2 λ_2	Mode3 λ_3	Mode4 λ_4
2×2	12.39	24.90	37.37	49.87
4×4	12.38	24.70	37.27	44.59
6×6	12.37	24.67	37.25	44.54
8×8	12.36	24.65	37.24	44.52
10×10	12.36	24.65	37.24	44.51
12×12	13.36	24.64	37.24	44.50

Table 4-12. First four mode natural frequencies of fiber-reinforced $[0_2/-45_2/45_2/90_2]_s$ laminated simply-supported plate with $a/b = 1, h/a = 0.016$ using trigonometric series solution (TSS) with *M*=12 and *N*=12 and ANSYS

Solution Type	Mode1 Frequency (Hz)	Mode2 Frequency (Hz)	Mode3 Frequency (Hz)	Mode4 Frequency (Hz)
TSS	452.7	902.4	1363.6	1629.8
ANSYS	445.3	885.8	1341.3	1601.4
Difference %	1.66	1.87	1.66	1.77

Figure 4-62 shows the first mode shape of the simply-supported plate using trigonometric series solution (TSS). While obtaining the first mode, order of the trigonometric series *M* and *N* are taken 12 in Figure 4-62.

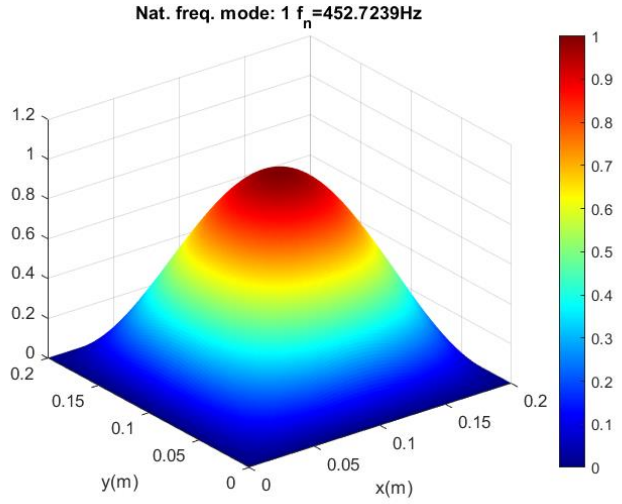

Figure 4-62. First mode shape of the fiber-reinforced $[0_2/-45_2/45_2/90_2]_s$ laminated simply supported plate with $a/b = 1,\ h/a = 0.016$ using the trigonometric series solution with M=12 and N=12

Second mode shape of the fiber-reinforced $[0_2/-45_2/45_2/90_2]_s$ laminated simply-supported plate is given in Figure 4-63. Trigonometric series solution (TSS) is used to obtain this mode shape with orders M=12 and N=12.

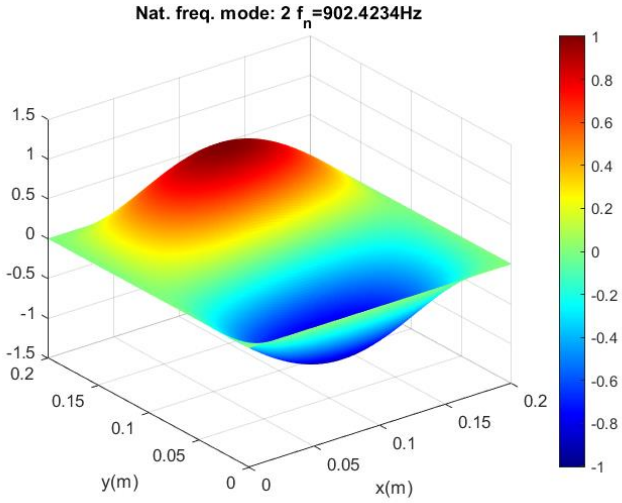

Figure 4-63. Second mode shape of the fiber-reinforced $[0_2/-45_2/45_2/90_2]_s$ laminated simply supported plate with $a/b = 1,\ h/a = 0.016$ using the trigonometric series solution with M=12 and N=12

Figure 4-64 and Figure 4-65 indicates the third and fourth mode shape of fiber-reinforced $[0_2/-45_2/45_2/90_2]_s$ laminated simply-supported plate using trigonometric series solution (TSS) with orders M=12 and N=12.

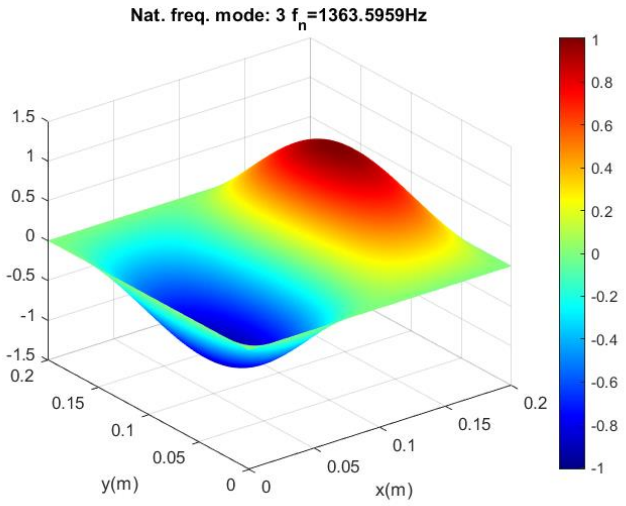

Figure 4-64. Third mode shape of the fiber-reinforced $[0_2/-45_2/45_2/90_2]_s$ laminated simply supported plate with $a/b = 1,\ h/a = 0.016$ using the trigonometric series solution with M=12 and N=12

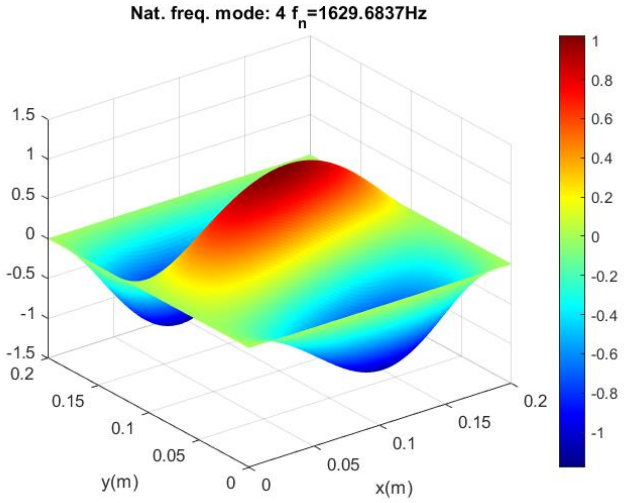

Figure 4-65. Fourth mode shape of the fiber-reinforced $[0_2/-45_2/45_2/90_2]_s$ laminated simply supported plate with $a/b = 1,\ h/a = 0.016$ using the trigonometric series solution with M=12 and N=12

Figure 4-66 shows the first mode shape of fiber-reinforced $[0_2/-45_2/45_2/90_2]_s$ laminated simply-supported plate using ANSYS.

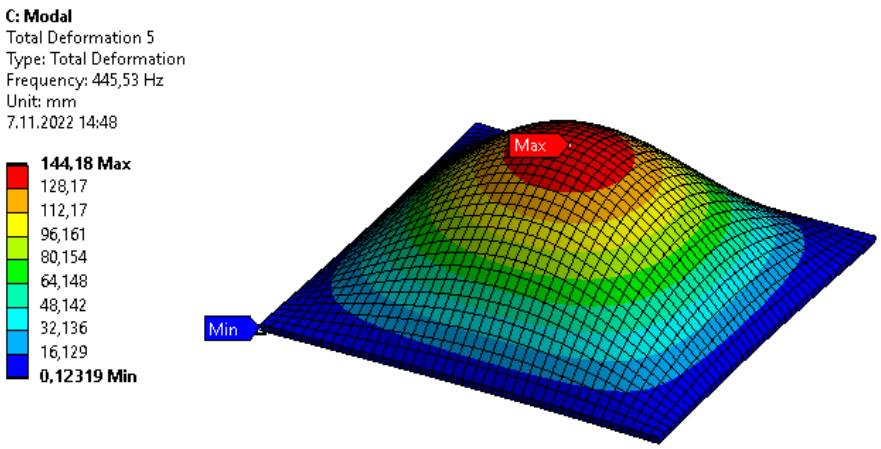

Figure 4-66. First mode shape of the fiber-reinforced $[0_2/-45_2/45_2/90_2]_s$ laminated simply supported plate with $a/b = 1$, $h/a = 0.016$ using ANSYS

Second mode shape of fiber-reinforced $[0_2/-45_2/45_2/90_2]_s$ laminated simply-supported plate is given in Figure 4-67. ANSYS is used to obtain second mode shape corresponding to second natural frequency.

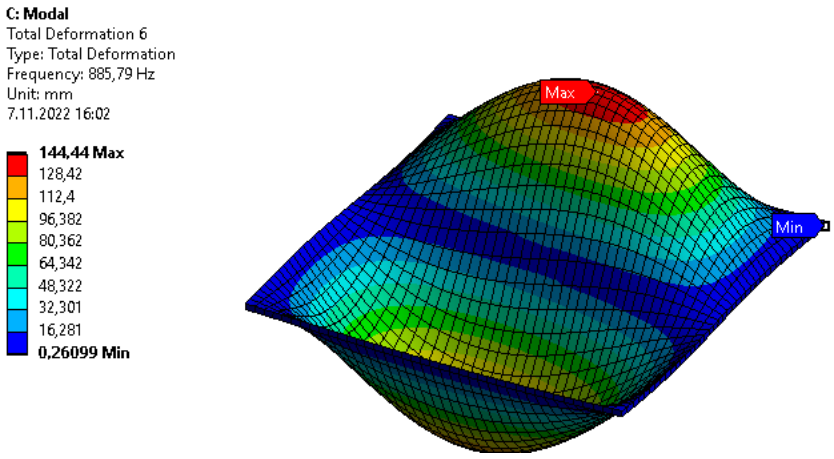

Figure 4-67. Second mode shape of the fiber-reinforced $[0_2/-45_2/45_2/90_2]_s$ laminated simply supported plate with $a/b = 1$, $h/a = 0.016$ using ANSYS

Figure 4-68 and Figure 4-69 shows the third and fourth mode shape of fiber-reinforced $[0_2/-45_2/45_2/90_2]_s$ laminated simply-supported plate using ANSYS.

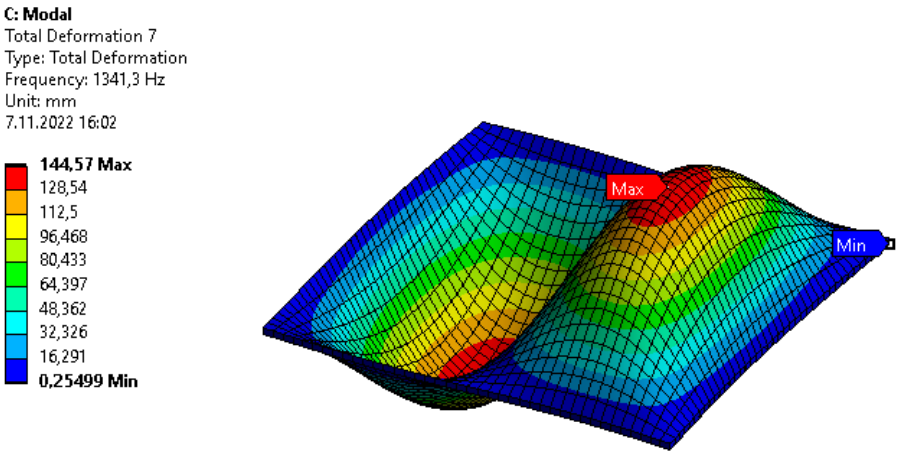

Figure 4-68. Third mode shape of the fiber-reinforced $[0_2/-45_2/45_2/90_2]_s$ laminated simply supported plate with $a/b = 1, h/a = 0.016$ using ANSYS

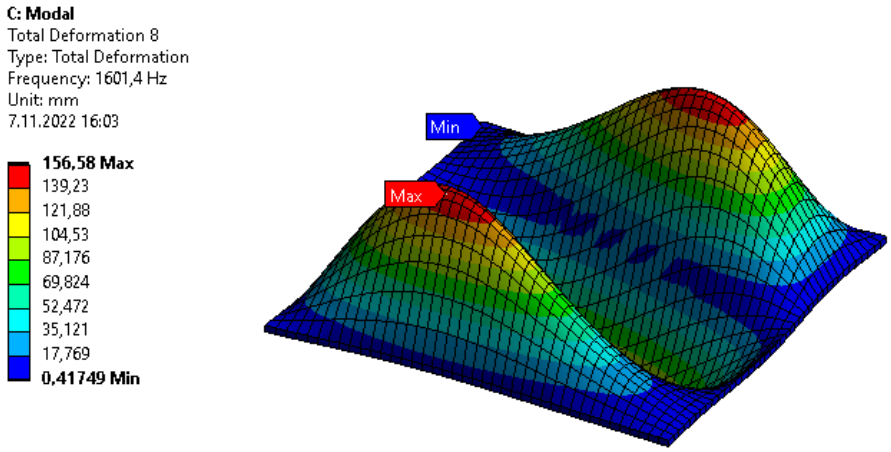

Figure 4-69. Fourth mode shape of the fiber-reinforced $[0_2/-45_2/45_2/90_2]_s$ laminated simply supported plate with $a/b = 1, h/a = 0.016$ using ANSYS

As seen in Table 4-12 and Figure 4-62-4-69, first four natural frequencies and mode shapes determined by TSS of simply-supported plate are verified with ANSYS.

4.3.2 Analysis for a Clamped Plate

The same material and geometric properties are used for a fiber-reinforced laminated plate described in the previous section. Boundary conditions are modified to clamp. Lamination sequence of clamped plate is $[0_2/-45_2/45_2/90_2]_s$. Trigonometric series solution and finite element analysis are used to obtain the natural frequencies and mode shapes of the fiber-reinforced clamped plate. In the trigonometric series solution (TSS), a convergence study of the frequency parameter λ is performed for the clamped plate by increasing the *M* and *N* orders of the Ritz solution. The results of the convergence study are shown in Table 4-13. When edges are clamped, the trigonometric shape function, $\sin(i\pi\xi)\sin(\pi\xi)\sin(j\pi\eta)\sin(\pi\eta)$, is used in the Rayleigh-Ritz method solution. Validation has been done for the first four modes' natural frequencies and mode shapes, using the finite element analysis program ANSYS and the trigonometric series solution with *M*=12 and *N*=12 in Table 4-14.

Table 4-13. Convergence study of frequency parameter $\lambda = \omega ab\sqrt{\rho h/D_0}$ for first four mode of fiber-reinforced $[0_2/-45_2/45_2/90_2]_s$ laminated clamped plate with $a/b = 1, h/a = 0.016$

Number of Series (M× N)	Mode1 λ_1	Mode2 λ_2	Mode3 λ_3	Mode4 λ_4
2 × 2	23.99	39.09	58.15	62.56
4 × 4	23.45	37.82	56.61	62.07
6 × 6	23.34	37.54	56.26	61.01
8 × 8	23.30	37.44	56.14	60.67
10 × 10	23.29	37.39	56.08	60.54
12 × 12	23.28	37.37	56.05	60.47

Table 4-14. First four mode natural frequencies of fiber-reinforced $[0_2/-45_2/45_2/90_2]_s$ laminated clamped plate with $a/b = 1$, $h/a = 0.016$ using trigonometric series solution (TSS) with *M*=12 and *N*=12 and ANSYS

Solution Type	Mode1 Frequency (Hz)	Mode2 Frequency (Hz)	Mode3 Frequency (Hz)	Mode4 Frequency (Hz)
TSS	852.2	1367.5	2051.1	2211.0
ANSYS	838.5	1341.3	1987.8	2161.9
Difference %	1.63	1.95	3.1	2.27

Figure 4-70 presents the first mode shape of the clamped plate using the trigonometric series solution with the order of the series *M* and *N* are selected 12.

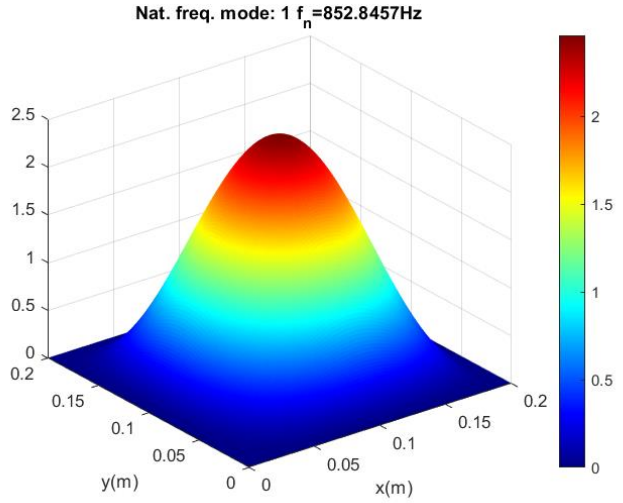

Figure 4-70. First mode shape of the fiber-reinforced $[0_2/-45_2/45_2/90_2]_s$ laminated clamped plate with $a/b = 1$, $h/a = 0.016$ using the trigonometric series solution with *M*=12 and *N*=12

Second mode shape of the fiber-reinforced $[0_2/-45_2/45_2/90_2]_s$ laminated clamped plate is expressed in Figure 4-71. Trigonometric series solution (TSS) is used to obtain this mode shape with orders *M*=12 and *N*=12.

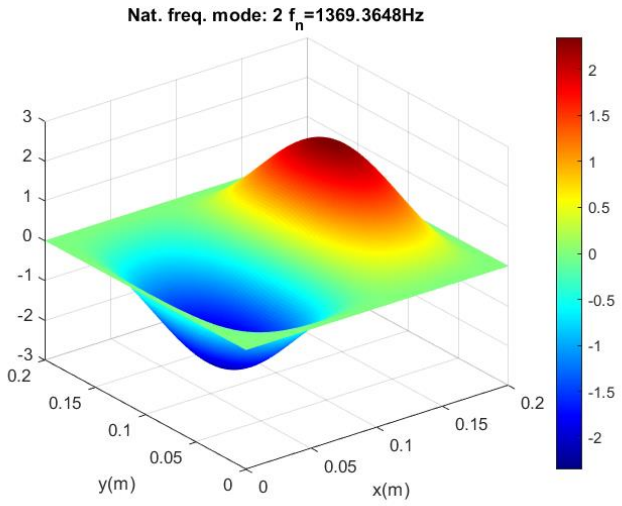

Figure 4-71. Second mode shape of the fiber-reinforced $[0_2/-45_2/45_2/90_2]_s$ laminated clamped plate with $a/b = 1, h/a = 0.016$ using the trigonometric series solution with M=12 and N=12

The third and fourth mode shape of fiber-reinforced $[0_2/-45_2/45_2/90_2]_s$ laminated clamped plate using trigonometric series solution (TSS) with orders M=12 and N=12 is given in Figure 4-72 and 4-73.

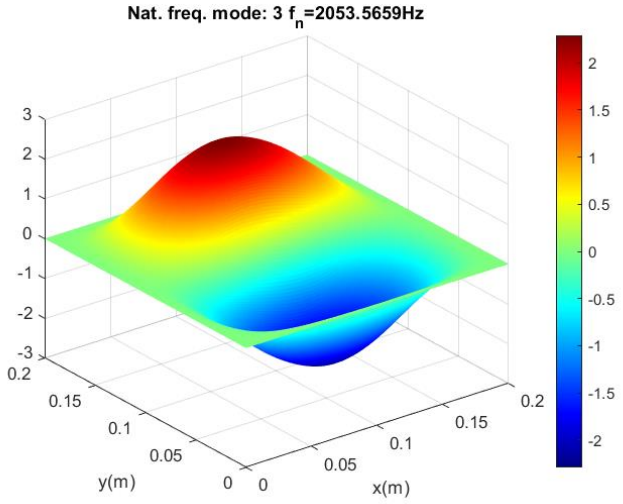

Figure 4-72. Third mode shape of the fiber-reinforced $[0_2/-45_2/45_2/90_2]_s$ laminated clamped plate with $a/b = 1, h/a = 0.016$ using the trigonometric series solution with M=12 and N=12

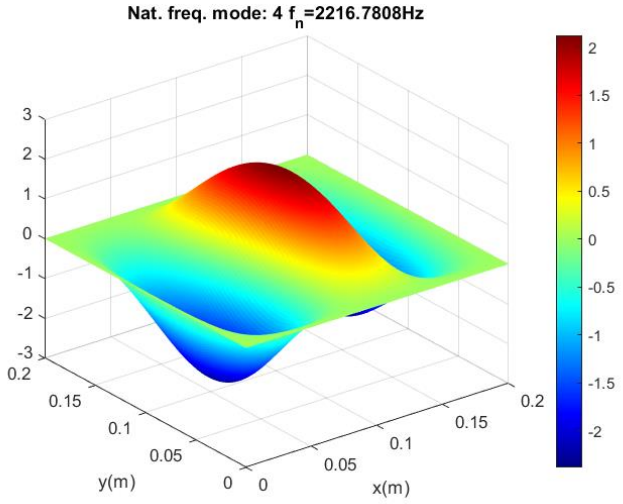

Figure 4-73. Fourth mode shape of the fiber-reinforced $[0_2/-45_2/45_2/90_2]_s$ laminated clamped plate with $a/b = 1, h/a = 0.016$ using the trigonometric series solution with M=12 and N=12

Figure 4-74 shows the first mode shape that found by ANSYS of fiber-reinforced $[0_2/-45_2/45_2/90_2]_s$ laminated clamped plate.

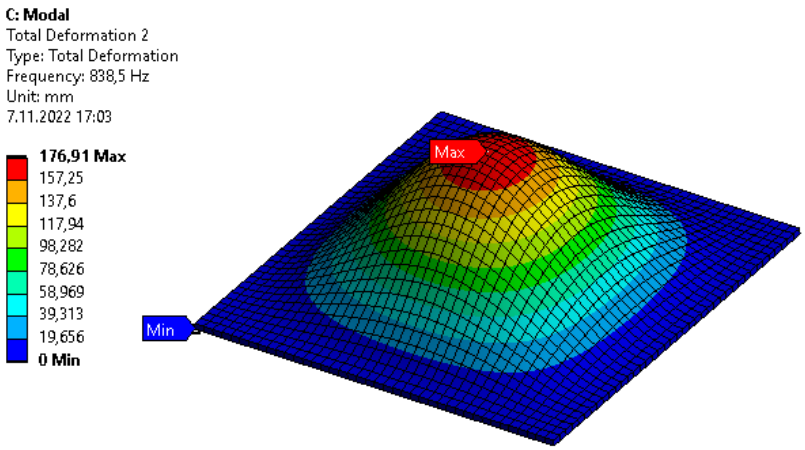

Figure 4-74. First mode shape of the fiber-reinforced $[0_2/-45_2/45_2/90_2]_s$ laminated clamped plate with $a/b = 1, h/a = 0.016$ using ANSYS

Second mode shape of fiber-reinforced $[0_2/-45_2/45_2/90_2]_s$ laminated clamped plate is given in Figure 4-75. ANSYS is used to determine second mode shape corresponding to second natural frequency.

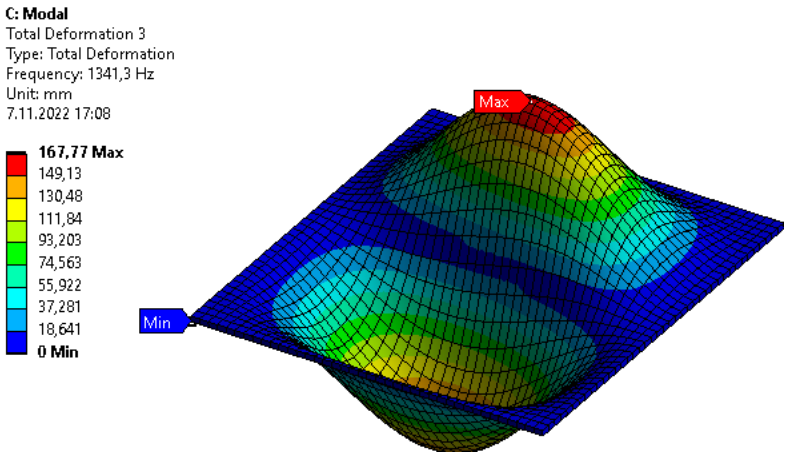

Figure 4-75. Second mode shape of the fiber-reinforced $[0_2/-45_2/45_2/90_2]_s$ laminated clamped plate with $a/b = 1, h/a = 0.016$ using ANSYS

The third and fourth mode shape of fiber-reinforced $[0_2/-45_2/45_2/90_2]_s$ laminated clamped plate using ANSYS is shown in Figure 4-76 and Figure 4-77.

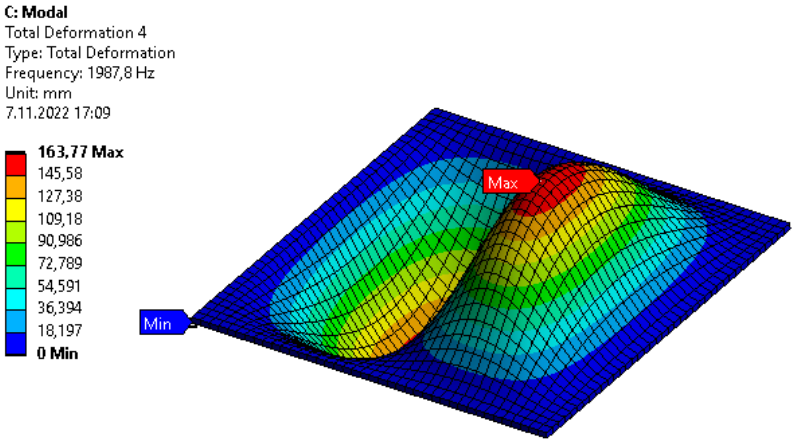

Figure 4-76. Third mode shape of the fiber-reinforced $[0_2/-45_2/45_2/90_2]_s$ laminated clamped plate with $a/b = 1, h/a = 0.016$ using ANSYS

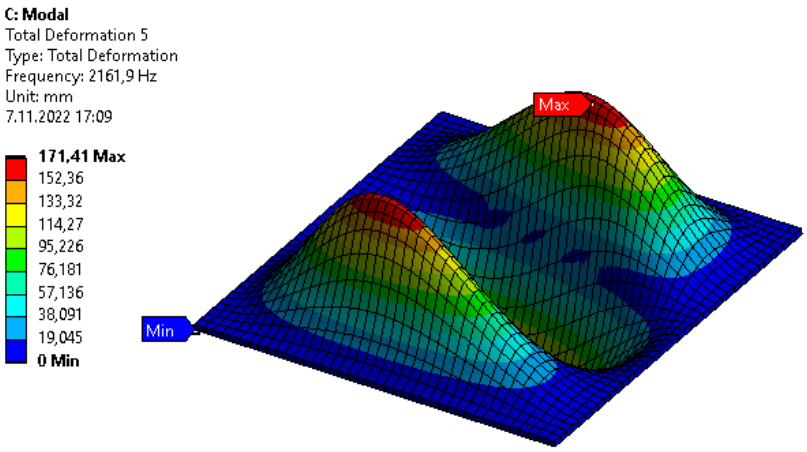

Figure 4-77. Fourth mode shape of the fiber-reinforced $[0_2/-45_2/45_2/90_2]_s$ laminated clamped plate with $a/b = 1, h/a = 0.016$ using ANSYS

Verification of natural frequencies and mode shapes of fiber-reinforced clamped plate has been done as seen in Table 4-13 and Figure 4-70-4-77.

4.3.3 Analysis for a Single Free and Three Clamped Plate

Natural frequencies and mode shapes of fiber-reinforced single free and three clamped plate are determined by the trigonometric series solution (TSS) and finite element analysis. The material and geometric properties of fiber-reinforced plate are taken in Table 4-9 and Table 4-10 as in the previous two sections. Lamination sequence of single free and three clamped plate is $[0_2/-45_2/45_2/90_2]_s$. In the trigonometric series solution (TSS), a convergence study of frequency parameter λ is done for a single free and three-clamped plate by increasing the *M* and *N* orders of the Ritz solution. The results of the convergence study using the trigonometric series solution are shown in Table 4–15. The trigonometric shape function, $(1-\cos\left(\frac{(2i-1)\pi}{2}\xi\right))\sin(j\pi\eta)\sin(\pi\eta)$, is used in the Rayleigh-Ritz method solution for this boundary conditions. Validation has been performed for the first four natural frequencies using the finite element analysis program ANSYS and the trigonometric series solution with *M*=12 and *N*=12 given in Table 4-16.

Table 4-15. Convergence study of frequency parameter $\lambda = \omega ab\sqrt{\rho h/D_0}$ for first four mode of fiber-reinforced $[0_2/-45_2/45_2/90_2]_s$ laminated single free and three clamped plate with $a/b = 1, h/a = 0.016$

Number of Series (M× *N*)	Mode1 λ_1	Mode2 λ_2	Mode3 λ_3	Mode4 λ_4
2 × 2	11.16	26.88	30.00	47.65
4 × 4	10.94	25.16	28.12	42.47
6 × 6	10.90	24.99	27.87	41.98
8 × 8	10.88	24.94	27.78	41.82
10 × 10	10.87	24.92	27.74	41.75
12 × 12	10.86	24.91	27.72	41.72

Table 4-16. First four mode natural frequencies of fiber-reinforced $[0_2/-45_2/45_2/90_2]_s$ laminated single free and three clamped plate with $a/b = 1$, $h/a = 0.016$ using trigonometric series solution (TSS) with M=12 and N=12 and ANSYS

Solution Type	Mode1 Frequency (Hz)	Mode2 Frequency (Hz)	Mode3 Frequency (Hz)	Mode4 Frequency (Hz)
TSS	397.4	911.6	1013.6	1525.7
ANSYS	392.8	897.6	998.1	1493.0
Difference %	1.17	1.55	1.55	2.19

Figure 4-78 shows the first mode shape of the single free and three clamped plate using trigonometric series solution (TSS). While obtaining the first mode, order of the trigonometric series M and N are taken 12.

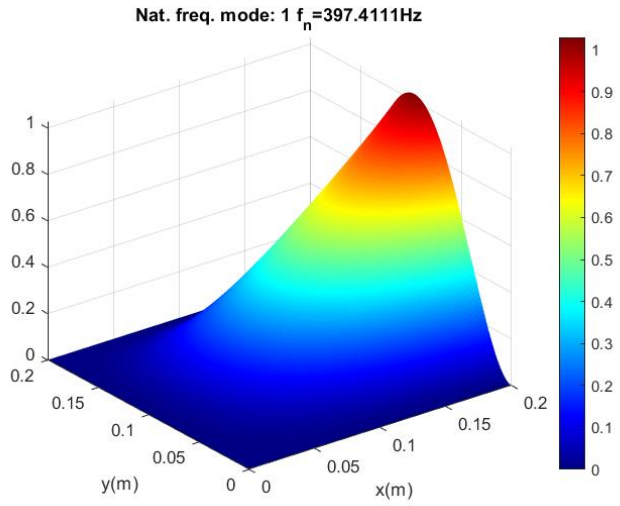

Figure 4-78. First mode shape of the fiber-reinforced $[0_2/-45_2/45_2/90_2]_s$ laminated single free and three clamped plate with $a/b = 1$, $h/a = 0.016$ using the trigonometric series solution with M=12 and N=12

Second mode shape of the fiber-reinforced $[0_2/-45_2/45_2/90_2]_s$ laminated single free and three clamped plate is given in Figure 4-79. Trigonometric series solution (TSS) is used to determine second mode shape with orders M=12 and N=12.

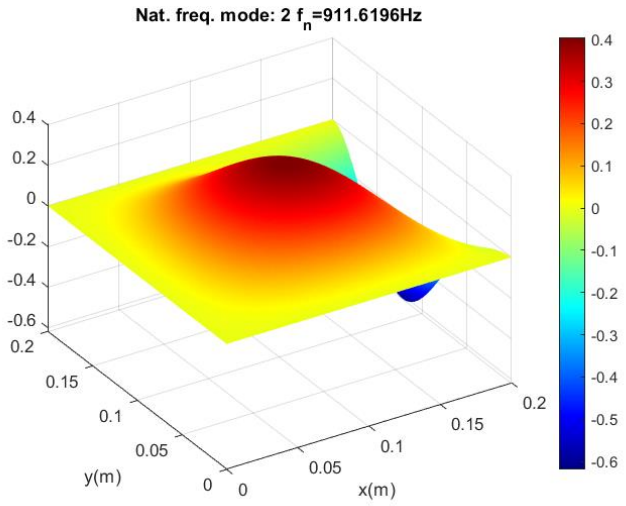

Figure 4-79. Second mode shape of the fiber-reinforced $[0_2/-45_2/45_2/90_2]_s$ laminated single free and three clamped plate with $a/b = 1, h/a = 0.016$ using the trigonometric series solution with M=12 and N=12

Figure 4-80 and Figure 4-81 indicates the third and fourth mode shape of fiber-reinforced $[0_2/-45_2/45_2/90_2]_s$ laminated single free and three clamped plate using trigonometric series solution (TSS) with orders M=12 and N=12.

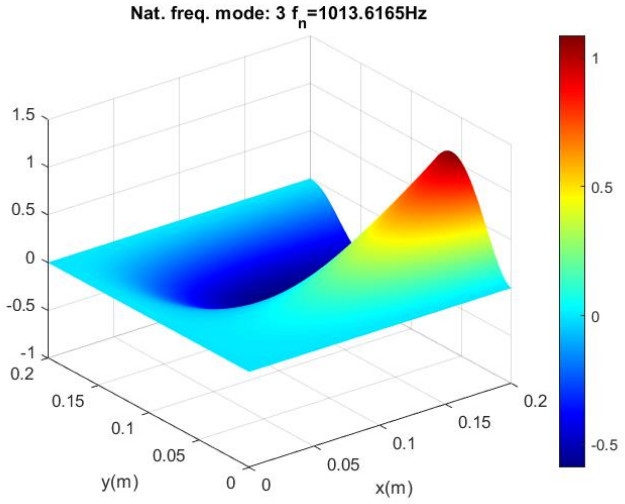

Figure 4-80. Third mode shape of the fiber-reinforced $[0_2/-45_2/45_2/90_2]_s$ laminated single free and three clamped plate with $a/b = 1, h/a = 0.016$ using the trigonometric series solution with M=12 and N=12

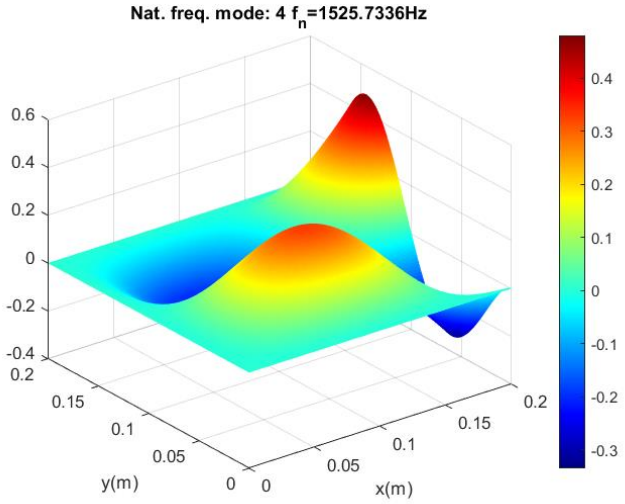

Figure 4-81. Fourth mode shape of the fiber-reinforced $[0_2/-45_2/45_2/90_2]_s$ laminated single free and three clamped plate with $a/b = 1, h/a = 0.016$ using the trigonometric series solution with M=12 and N=12

Figure 4-82 shows the first mode shape of fiber-reinforced $[0_2/-45_2/45_2/90_2]_s$ laminated single free and three clamped plate using ANSYS.

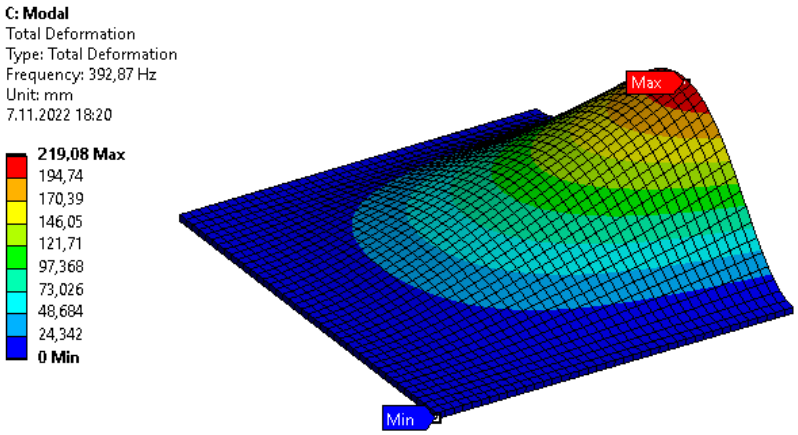

Figure 4-82. First mode shape of the fiber-reinforced $[0_2/-45_2/45_2/90_2]_s$ laminated single free and three clamped plate with $a/b = 1$, $h/a = 0.016$ using ANSYS

Second mode shape of fiber-reinforced $[0_2/-45_2/45_2/90_2]_s$ laminated single free and three clamped plate is given in Figure 4-83. ANSYS is used to obtain second mode shape of this plate.

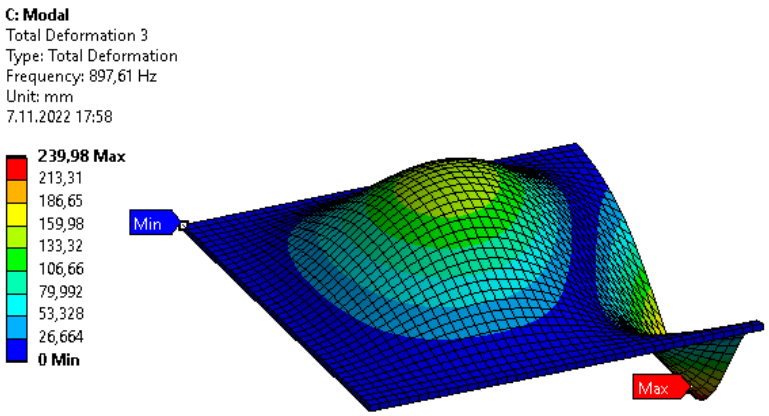

Figure 4-83. Second mode shape of the fiber-reinforced $[0_2/-45_2/45_2/90_2]_s$ laminated single free and three clamped plate with $a/b = 1$, $h/a = 0.016$ using ANSYS

Figure 4-84 and Figure 4-85 shows the third and fourth mode shape of fiber-reinforced $[0_2/-45_2/45_2/90_2]_s$ laminated single free and three clamped plate using ANSYS.

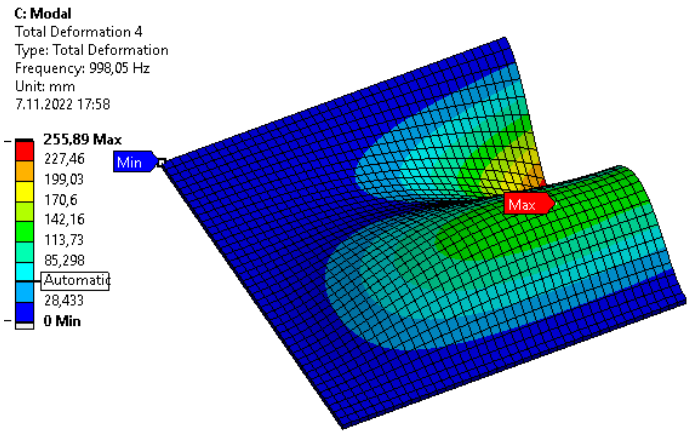

Figure 4-84. Third mode shape of the fiber-reinforced $[0_2/-45_2/45_2/90_2]_s$ laminated single free and three clamped plate with $a/b = 1$, $h/a = 0.016$ using ANSYS

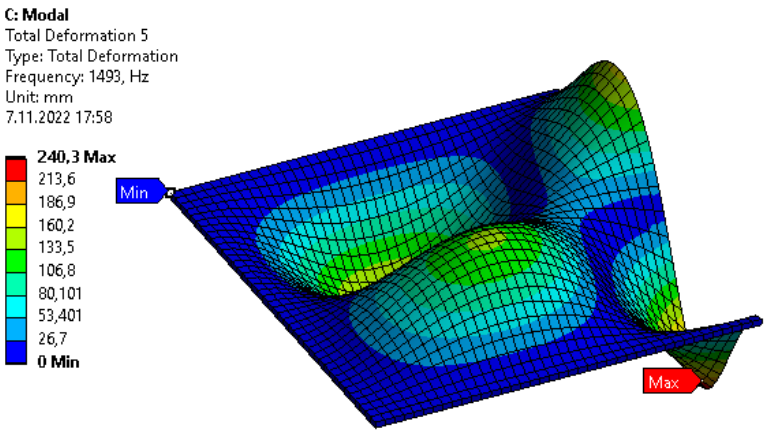

Figure 4-85. Fourth mode shape of the fiber-reinforced $[0_2/-45_2/45_2/90_2]_s$ laminated single free and three clamped plate with $a/b = 1$, $h/a = 0.016$ using ANSYS

4.4 Parametric Study

Changing the parameters of a fiber-reinforced laminated plate affects the static bending and free vibration results. Classical lamination plate theory assumes that a fiber-reinforced plate is thin. If thickness is increased too much then results will deviate from reality. Also, the orientation of the fiber angle in the lamina affects the static bending and free vibration results of the problem. Different fiber angles have been laminated so that the strength and natural frequency of different laminated fiber angles can be understood. Finally, the aspect ratio of the fiber-reinforced laminated plate has been analyzed to understand its effects on the static bending and free vibration results.

4.4.1 Effects of Thickness to Length Ratio (h/a) on Static Bending Results

The theory used in analytical solutions assumes the plate is thin. The thickness-to-length ratio is investigated for the fiber-reinforced plate to understand its effects on the maximum deflection. The trigonometric series solution (TSS) and the finite element method are utilized to determine the effects of thickness to length ratio on bending results. The material and geometric properties of the fiber-reinforced laminated plate used in the analysis are taken from Table 4-1 and Table 4-2 [49]. The boundary conditions of the fiber-reinforced plate are simply-supported, clamped, single free and three clamped. Firstly, the plate's layer thickness, t, is taken as 0.2 mm, and then increased by 0.05 mm at each step, up to 0.5 mm and analyzed. Thus, the total thickness of the plate, h, is increased from 3.2 mm to 8 mm, as given in Table 4-17. The lamination sequence of the fiber-reinforced laminated plate is $[0_2/-45_2/45_2/90_2]_s$. Table 4-18 shows the validation for the maximum deflection of fiber-reinforced plate with different thicknesses using the finite element analysis program ANSYS and the trigonometric series solution with M=12 and N=12.

Table 4-17. Thickness to length ratio (h/a) of the fiber-reinforced $[0_2/-45_2/45_2/90_2]_s$ laminated plate

h/a	h (mm)	t (mm)	a (mm)
0.016	3.2	0.20	200
0.020	4.0	0.25	200
0.024	4.8	0.30	200
0.028	5.6	0.35	200
0.032	6.4	0.40	200
0.036	7.2	0.45	200
0.040	8.0	0.50	200

Table 4-18. Effects of h/a ratio on the maximum deflection of the fiber-reinforced $[0_2/-45_2/45_2/90_2]_s$ laminated simply-supported (SSSS), clamped (CCCC), single free and three clamped (CFCC) plate with $q = 0.01$ MPa, $a/b = 1$, using trigonometric series solution (TSS) with M=12 and N=12 and ANSYS

h/a	Maximum Deflection (mm)					
	SSSS Plate $w_0(a/2, b/2)$		CCCC Plate $w_0(a/2, b/2)$		CFCC Plate $w_0(a, b/2)$	
	TSS	FEM	TSS	FEM	TSS	FEM
0.016	0.4161	0.4089	0.1169	0.1204	0.6096	0.6267
0.020	0.2130	0.2101	0.0598	0.0626	0.3121	0.3234
0.024	0.1233	0.1222	0.0346	0.0368	0.1806	0.1887
0.028	0.0776	0.0773	0.0218	0.0237	0.1137	0.1201
0.032	0.0520	0.0521	0.0146	0.0163	0.0762	0.0813
0.036	0.0365	0.0368	0.0103	0.0117	0.0535	0.0577
0.040	0.0266	0.0271	0.0075	0.0087	0.0390	0.0426

The numerical results from Table 4-18 are plotted. Effects of thickness-to-length ratio on the bending results of the fiber-reinforced laminated plate with different boundary conditions are given in Figure 4-86 using ANSYS and trigonometric series solution (TSS).

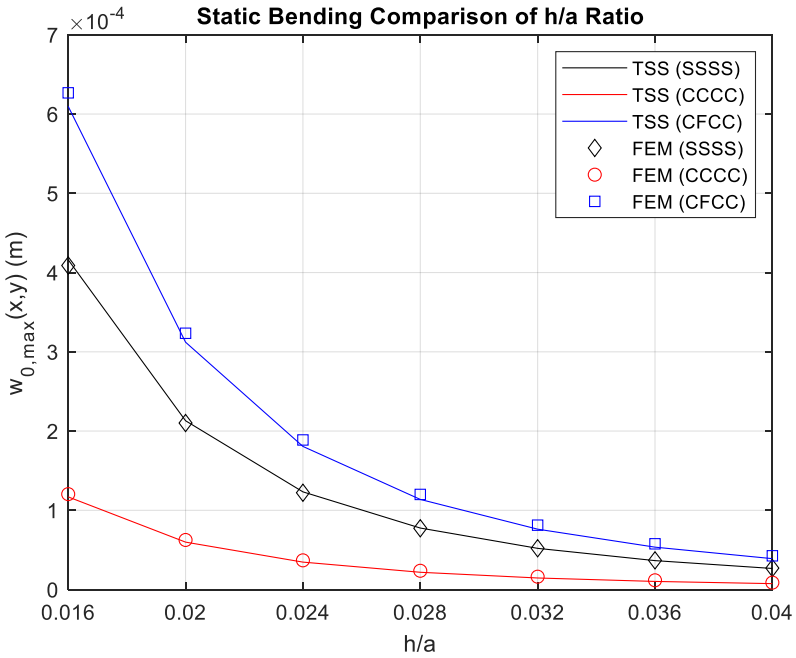

Figure 4-86. Effects of h/a ratio on the maximum deflection of the fiber-reinforced $[0_2/-45_2/45_2/90_2]_s$ laminated simply supported, clamped, and single free three clamped plate with $q = 0.01$ MPa, $a/b = 1$ using trigonometric series solution (TSS) with M=12 and N=12 and ANSYS

Figure 4-86 shows that if the ply thickness increases, maximum deformation decreases as the stiffness of plate increases. Also, there is a region where maximum deflection decreases sharply. There is an optimum range of h/a between 0.016 and 0.02 for achieving bending results correctly simulated thin laminated composite plates.

4.4.2 Effects of Thickness to Length Ratio (h/a) on Free Vibration Results

The thickness-to-length ratio is studied for fiber-reinforced plates to learn more about how it affects the fundamental natural frequency. The trigonometric series solution (TSS) and the finite element method are used in the different thickness-to-length ratio analyses. The material and geometric properties of the fiber-reinforced laminated plate are taken from Table 4-1 and Table 4-2 [49]. The boundary conditions of the fiber-reinforced plate are simply supported (SSSS), clamped (CCCC), and single free three clamped (CFCC). The thickness variation of plies is shown in Table 4-17, given in the previous section. The lamination sequence of the fiber-reinforced laminated plate is $[0_2/-45_2/45_2/90_2]_s$. Table 4-19 expresses the verification for the fundamental natural frequency of fiber-reinforced plate with different thickness to length ratio using the finite element analysis program, ANSYS and the trigonometric series solution with order M=12 and N=12.

Table 4-19. Effects of h/a ratio on the natural frequency of the fiber-reinforced $[0_2/-45_2/45_2/90_2]_s$ laminated simply-supported (SSSS), clamped (CCCC), single free and three clamped (CFCC) plate with, $a/b = 1$, using trigonometric series solution (TSS) with M=12 and N=12 and ANSYS

h/a	Natural Frequency, f_n (Hz)					
	SSSS Plate		CCCC Plate		CFCC Plate	
	TSS	FEM	TSS	FEM	TSS	FEM
0.016	452.73	450.60	825.76	840.40	398.08	393.09
0.020	565.92	562.05	1032.21	1042.12	497.60	489.42
0.024	679.01	672.73	1238.65	1238.40	597.12	584.62
0.028	792.28	782.48	1445.08	1429.16	696.64	678.54
0.032	905.46	891.17	1651.53	1612.00	796.17	771.03
0.036	1018.65	998.67	1857.97	1789.01	895.69	861.97
0.040	1131.83	1104.90	2064.41	1960.02	995.21	951.26

The theory used in analytical solutions assumes the plate is thin. The thickness-to-length ratio is investigated for three boundary conditions to understand its effects on fundamental natural frequency. Thus, its effect on the natural frequency can be examined as the plate thickness increases. Figure 4-87 shows the effects of thickness-to-length ratio on free vibration results.

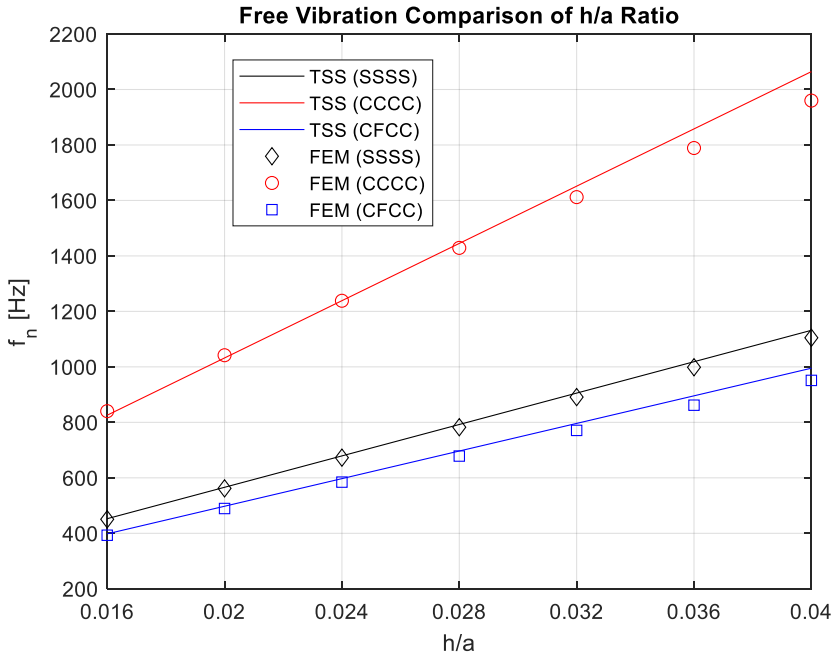

Figure 4-87. Effects of h/a ratio on the fundamental frequency of the fiber-reinforced $[0_2/-45_2/45_2/90_2]_s$ laminated simply supported, clamped, and single free three clamped plate with, $a/b = 1$ using trigonometric series solution (TSS) with *M*=12 and *N*=12 and ANSYS

The trigonometric series approach used Kirchhoff's hypothesis that utilized the thin plate assumption. Figure 4-87 shows that the fundamental frequency increases when the thickness-to-length ratio rises. This situation occurs because of the increase in the plate's stiffness when the thickness of the plate increases.

4.4.3 Effects of Lamination Angles on Static Bending Results

The different fiber orientation angles of the fiber-reinforced plate are studied to understand their effects on the maximum deflection. The trigonometric series solution (TSS) and the finite element method are used to determine how the lamination angle affects the static bending results. The material properties of the fiber-reinforced laminated plate are taken from Table 4-1 [49], except for the thickness of the ply. The ply thickness, t, is selected as 0.5 mm, so the total thickness of the fiber-reinforced plate, h, is 4 mm. The geometric properties of the fiber-reinforced plate in the different lamination angle problem are shown in Table 4-20. Eight plies are symmetrically laminated in the fiber-reinforced plate. To understand the effects of fiber orientation, plies with different fiber orientation angles are laminated symmetrically with their minus angles, as seen in Table 4-21. The boundary conditions of the fiber-reinforced plate are simply supported (SSSS), clamped (CCCC), and single-free three-clamped (CFCC). Table 4-22 presents the validation for the maximum deflection of the fiber-reinforced plate with different lamination angles using the finite element analysis program ANSYS and the trigonometric series solution with M=12 and N=12.

Table 4-20. Geometric properties of fiber-reinforced plate for different lamination angle problem

Name	Geometric Parameter	Value	Unit
X axis Dimension	a	0.2	m
Y axis Dimension	b	0.2	m
Uniform Load	q	10000	$\mathrm{N/m^2}$
Number of Plies	n	8	-

Table 4-21. Lamination type of the fiber-reinforced plate in different lamination angle problem for maximum deflection

Lamination Type No.	Lamination Sequence $[\theta/-\theta/\theta/-\theta]_s$	Ply Thickness t (mm)	Plate Thickness h (mm)
1	$[0/-0/0/-0]_s$	0.5	4.0
2	$[15/-15/15/-15]_s$	0.5	4.0
3	$[30/-30/30/-30]_s$	0.5	4.0
4	$[45/-45/45/-45]_s$	0.5	4.0
5	$[60/-60/60/-60]_s$	0.5	4.0
6	$[75/-75/75/-75]_s$	0.5	4.0
7	$[90/-90/90/-90]_s$	0.5	4.0

Table 4-22. Effects of lamination angle on the maximum deflection of the fiber-reinforced simply-supported (SSSS), clamped (CCCC), single free and three clamped (CFCC) plate with, $q = 0.01$ MPa, $h/a = 0.02$, $a/b = 1$, using trigonometric series solution (TSS) with M=12 and N=12 and ANSYS

Lamination Type No.	Maximum Deflection (mm)					
	SSSS Plate $w_0(a/2, b/2)$		CCCC Plate $w_0(a/2, b/2)$		CFCC Plate $w_0(a, b/2)$	
	TSS	FEM	TSS	FEM	TSS	FEM
1	0.2738	0.2623	0.0548	0.0583	0.7542	0.75909
2	0.2352	0.2279	0.0573	0.0611	0.6352	0.6215
3	0.1818	0.1789	0.0622	0.0632	0.3806	0.3829
4	0.1619	0.1613	0.0637	0.0641	0.1913	0.2011
5	0.1778	0.1789	0.0598	0.0632	0.1012	0.1085
6	0.2241	0.2279	0.0537	0.0612	0.06224	0.07219
7	0.2569	0.2623	0.0508	0.0509	0.05011	0.05749

Figure 4-88 shows the effects of fiber orientation angles in lamina on the maximum deflection of fiber-reinforced simply supported (SSSS), clamped (CCCC), and single free three clamped (CFCC) plate. Numerical results are taken from Table 4-22.

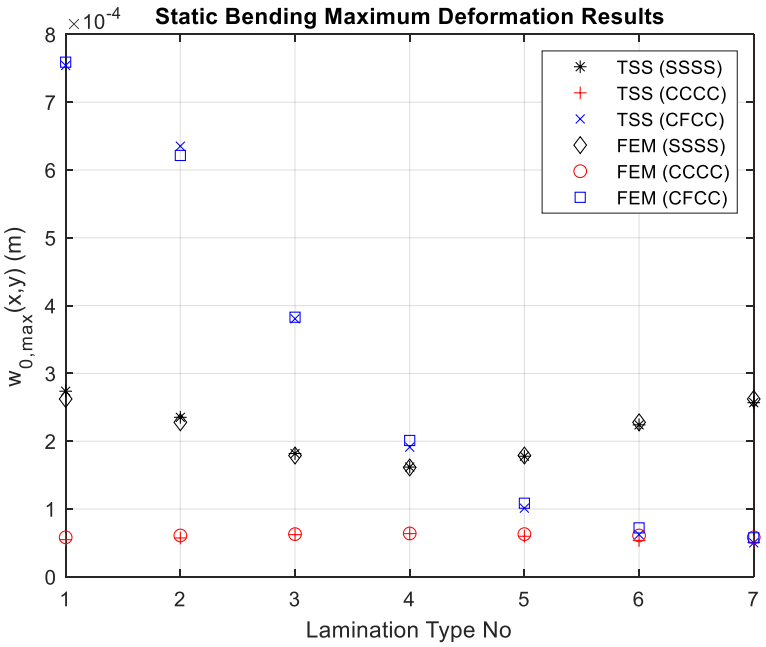

Figure 4-88. Effects of lamination angle on the maximum deflection of the fiber-reinforced laminated simply supported, clamped, and single free three clamped plate with $q = 0.01$ MPa, $h/a = 0.02$, $a/b = 1$, using trigonometric series solution (TSS) with M=12 and N=12 and ANSYS

Figure 4-88 shows that the fiber orientation angles of layers react differently. The strongest fiber orientation layer is 45°, and the weakest is 90° and 0° for simply supported boundaries. When edges are clamped, all lamination angles give almost the same result because all degrees of freedom are fixed when boundaries are clamped. The strongest fiber orientation angle in the single free and three-clamped edges is 90°, and the weakest fiber orientation angle is 0° because one edge is free in the x direction.

4.4.4 Effects of Lamination Angles on Free Vibration Results

The effects of the different fiber orientation angles on the fundamental natural frequency are employed for the fiber-reinforced plate. The trigonometric series solution (TSS) and the finite element method are used in the different lamination angle analyses. The material and geometric properties of the fiber-reinforced laminated plate used in this problem are taken from Table 4-1 [49] and Table 4-20. The ply thickness, t, is selected as $0.4\,\text{mm}$, so the total thickness of the fiber-reinforced plate, h, is $3.2\,\text{mm}$. The boundary conditions of the fiber-reinforced plate are simply supported (SSSS), clamped (CCCC), and single free three clamped (CFCC). In order to understand the effects of lamination angles on the fundamental natural frequency, seven different lamination sequences given in Table 4-23 are used. In this table, the thicknesses of the ply and plate are also provided. As seen in Table 4-23, eight plies are laminated symmetrically. Table 4-24 indicates the verifying natural frequency of the fiber-reinforced plate with different lamination angles using the finite element analysis program ANSYS and the trigonometric series solution with M=12 and N=12.

Table 4-23. Lamination type of the fiber-reinforced plate in different lamination angle problem for fundamental natural frequency

Lamination Type No.	Lamination Sequence $[\theta/-\theta/\theta/-\theta]_s$	Ply Thickness t (mm)	Plate Thickness h (mm)
1	$[0/-0/0/-0]_s$	0.4	3.2
2	$[15/-15/15/-15]_s$	0.4	3.2
3	$[30/-30/30/-30]_s$	0.4	3.2
4	$[45/-45/45/-45]_s$	0.4	3.2
5	$[60/-60/60/-60]_s$	0.4	3.2
6	$[75/-75/75/-75]_s$	0.4	3.2
7	$[90/-90/90/-90]_s$	0.4	3.2

Table 4-24. Effects of lamination angle on the fundamental natural frequency of the fiber-reinforced simply-supported (SSSS), clamped (CCCC), single free and three clamped (CFCC) plate with, $q = 0.01$ MPa, $h/a = 0.02$, $a/b = 1$, using trigonometric series solution (TSS) with M=12 and N=12 and ANSYS

Lamination Type No.	Natural Frequency, f_n (Hz)					
	SSSS Plate		CCCC Plate		CFCC Plate	
	TSS	FEM	TSS	FEM	TSS	FEM
1	400.24	398.86	864.60	848.94	262.49	261.97
2	430.85	429.76	852.79	849.87	284.14	287.90
3	488.60	487.13	830.80	827.98	363.01	365.13
4	517.25	513.71	826.40	823.76	503.93	499.30
5	494.20	487.13	847.56	841.98	669.72	666.44
6	441.51	439.76	880.16	879.87	804.49	791.15
7	413.20	410.87	895.38	888.99	856.78	848.97

Natural frequencies of the fiber-reinforced plate with different fiber orientation layers are determined by the trigonometric series solution (TSS) and the finite element analysis program, ANSYS, as seen in Table 4-24. The results are close to each other. The effects of lamination angles on the fundamental natural frequencies are shown in Figure 4-89.

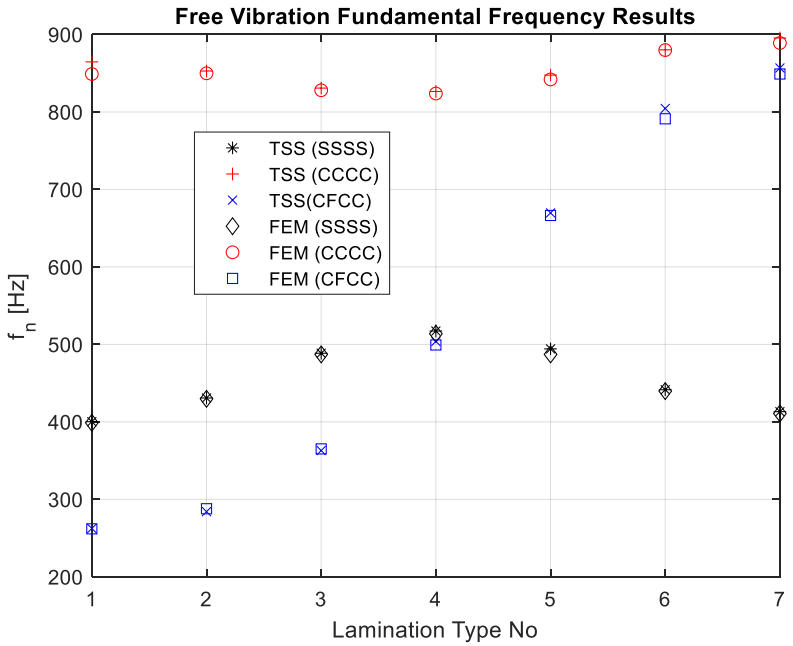

Figure 4-89. Effects of lamination angle on the fundamental natural frequency of the fiber-reinforced laminated simply supported, clamped, and single free three clamped plate with $h/a = 0.02$, $a/b = 1$, using trigonometric series solution (TSS) with M=12 and N=12 and ANSYS

The results of three different boundary conditions are shown in Figure 4-89. These boundary conditions have different critical fundamental frequencies depending on the lamination angle. The critical fiber-orientation angles are 90° and 0° when boundaries are simply supported. However, 45° of fiber orientation is more crucial to the free vibration problem if the edges are clamped. Lastly, a 0° lamination angle is important when boundaries are single-free and three-clamped since the free edge is in the x direction.

4.4.5 Effects of Aspect Ratio (a/b) on Static Bending Results

In the analysis made in previous sections, the in-plane dimensions of the fiber-reinforced plate were equal. In order to understand the effects of the aspect (a/b) ratio on the maximum deflection of the fiber-reinforced plate, the analysis of various aspect ratios of the plate is made by the trigonometric series solution (TSS) and finite element method. The material and geometric properties of the fiber-reinforced plate are taken from Table 4-1 [49] and Table 4-25. The boundary conditions of the fiber-reinforced plate are simply-supported, clamped, single free and three clamped. Firstly, the plate's aspect ratio, a/b , is taken as 1 , then increased by 0.5 at each step, up to 3. Thus, the transverse dimension of plate b is decreased from 200 mm to 66.67 mm , as given in Table 4-25. The lamination sequence of the fiber-reinforced laminated plate is $[0_2/-45_2/45_2/90_2]_s$. Ply thickness, t is selected as 0.2 mm so the total thickness of fiber-reinforced plate, h is 3.2 mm. Table 4-26 shows the validation for the maximum deflection of fiber-reinforced plate with different aspect ratios using the finite element analysis program ANSYS and the trigonometric series solution with M=12 and N=12.

Table 4-25. Geometric properties of fiber-reinforced plate for different aspect ratio problem

Aspect Ratio a/b	Longitudinal Dimension a (mm)	Transverse Dimension b (mm)	Uniform Load q (MPa)
1	200	200	0.01
1.5	200	133.34	0.01
2	200	100	0.01
2.5	200	80	0.01
3	200	66.67	0.01

Table 4-26. Effects of aspect ratio on the maximum deflection of the fiber-reinforced $[0_2/-45_2/45_2/90_2]_s$ laminated simply-supported (SSSS), clamped (CCCC), single free and three clamped (CFCC) plate with, $q = 0.01$ MPa, $h/a = 0.016$ using trigonometric series solution (TSS) with M=12 and N=12 and ANSYS

Aspect Ratio	Maximum Deflection (mm)					
	SSSS Plate		CCCC Plate		CFCC Plate	
a/b	$w_0(a/2, b/2)$		$w_0(a/2, b/2)$		$w_0(a, b/2)$	
	TSS	FEM	TSS	FEM	TSS	FEM
1	0.4161	0.4089	0.1169	0.1204	0.6096	0.6268
1.5	0.2077	0.2064	0.0626	0.0648	0.1311	0.1373
2	0.1040	0.1031	0.0291	0.0304	0.0410	0.0430
2.5	0.0548	0.0538	0.0138	0.0146	0.0167	0.0176
3	0.0307	0.0291	0.0700	0.0074	0.0800	0.0085

The composite plate may not always be square; it may have different dimensions in the x and y directions. To understand the effects of aspect ratio on the fiber-reinforced plate, static bending analysis is made for different aspect ratios. Three different boundary conditions are used in these calculations. The numerical results are taken from Table 4-26 and plotted for better examination. Figure 4-90 shows the effects of aspect ratio on the static bending results of the fiber-reinforced plate.

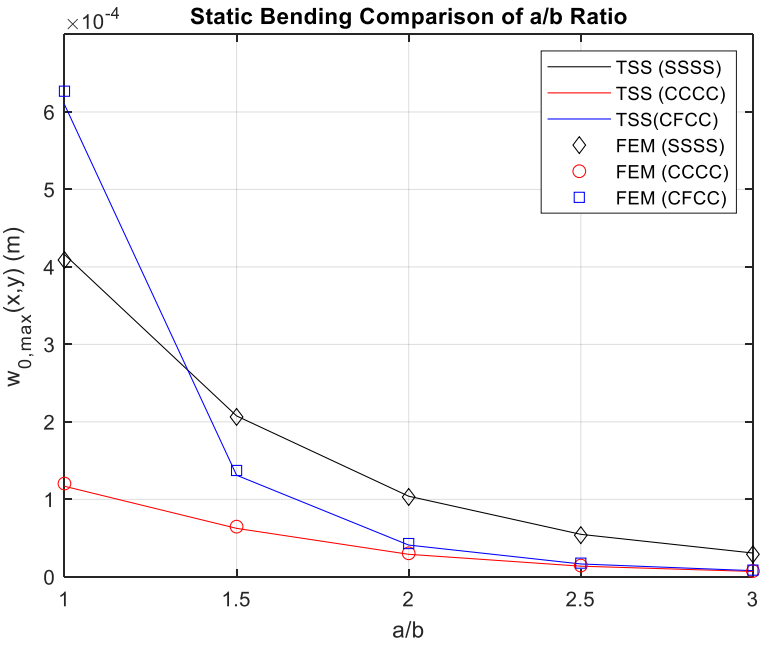

Figure 4-90. Effects of a/b ratio on the maximum deflection of the fiber-reinforced $[0_2/-45_2/45_2/90_2]_s$ laminated simply supported, clamped, and single free three clamped plate with $q = 0.01$ MPa, $h/a = 0.016$ using trigonometric series solution (TSS) with M=12 and N=12 and ANSYS

Aspect ratio effects behave similarly on the fiber-reinforced plate for three boundary conditions. If the aspect ratio of the fiber-reinforced plate increases, the maximum deflection decreases since stiffness of plate increases, as seen in Figure 4-90. When the plate boundaries are clamped, maximum deflection falls slower because all degrees of freedom are fixed. However, while a composite plate has free boundary conditions, maximum deformation decreases sharply.

4.4.6 Effects of Aspect Ratio (a/b) on Free Vibration Results

In the previous section, the effects of aspect ratio on the maximum static bending were examined. The aspect ratio also has certain effects on the fundamental natural frequency of the fiber-reinforced plate. In order to understand these effects, the trigonometric series solution (TSS) and finite element method are used for different aspects ratio of the plate. The material and geometric properties of the fiber-reinforced laminated plate are taken from Table 4-1 [49] and Table 4-25, as in the previous section. The boundary conditions of the fiber-reinforced plate are simply-supported, clamped, single free and three clamped. The change in aspect ratio is given in Table 4-25. The lamination sequence of the fiber-reinforced laminated plate is $[0_2/-45_2/45_2/90_2]_s$. Ply thickness, t is selected as 0.2 mm so the total thickness of fiber-reinforced plate, h is 3.2 mm. Table 4-27 demonstrates the validation for the fundamental natural frequency of fiber-reinforced plate with different aspect ratios using the finite element analysis program ANSYS and the trigonometric series solution with M=12 and N=12.

Table 4-27. Effects of aspect ratio on the fundamental natural frequency of the fiber-reinforced $[0_2/-45_2/45_2/90_2]_s$ laminated simply-supported (SSSS), clamped (CCCC), single free and three clamped (CFCC) plate with, $h/a = 0.016$ using trigonometric series solution (TSS) with M=12 and N=12 and ANSYS

Aspect Ratio	Natural Frequency, f_n (Hz)					
	SSSS Plate		CCCC Plate		CFCC Plate	
a/b	TSS	FEM	TSS	FEM	TSS	FEM
1	452.65	450.15	838.71	840.44	391.39	393.09
1.5	640.28	636.71	1155.51	1154.30	805.29	805.92
2	904.65	898.12	1680.99	1672.02	1394.31	1389.20
2.5	1246.19	1235.70	2405.21	2378.40	2155.74	2134.91
3	1664.84	1654.8	3316.29	3257.61	3088.65	3038.52

Figure 4-91 shows the effects of aspect ratio (a/b) on the fundamental natural frequency of the fiber-reinforced plate using numerical results from the Table 4-27.

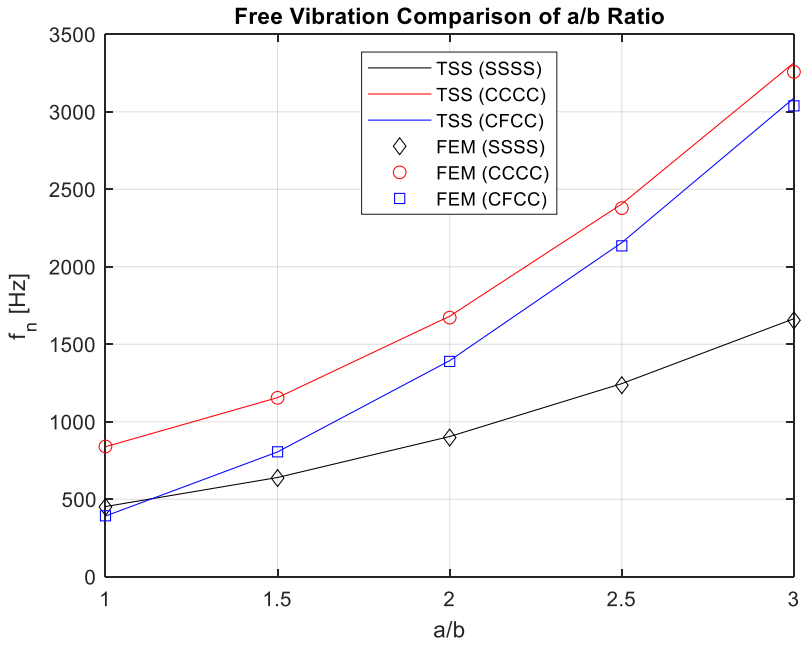

Figure 4-91. Effects of a/b ratio on the fundamental frequency of the fiber-reinforced $[0_2/-45_2/45_2/90_2]_s$ laminated simply supported, clamped, and single free three clamped plate with, $h/a = 0.016$ using trigonometric series solution (TSS) with M=12 and N=12 and ANSYS

When the Figure 4-91 is examined, it can be understood that when the aspect ratio increases with decreasing transverse dimension, natural frequencies of different boundaries increase since the stiffness of plate increases. When boundaries are clamped, or a single free and three clamped, fundamental frequency increases more than when all edges are simply supported. The reason for this situation can be explained as follows: if there is a clamped boundary condition on a fiber-reinforced plate, all degrees of freedom are limited.

4.5 Comparison with Different Approximation Method

In this section, the new developed trigonometric series solution (TSS) method is compared with a study in the literature. Deflection and free vibration of symmetrically laminated, quasi-isotropic, thin rectangular plates for different boundary conditions were studied by Altunsaray and Bayer in 2013 [49]. This study examines the maximum deflection and the natural frequency of thin rectangular plates that are simply supported and clamped from four edges. The effects of changes in aspect ratio and orientation angle on the results of static bending and free vibration problems according to the Classical Lamination Plate Theory are parametrically calculated using the Galerkin Method. The obtained results are compared with the software package ANSYS, which conducts analyses using the Finite Elements Method (FEM). While making the comparison, the methods in the article [49] are compared with the trigonometric series solution method with M and N taken as 12. The stacking sequences used in the comparison are given in Table 4-28. Material and geometric properties of the fiber-reinforced plate are taken from Tables 4-1 and 4-2. The comparison of the maximum deflections of the fiber-reinforced simply supported and clamped plate according to different aspect ratios are given in Tables 4-29 and 4-30.

Table 4-28. Different lamination types for comparison of TSS with the literature [49]

Lamination Type No.	Lamination Sequence	Ply Thickness t (mm)	Plate Thickness h (mm)
1	$[0_2/-45_2/45_2/90_2]_s$	0.2	3.2
2	$[-45_2/0_2/45_2/90_2]_s$	0.2	3.2
3	$[45_2/-45_2/0_2/90_2]_s$	0.2	3.2
4	$[90_2/-45_2/45_2/0_2]_s$	0.2	3.2

Table 4-29. Effects of aspect ratio and stacking sequence on the maximum deflection of the fiber-reinforced laminated simply-supported (SSSS) plate, $q = 0.01$ MPa, $h/b = 0.016$ using trigonometric series solution (TSS) with M=12 and N=12 and Altunsaray and Bayer [49] results

a/b	Method	Lamination Scheme Type No. $w_0(a/2, b/2)$ (mm)			
		1	2	3	4
1	Altunsaray and Bayer [49]	0.401	0.347	0.318	0.407
	Present	0.416	0.376	0.330	0.404
	FEM	0.416	0.392	0.339	0.416
1.4	Altunsaray and Bayer [49]	0.891	0.691	0.600	0.507
	Present	0.919	0.748	0.618	0.569
	FEM	0.923	0.778	0.625	0.568
2.0	Altunsaray and Bayer [49]	1.623	1.178	0.996	0.729
	Present	1.665	1.267	1.020	0.701
	FEM	1.655	1.287	1.006	0.680

Different approximation methods, Galerkin and Ritz, are given and validated with ANSYS in Table 4-29 for maximum deflection of simply supported plate. These results show that the proposed trigonometric series solution (TSS) method has better accuracy than the Galerkin method, which is given in the literature study [49].

Table 4-30. Effects of aspect ratio and stacking sequence on the maximum deflection of the fiber-reinforced laminated clamped (CCCC) plate, $q = 0.01$ MPa, $h/b = 0.016$ using trigonometric series solution (TSS) with M=12 and N=12 and Altunsaray and

a/b	Method	Lamination Scheme Type No. $w_0(a/2, b/2)$ (mm)			
		1	2	3	4
1	Altunsaray and Bayer [49]	0.116	0.119	0.121	0.116
	Present	0.119	0.127	0.125	0.114
	FEM	0.121	0.130	0.127	0.120
1.4	Altunsaray and Bayer [49]	0.276	0.237	0.216	0.142
	Present	0.283	0.255	0.222	0.140
	FEM	0.284	0.257	0.224	0.145
2.0	Altunsaray and Bayer [49]	0.463	0.350	0.300	0.149
	Present	0.475	0.371	0.306	0.148
	FEM	0.473	0.370	0.306	0.149

The maximum deformation of fiber-reinforced clamped plate according to the different aspect ratios are given in Table 4-30 with trigonometric series solution (TSS) method and literature example [49] and results are validated using FEM. The results show that the developed method gives better results than the literature study [49].

The natural frequency of the fiber-reinforced simply-supported and clamped plates according to different aspect ratios are compared in Table 4-31 and Table 4-32. The

results are obtained using the trigonometric series solution (TSS) method and are compared with the literature [49] that used Galerkin method and FEM.

Table 4-31. Effects of aspect ratio and stacking sequence on the natural frequency of the fiber-reinforced laminated simply-supported (SSSS) plate, $h/b = 0.016$ using trigonometric series solution (TSS) with M=12 and N=12 and Altunsaray and Bayer [49] results

a/b	Method	Lamination Scheme Type No. Natural Frequency, f_n (Hz)			
		1	2	3	4
1	Altunsaray and Bayer [49]	454.7	483.6	510.9	454.7
	Present	452.6	471.6	507.4	459.2
	FEM	447.6	461.2	494.9	447.6
1.4	Altunsaray and Bayer [49]	306.1	343.5	373.3	380.6
	Present	304.4	334.1	370.8	387.4
	FEM	301.2	327.4	363.3	376.7
2.0	Altunsaray and Bayer [49]	227.4	263.6	290.5	341.1
	Present	226.2	257.1	288.9	349.4
	FEM	224.3	253.3	284.7	339.2

Table 4-32. Effects of aspect ratio and stacking sequence on the natural frequency of the fiber-reinforced laminated clamped (CCCC) plate, $h/b = 0.016$ using trigonometric series solution (TSS) with M=12 and N=12 and Altunsaray and Bayer [49] results

a/b	Method	Lamination Scheme Type No. Natural Frequency, f_n (Hz)			
		1	2	3	4
1	Altunsaray and Bayer [49]	856.3	849.1	844.3	856.3
	Present	852.8	827.8	836.8	860.6
	FEM	842.5	815.8	823.3	842.5
1.4	Altunsaray and Bayer [49]	560.5	602.8	629.3	759.6
	Present	557.9	585.7	623.8	776.9
	FEM	553.7	579.9	616.8	748.8
2.0	Altunsaray and Bayer [49]	429.3	490.3	527.0	719.3
	Present	427.3	478.5	522.7	737.9
	FEM	425.2	475.4	518.9	710.1

As can be seen from the natural frequency results for simply supported and clamped fiber-reinforced plates given in the Table 4-31 and 4-32, the newly developed trigonometric series solution (TSS) gave results closer to the results calculated by the finite element method.

CHAPTER 5

CONCLUSION

This study developed a new trigonometric series expansion method to obtain the static bending and free vibration behaviors of symmetrically laminated fiber-reinforced plates. Kirchhoff's (Classical Laminated Plate) theory is applied in the analytical formulation of both bending and free vibration problems. Governing partial differential equations is derived by employing Hamilton's principle. The effects of boundary conditions on static bending and free vibration problems are investigated. The boundary conditions are satisfied by expanding mid-plane displacement into a series of trigonometric shape functions. When the Rayleigh-Ritz method is used to obtain approximating static bending results, the coefficients of the trigonometric series form a linear system. For the free vibration problems, the eigenvalue equation is obtained by solving the minimization of the energy theory of the fiber-reinforced plate with the Rayleigh-Ritz method. Natural frequencies and mode shapes of the fiber-reinforced plate are determined by solving this equation. Using plate elements that incorporate first-order shear deformation theory, finite element models for both bending and free vibrations are constructed by ANSYS. Numerical results are obtained for simply supported and clamped composite plates as well as those for a plate with single free and three clamped edges. The developed trigonometric series approach is validated by comparing the results of finite element studies and a study in the literature [49]. Comparisons of this study's results to those of finite element analysis and literature show the accuracy of the trigonometric series solution method used in this study. Further results illustrate the influences of geometric and material parameters upon the static bending and the free vibration responses of the fiber-reinforced plate.

The following outcomes were made from the results obtained in bending problems.

- The minimum deformation occurred in the fiber-reinforced clamped plate because all degree of freedom are limited along the boundaries.
- The maximum deformation occurred due to the free boundary condition in the plate with single-free and three-clamped.

A few inferences have also been made from the transverse stress results. Transverse stresses were examined separately for each layer. Since each layer was laminated at a different angle, it was observed in which directions more stress occurred on these layers.

- The highest normal stress in the x and y directions was determined in the layers that have 0° and 90° of fiber-orientation, respectively, due to the fact that the orientations of the fibers are parallel to the x and y axes.
- The highest shear stress was calculated in layers with a fiber orientation of $45°$ or $-45°$ because these fiber orientations are laminated along the shear direction of the plies.

The stresses of each of the plies along the thickness of the laminate are also compared.

- For the σ_{xx}, it is observed that the maximum stress occurs at 0° fiber oriented layers as expected.
- For the σ_{yy}, the maximum stress occurs at 45° and -45° fiber oriented layers. Normally, 90° fiber oriented layers are expected to have highest stress but as they are at midplane of the laminate, they are subjected to less deformation than 45° and -45° layers. This causes these fibers have higher stress than 90° fiber oriented layers.
- For the σ_{xy}, the maximum stress occurs at 45° and -45° fiber oriented layers which is expected.

Modal analysis is also performed in this study for three different boundary conditions.

- The lowest first natural frequency of the symmetrically laminated fiber-reinforced plate was found in single-free and three-clamped boundary conditions which is a result of having a free edge.
- The highest value was obtained on the clamped plate since all degrees of freedom are limited along the boundaries in this case.

The effects of some geometric parameters on the results are investigated as well.

- Firstly, the thickness-to-length ratio was examined. It is observed that as the thickness increases, maximum deflection decreases and natural frequency increases since the stiffness of the plate increases.
- Second parametric study was carried out to understand how the fiber-orientation angles of the layers behave in static bending and free vibration problems. Strongest fiber-orientation layer is 45° in simply-supported plate. When all edges are clamped, all lamination angles give almost the same result because all degree of freedoms are limited along boundaries. For single-free and three clamped plate, strongest lamination angle is 90° degrees since the free edge is in x direction. For natural frequencies, critical lamination angle is 0° and 90° for simply supported plate. For clamped plate, 45° fiber oriented layers are critical. Since the free edge is in x direction, 0° fibers are most critical for single free and three clamped plate.
- Finally, a parametric study is carried out to understand how the aspect ratio affects the results. It is seen that while the transverse dimension decreases, stiffness of the plate increases. It is also observed that as the aspect ratio increases, maximum deflection decreases while natural frequency increases.

Another comparison is made for bending and free vibration analysis for simply supported and clamped plate between the study carried out in this thesis and a different approximation method existing in the literature [49].

- It is seen that the accuracy of the proposed method in this study, leads to results with higher accuracy than the method employed in the literature study.

The developed method in this study can be used accurately for static bending and free vibration analysis of a fiber-reinforced laminated plate with different types of boundary conditions. The proposed method leads to rapid convergence, possesses computational efficiency, and could be useful in design and optimization studies involving laminated fiber-reinforced structures. In the future, this method may be used with unsymmetrical fiber-reinforced plates and solving this method under thermal loads may be an exciting area of study.

REFERENCES

[1] Carrera, E., 2003, “Theories and finite elements for multilayered plates and shells: a unified compact formulation with numerical assessment and benchmarking,” Archives of Computational Methods in Engineering, 10(3), pp. 215–296.

[2] Reddy, J. N., 2004, Mechanics of laminated composite plates and shells: theory and analysis, CRC Press.

[3] Liew, K. M., Pan, Z. Z., and Zhang, L. W., 2019, “An overview of layerwise theories for composite laminates and structures: Development, numerical implementation and application,” Composite Structures, 216, pp. 240–259.

[4] Kreja, I., 2011, “A literature review on computational models for laminated composite and sandwich panels,” Open Engineering, 1(1), pp. 59–80.

[5] Srinivas, S. and Rao, A. K., 1970, “Bending, vibration and buckling of simply supported thick orthotropic rectangular plates and laminates,” International Journal of Solids and Structures, 6(11), pp. 1463–1481.

[6] Pagano, N. J., 1970, “Exact solutions for rectangular bidirectional composites and sandwich plates,” Journal of Composite Materials, 4(1), pp. 20–34.

[7] Ye, J. and Soldatos, K. P., 1994, “Three-dimensional vibration of laminated cylinders and cylindrical panels with symmetric or antisymmetric cross-ply lay-up,” Composites Engineering, 4(4), pp. 429–444.

[8] Fan, J. and Ye, J., 1990, “An exact solution for the statics and dynamics of laminated thick plates with orthotropic layers,” International Journal of Solids and Structures, 26(5-6), pp. 655–662.

[9] Vel, S. S. and Batra, R. C., 2001, “Exact solution for rectangular sandwich plates with embedded piezoelectric shear actuators,” AIAA Journal, 39(7), pp. 1363–1373.

[10] Vel, S. S. and Batra, R. C., 1999, “Analytical solution for rectangular thick laminated plates subjected to arbitrary boundary conditions,” AIAA Journal, 37(11), pp. 1464– 1473.

[11] Vel, S. S. and Batra, R. C., 2000, “Three-dimensional analytical solution for hybrid multilayered piezoelectric plates,” Journal of Applied Mechanics, 67(3), pp. 558–567.

[12] Rohwer K., Friedrichs S., Wehmeyer C., Analyzing laminated structures from fibre-reinforced composite material - an assessment, Technische Mechanik 25, 2005, 59-79

[13] Jones R. M., Mechanics of composite materials, Second Editions, Taylor & Francis, Inc., Philadelphia, PA, 1999

[14] Sun C.T., Chin, H., Analysis of asymmetric composite laminates, AIAA Journal 26, 1988, 714-718

[15] Reissner, E. and Stavsky, Y., 1961, “Bending and stretching of certain types of heterogeneous aeolotropic elastic plates,” Journal of Applied Mechanics, 28(3), pp. 402–408.

[16] Whitney J. M., Pagano, N. J., Shear deformation in heterogeneous anisotropic plates, Journal of Applied Mechanics, Trans. ASME 37, 1970, 1031-1036

[17] Dong S. B., Tso F. K. W., On a laminated orthotropic shell theory including transverse shear deformation, Journal of Applied Mechanics, Trans. ASME 39, 1972, 1091-1096

[18] Chandrashekhara K., Pavan Kumar D. V. T. G., Static response of composite circular cylindrical shells studied by different theories, Meccanica 33, 1998, 11-27

[19] Reddy J. N., A simple higher-order theory for laminated composite plates, Journal of Applied Mechanics, Trans. ASME 51, 1984, 745-752

[20] Khdeir A. A., Reddy J. N., Librescu L., Analytical solution of a refined shear deformation theory for rectangular composite plates, Int. Journal of Solids & Structures 23, 1987, 1447-1463

[21] Meirovitch, L. and Kwak, M. K., 1990, "Convergence of the classical Rayleigh-Ritz method and the finite element method," AIAA Journal, 28(8), pp. 1509–1516.

[22] Wang, C. M., Wang, Y. C., and Reddy, J. N., 2002, "Problems and remedy for the Ritz method in determining stress resultants of corner supported rectangular plates," Computers and Structures, 80(2), pp. 145–154.

[23] Ilanko, S., Monterrubio, L., and Mochida, Y., 2015, The Rayleigh-Ritz Method for Structural Analysis, John Wiley & Sons.

[24] Kapania, R. K. and Liu, Y., 2000, "Static and vibration analyses of general wing structures using equivalent-plate Models," AIAA Journal, 38(7), pp. 1269–1277.

[25] Bhat, R., 1985, "Natural frequencies of rectangular plates using characteristic orthogonal polynomials in Rayleigh-Ritz method," Journal of Sound and Vibration, 102(4), pp. 493–499.

[26] Bhat, R., 1987, "Flexural vibration of polygonal plates using characteristic orthogonal polynomials in two variables," Journal of Sound and Vibration, 114(1), pp. 65–71.

[27] Bhat, R., 1987, “Rayleigh-Ritz method with separate deflection expressions for structural segments,” Journal of Sound and Vibration, 115(1), pp. 174–177.

[28] Bhat, R., 2015, “Vibration of beams using novel boundary characteristic orthogonal polynomials satisfying all boundary conditions,” Advances in Mechanical Engineering, 7(4), p. 1687814015578355.

[29] A.W. Leissa, The free vibration of rectangular plates, Journal of Sound and Vibration, Volume 31, Issue 3, 1973, Pages 257-293.

[30] Arthur W. Leissa, Yoshihiro Narita, Vibration studies for simply supported symmetrically laminated rectangular plates, Composite Structures, Volume 12, Issue 2, 1989, Pages 113-132.

[31] K.M. Liew, K.Y. Lam, A Rayleigh-Ritz approach to transverse vibration of isotropic and anisotropic trapezoidal plates using orthogonal plate functions, International Journal of Solids and Structures, Volume 27, Issue 2, 1991, Pages 189-203.

[32] Chow, S. T., Liew, K. M., & Lam, K. Y. (1992). Transverse vibration of symmetrically laminated rectangular composite plates. *Composite Structures*, *20*(4), 213-226.

[33] Geannakakes, G. N. (1995). Natural frequencies of arbitrarily shaped plates using the Rayleigh-Ritz method together with natural co-ordinate regions and normalized characteristic orthogonal polynomials. *Journal of Sound and Vibration*, *182*(3), 441-478.

[34] Chai, G. B. (1994). Free vibration of generally laminated composite plates with various edge support conditions. *Composite Structures*, *29*(3), 249-258.

[35] Wang, S. (1997). Vibration of thin skew fibre reinforced composite laminates. *Journal of sound and vibration*, *201*(3), 335-352.

[36] Cheung, Y. K., & Zhou, D. (1999). The free vibrations of rectangular composite plates with point-supports using static beam functions. *Composite Structures*, *44*(2-3), 145-154.

[37] Cheung, Y. K., & Zhou, D. (2001). Free vibrations of rectangular unsymmetrically laminated composite plates with internal line supports. *Computers & Structures*, *79*(20-21), 1923-1932.

[38] Anlas, G., & Göker, G. (2001). Vibration analysis of skew fibre-reinforced composite laminated plates. *Journal of sound and vibration*, *242*(2), 265-276.

[39] Amirahmadi, S., & Ansari, R. (2009). Buckling and vibration analysis of angle-ply symmetric laminated composite plates with fully elastic boundaries.

[40] Chakraverty, S., & Pradhan, K. K. (2014). Free vibration of functionally graded thin rectangular plates resting on Winkler elastic foundation with general boundary conditions using Rayleigh–Ritz method. *International Journal of Applied Mechanics*, *6*(04), 1450043.

[41] Chakraverty, S., & Behera, L. (2014). Free vibration of rectangular nanoplates using Rayleigh–Ritz method. *Physica E: Low-dimensional Systems and Nanostructures*, *56*, 357-363.

[42] Deghboudj, S., Boukhedena, W., & Satha, H. (2021). Free Vibration Analysis of Symmetric Laminated Composite Thin Rectangular Plate and Passive Control with Attached Patches. *Journal of Failure Analysis and Prevention*, *21*(4), 1240-1251.

[43] Nguyen, T. K., Nguyen, N. D., Vo, T. P., & Thai, H. T. (2017). Trigonometric-series solution for analysis of laminated composite beams. *Composite Structures*, *160*, 142-151.

[44] Carroll, K., & Gutierrez-Miravete, E. (2014, November). A Comparison of Computed Deflections of Symmetric Angle-Ply Laminate Plates by the Ritz Method and the Finite Element Method. In *ASME International Mechanical Engineering*

Congress and Exposition (Vol. 46583, p. V009T12A004). American Society of Mechanical Engineers.

[45] Narita, Y., & Leissa, A. W. (1990). Buckling studies for simply supported symmetrically laminated rectangular plates. *International Journal of Mechanical Sciences*, *32*(11), 909-924.

[46] Patnaik, S. N. (2001). *Stress formulation in three-dimensional elasticity* (Vol. 210515). National Aeronautics and Space Administration, Glenn Research Center.

[47] Ritz, W. (1909). Über eine neue Methode zur Lösung gewisser Variationsprobleme der mathematischen Physik.

[48] Yavuz, M. T., & Ozkol, I. (2021). Comparison of Some Numerical Approaches for Determination of Dynamic Characteristics in Beam and Plate Elements. *Avrupa Bilim ve Teknoloji Dergisi*, (28), 1454-1468.

[49] Altunsaray, E., & Bayer, İ. (2013). Deflection and free vibration of symmetrically laminated quasi-isotropic thin rectangular plates for different boundary conditions. *Ocean Engineering*, *57*, 197-222.